MARINE HEAT WAVES IN THE INDIAN OCEAN AND THEIR IMPACTS ON ATMOSPHERIC CONVECTION

by

SARANYA, J. S

(2015-20-022)

THESIS

Submitted in partial fulfillment of the requirements for the degree of

BSc-MSc (Integrated) CLIMATE CHANGE ADAPTATION

FACULTY OF AGRICULTURE
Kerala Agricultural University

ACADEMY OF CLIMATE CHANGE EDUCATION AND RESEARCH
VELLANIKKARA, THRISSUR - 680 656
KERALA, INDIA
2020

DECLARATION

I, hereby declare that this thesis entitled "**MARINE HEAT WAVES IN THE INDIAN OCEAN AND THEIR IMPACTS ON ATMOSPHERIC CONVECTION**" is a legitimate record of work done by me during the period of research and the contents of this thesis have not been presented earlier for any Degree or Diploma of any other University or society.

Vellanikkara, **Saranya. J. S**

Date: (2015-20-022)

CERTIFICATE

Certified that this thesis entitled "**MARINE HEAT WAVES IN THE INDIAN OCEAN AND THEIR IMPACTS ON ATMOSPHERIC CONVECTION**" is a bonafide record of work done independently by **Ms. Saranya. J.S** student of Academy Of Climate Change Education And Research, Kerala Agricultural University vellanikkara, Thrissur - 680 656, Kerala, India, under my guidance and supervision and that it has not previously formed the basis for the award of any degree, diploma, fellowship or associateship to her.

Vellanikkara,
Date:

Dr. P. O. Nameer
(Major Advisor, Advisory Committee)
Professor and Special Officer,
Academy of Climate Change Education and Research, Vellanikkara.

CERTIFICATE

We, the undersigned members of the advisory committee of Ms. Saranya, J.S., (2015-20-022) a candidate for the degree of BSc-MSc (Integrated) Climate Change Adaptation agree that the thesis entitled "**MARINE HEAT WAVES IN THE INDIAN OCEAN AND THEIR IMPACTS ON ATMOSPHERIC CONVECTION**" may be submitted by Ms. Saranya. J.S., (2015-20-022) in partial fulfillment of the requirement for the degree.

ACKNOWLEDGMENTS

The outcome of my thesis required a lot of guidance and assistance from many people. I am incredibly privileged to have got this all along with the completion of my thesis. I wish to extend my profound gratitude to my guide, Dr. Roxy Mathew Koll, for his encouragement, support, and patience towards me, all though he had a busy schedule. He was always there to help me when I stuck in my analysis. Moreover, he gave me a chance to think freely and do work independently. His criticism and the way of handling the research question helped me a lot and will help in the future. I want to thank Dr.Vinu Valsala, the Academic head, Dr. R. Krishnan, the Executive Director, CCCR, and Prof. Ravi S Nanjundiah, the Director helping me to do my thesis at Indian Institute of Tropical Meteorology. I am deeply grateful to Dr. PO Nameer, Special Officer, ACCER, KAU, Vellanikkara for his support and cooperation throughout the research period. I gratefully acknowledge Jineesh. V.K, Dr. Gopakumar, Krishnapriya for their support throughout my research work. I am indebted to Mr. Panini Dasgupta, Ph.D. student, and groupmate at IITM for his support and priceless contribution to my thesis. He teaches me the python and other basic concepts of different subjects. He is always there for any help. His encouragement made me curious about my thesis. Thank my best friend, Athira, K. S, who always helped and stood by my side throughout the study period. Next, I like to remember Ajay Anand, Jyoti Jadav, Sreeraj, Sai prasad, Akash, Nivya, Vismaya, Aswin Sagar for their help and cooperation; we had lots of funny moments together throughout the research period. I gratefully acknowledge the group mates Vineet, Sophia, Aditi, and Vivek for their help and cooperation during the study period. I am extending my sincere gratitude towards my batch mates for their care and affection**.** Finally, I must convey my very deep gratitude to my family for providing me with support encouragement and prayers throughout my years of study. This accomplishment would not have been possible without them.

TABLE OF CONTENTS

LIST OF TABLES

LIST OF FIGURES

SYMBOLS AND ABBREVIATIONS

MHW	Marine heatwave
OISST	Optimum Interpolated Sea Surface Temperature
SST	Sea Surface Temperature
ENSO	El Niño Southern Oscillation
IOD	Indian Ocean Dipole
SSTA	Sea Surface Temperature Anomaly
OLR	Outgoing long wave Radiation
JJAS	June to September
BoB	Bay of Bengal
MJO	Madden-Julian Oscillation
MISO	Monsoon Intra seasonal Oscillation
DSWRF	Downward Short Wave Radiation Flux
ULWRF	Upward Long wave Radiation Flux
SHTFL	Sensible Heat Flux
LHTFL	Latent Heat Flux

CHAPTER 1
INTRODUCTION

According to the Special Report on the Ocean and Cryosphere (SROCC) of the Intergovernmental Panel on Climate Change (IPCC), the global ocean will continue to warm during the 21st century. By 2100, the ocean warming in the top 2000 m was estimated to be 5 to 7 times higher under the business-as-usual scenario (or 2-4 times higher under low emission scenario) relative to the temperature reported since 1970 (very likely). Under this warming scenario, we can expect a rise in extreme temperature events in the ocean, similar to what is projected over the land. Marine heatwaves (MHWs) are a relatively new concept, which is an outcome of a warming ocean. They are similar to heat waves over the land but have some differences in their identification and definition. As for the most recent definition, Hobday *et al.* (2016) call it a discrete prolonged anomalous warm water event. Schaeffer *et al.* (2017) opine that MHWs are uncertain and cavernous in the ocean. MHWs are reported worldwide, the 2003 Mediterranean Sea MHW, 2011 West Australian MHW, 2015/16 Tasman Sea MHW are some of them. Numerous studies indicate that these significant events can cause habitat destruction and affect ocean biology adversely. Coral bleaching, seagrass destruction, loss of kelps forest are some of them. The fisheries sector all over the world is also affected by these events. For example, lobsters have been adversely affected (Mills *et al.,* 2013).

Furthermore, model studies in the northeast Pacific fishery show that the impacts on the fishing will be tremendous. Fish production will resentfully affect, and this impact might quadruple compared with the mean change (Cheung and Frölicher, 2020). MHWs can reduce primary productivity, which further affects several species. It was also reported that

middle Atlantic bight MHW accelerated the dying of the Humpback Whales, through the change in the position of shelf breakfront in to onshore, which also shift the Whales position from the cross-shelf because Whales usually track shelf-break front due to the upwelling feature (Gawarkiewicz *et al*., 2019).

According to Schlegel *et al.* (2017), local-scale changes can sway the MHW events. These events are expected to increase in the future due to global warming (Frölicher *et al.,* 2018; Oliver *et al*., 2018). In a recent study, Oliver *et al.* (2018) showed that globally, there is a yearly 54% increase in the count of MHW days and also indicated a further increase shortly. The causes of the formation of these events are different. Most of them are associated with ENSO events. The synoptic conditions can also trigger them, like weakening of wind, air temperature rise and less interaction between the ocean and atmosphere (Bond *et al.,* 2015; Chen *et al.,* 2015, Schaeffer and Roughan 2017). Darmaraki *et al.* (2019) point out that, soon, due to the warming trend, the MHWs will become more influential in terms of their duration and intensity, which may threaten the marine ecosystem in the Mediterranean Sea. According to a recent study, it has been found that the warming caused by the MHW in the north Pacific (called the "The Blob") lasts in the subsurface layer until March 2018. And in addition to that, MHWs impact the coastal ecosystem because the remnants of MHWs may continue in the coastal water for up to 4 years (Jackson *et al*., 2018).

Although we are well aware of extreme temperature events in the Pacific and Atlantic oceans, in the Indian Ocean, we do not have many studies related to MHWs in the Indian Ocean. In the Indian Ocean, especially the southeast Indian Ocean, coral bleaching due to the MHWs were reported, mostly associated with the El Niño-Southern Oscillation

(ENSO) and Madden-Julian Oscillations (MJO) riding over a global warming signal (Zhang *et al.,* 2017).

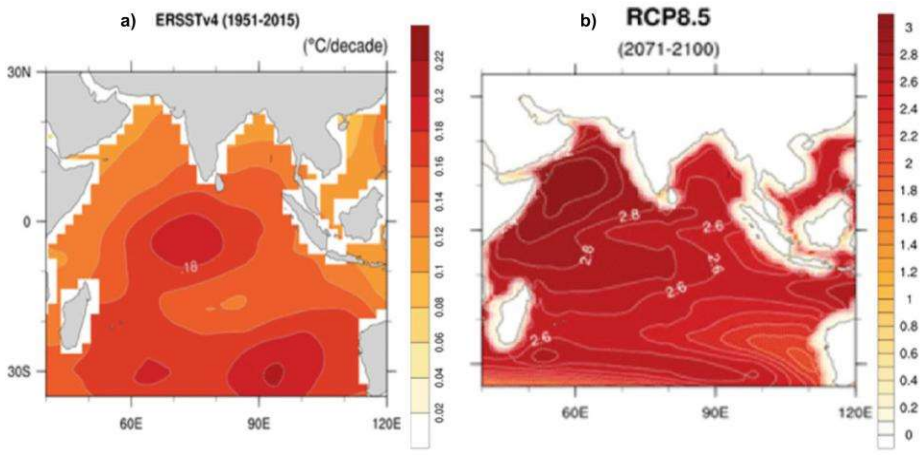

Figure 1.1: a) Observed change in Sea Surface Temperature (SST) using Extended Reconstructed Sea Surface Temperature, version 4 (ERSST v4) during 1951-2015, b) projected change in the SST over Indian Ocean (RCP8.5 for 2070-2099) (Roxy *et al.*, 2020).

The northern Indian Ocean is a crucial region because it supports significant marine primary productivity and its role in modulating the intra-seasonal and inter-annual variability of the Indian summer monsoon. Hence a better understanding of this extreme event in the Indian Ocean is crucial for the food and water security over the Indian subcontinent. Under this circumstance, this study's main objective is to analyze the MHWs in the Indian Ocean and their impacts on the atmospheric conditions (convection, monsoon).

CHAPTER 2
REVIEW OF LITERATURE

MHWs are anomalous warm water events. The Intergovernmental Panel on Climate Change (IPCC) defines the extreme event as an event that occurs when the observed values of weather and climate exceed threshold values (IPCC Special report 2011). Extreme events frequently occur due to change in the climate and weather; they are either due to the accumulation of normal weather phenomena (e.g., flood) or by impacts of large scale phenomena such as El Niño.

Among different types of extreme weather events, temperature extreme is more critical due to human interference with nature, and the resultant increase in global temperature (Stott *et al.,* 2016). There are several extreme events occurs in the ocean apart from temperature extremes, like periods of high upwelling (Feely *et al.,* 2008; Evans *et al.,* 2015*;* Benthuysen *et al.*, 2016*)* and dead zones formation (Diaz and Rosenberg, 2008*;* Stramma *et al.,* 2010). But the extreme temperature events in the oceanic region have a crucial role in biology, food, water security of the society, and even in the atmospheric process. There are several studies related to atmospheric heatwaves other than MHWs. MHWs are in their early childhood stage, and they got the framework recently. In Addition to this, the overall broad range impacts of MHWs are still unknown; it is an emerging research topic in the context of anthropogenic climate change. MHWs are already occurring as a response to anthropogenic climate change and have increased dramatically in frequency and duration since the early 20th century (Oliver *et al.,* 2018). In this study, we focus on the in-depth analysis of one of the extreme temperature events, MHWs in the Indian Ocean, and their impacts on atmospheric convection, in a changing climate.

2.1 Extreme Temperature Events

A positive deviation from standard long-term temperature levels is called the heatwave; a natural disaster can occur both in the atmosphere and in the ocean (Perkins-Kirkpatrick *et al.,* 2016). Later Perkins and Alexander (2012) brought forward the concept of using percentile as a criterion for the definition of the heatwave and proposed that the temperature above the threshold would last for at least three days. The indispensable feature of a heatwave is the heavy stationary anticyclone that lasts for an extended period (Charney and DeVore, 1979). Owing to the wide temperature variability during the summer season, extreme temperatures occur more in the summer compared with the other season. The atmospheric heatwaves are well known and well studied probably because these have a direct impact on human life; likewise, MHWs should have implications for ocean ecosystems, and sooner or later will affect humans too. These extreme temperature events will increase in the future due to the anthropogenic global warming condition (Orlowsky and Seneviratne, 2012). MHWs are new in the sense that only very few studies out there and defining the MHWs got the framework recently (Hobday *et al.*, 2016).

2.2 Marine Heat Waves and their Quantification

Sorte *et al*. (2010) provided a detailed definition in earlier periods, "Marine Heat Waves are temperature extreme in the ocean that persist 3-5°C anomalies for at least three to five days". In general, extremes are calculated based on absolute thresholds rather than a comparative measure, so that this approach often accomplishes the detection of MHW. This helps us compare different MHWs globally and at various times (Marbà *et al.,* 2015).

Hobday *et al*. elucidate, MHWs based on Perkins and Alexander's (2013) research, according to Hobday *et al.* (2016) MHWs are characterized as an anomalously warm water event that can last for at least five constitutive days. MHW lasts for more than five days and has a break of 1 to 2 days in the warming cycle, where it is described as a continuous occurrence. The concept discrete means, it should have a well-defined start and end, prolonged; MHW should last at least five days for a given area, and an abnormally warm implies that the MHW should be above the percentile measured from the baseline temperature. There are collections of MHW matrices that describe duration, mean, average, and cumulative intensities. The duration of the MHW specified as the time between the appropriate start and end dates; the mean and maximum concentrations shall be the mean and maximum temperature anomaly for the entire MHW cycle. Finally, the overall temperature anomaly over the lifespan of the event is expressed as cumulative intensities. From Figure 2.1, we can find out the MHW as per the Hobday definition.

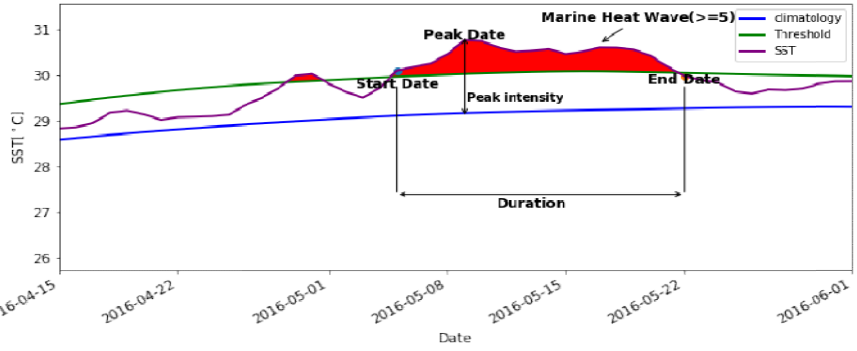

Figure 2.1: Schematic representation of Marine Heat Wave.

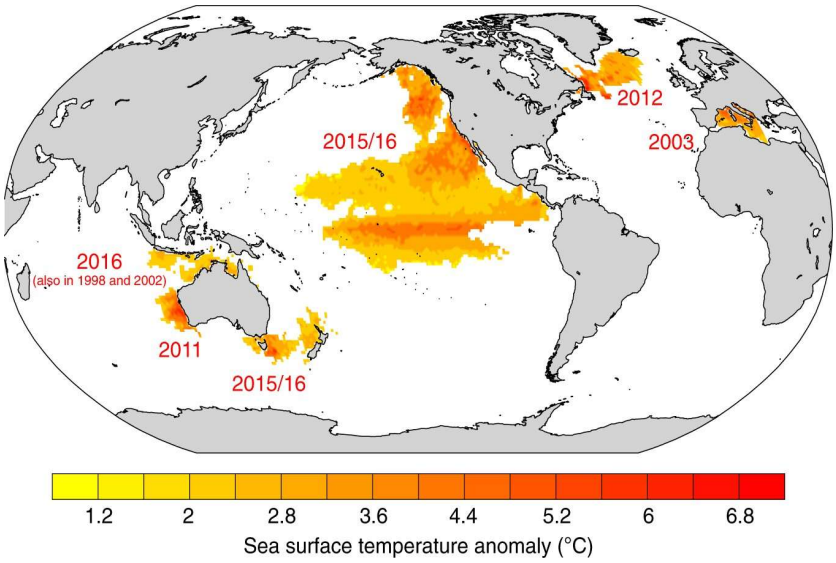

Figure 2.2: Some of the Marine Heat Waves have recorded and evaluated to date. The yellow regions show the SST anomaly above the 99th percentile (threshold) (Thomas L. Frolicher, 2017).

The naming and categorization of extreme events is a long process. The name of an incident is typically used to classify them and for the quantitative analyses of these events across the globe. MHW is specified by the 90th percentile method (Hobday *et al.,* 2016). MHWs are categorized based on the strength of the sea surface temperature anomaly determined from the area's long-term climatology (Hobday *et al.*, 2016). MHW categories are specified by the 90th percentile method, which distinguishes various categories based on multiples. First, calculate the difference between threshold and climatology. Then the multiples of these values are categorized as moderate (1–2×, Category I), strong (2-, Category II), severe (3–4×, Category III) and extreme (> 4×, Category IV).

So far, various MHW events have been recorded. From such (Hughes *et al.,* 2017) significant bleaching of coral reefs resulted in the Great Barrier Reef in 2016, the MHW lasted for 55 days and is 2.15 degrees Celsius above climatology. For 45 percent of the time, it was Category 2. It is known as the Great Barrier Reef 2016 – Category II (Strong) MHW. Western Australia 1999 – Category III (Severe) was an MHW that happened on the western coast of Australia that lasted 132 days. Mostly it was graded as Category 3. In 2012, the Northwest Atlantic Ocean experienced MHW, that event lasted 132 days and was classified under the extreme for 2 percent days. Moderate for 23 percent, with an average strength of 4.30° C. Figure 2.2 gives the latest MHWs reported worldwide.

The naming of MHW is performed in the same manner as the hurricanes, but the researchers say it is not identical to the naming of cyclones. The name of the ocean heatwaves will have a particular location. This would also avail of the oceanic situation during that event (Oliver *et al.,* 2017). The name also should contain the year in which that happened and the category that events belonged for a longer time. Hobday *et al.* (2016) proposed that the naming of MHWs would begin only after hitting Category 2 to prevent too many names for a single occurrence. The proposed naming scheme is as follows: Field & peak year Eg: Tasman Sea 2015 MHW.

Roxy *et al.* (2014) have indicated that the Indian Ocean has been warming steadily over the last five decades. Frolicher *et al.* (2018) proposed a high risk of MHW due to a change in temperature. The occurrences of MHW will be high in the tropical and the Arctic Ocean, less in the Southern Ocean. Also, MHWs are reported in all ocean basins. Due to anthropogenic climate change, the mean temperatures of the world oceans increase, leading to an increase in the intensity and frequency of the MHW events. Owing to human-made warming, the rate of underwater heatwaves is also rising

(Hobday *et al.,* 2016; Frölicher, 2019). Oliver *et al.* (2018) point out that from 1925 to 2016, the frequency and duration of MHW increased by 34% and 17%.

2.2.2 Marine Heat Wave Events and their Potential Impacts

Even though this is an emerging topic, several MHW events have been documented until now. The most important events occurred in 1999, 2011/2012, and 2015/16. Western Australia 1999 – severe MHW occurred and lasted for 132 days along the Australian west coast. It was categorized as severe (2% of days) and was moderate for 86% of its duration for a short period. There are no studies reported on this event's impact, probably due to the lack of sufficient data. The first identified MHW was the Mediterranean Sea 2003 event. This event reported an SST anomaly of 1°C -3°C. The Mediterranean Sea 2006 MHW lasted for 33-days, grouped as strong for 21% of days, and had a maximum intensity of 3.99°C (Kersting *et al.,* 2013*;* Marbà and Duarte, 2010). During 2011 another one having 6.5°C as the maximum intensity anomaly between the event and lasted for two months. It is named Ningaloo Nino and made February the warmest month of the same year (Pearce and Feng, 2013*;* Wernberg *et al.,* 2013). This event was due to the strong La Nina of 2010/11 and the transport of warm water into the high latitudes (Pearce and Feng, 2013). In 2012 MHW events in the Northwest Atlantic had a wide range of impacts on the fisheries sector. This had a duration of 132 days and was severe for 2% of days and strong for 23 % of days (maximum intensity of 4.30°C) (Mills *et al.,* 2013). Based on the records, the longest MHW (17 months) in the globe occurred in northeast Pacific nicknamed as "The Blob" (Northeast Pacific Blob 2015 – Category III (Severe)) with a maximum SST anomaly of 6.2°C, (Bond *et al.*, 2015). According to Emanuele Di Lorenzo. (2016) it was due to the strong El Nin˜o of 2014/15, and NE Pacific had an intense sea level pressure anomaly that stored the heat in this region. Reed *et al.* (2016) reported that the MHW

event occurred in Off Santa Barbara, California; during summer 2015 not had a catastrophic impact on ocean biology even though this event had a maximum intensity of 5.10°C. The lack of a strong impact may be due to the thermal tolerance of species in that region. Oliver *et al.* (2017) reported the Tasman Sea MHW 2015/16, SST anomaly of 2.9°C, and found there for 251 days. Further, Schlegel *et al*. (2017) said that this MHW was due to the presence of small scale eddies and wind path changes. Great Barrier Reef 2016 – MHW, had a profound impact on the coral bleaching with 2.15°C of maximum intensity and retained for 55 days (Hughes *et al.,* 2017). The studies in the Indian Ocean region are very less compared with other oceans.

The extreme temperature rise that persists for a long time in a location leads to numerous impacts on different ecological, socioeconomic, and atmospheric conditions. Because this is an emerging research topic, most of the effects are not well known. Again, these impacts have a wide range of variations among different species. MHW that occurred in summer days has some impact. When this kind of MHW occurs in colder days, the consequences are even worse.

The first and most visible impact of MHW is coral bleaching. Several studies reported the widespread bleaching of coral reefs. Coral reefs are essential organisms in the marine ecosystem; they provide several services starting from home for many fish species and other aquatic organisms to the aesthetic purpose of human communities. They are generally found between the tropics of Cancer and Capricorn. Coral bleaching is the process of death of algae, the zooxanthellae. They are responsible for the pigmentation of corals. Bleaching usually happens when these corals are exposed to warm water. The temperature of the water is higher than the reasonable condition and persistent warm water in that region for a long time (Muller-Parker *et al.,* 2015). Bleaching occurs only when the temperature rise in an area will last for 4 to 8 weeks; otherwise,

the average summer temperature rise will not cause any bleaching event even though corals are temperature sensitive organisms. Studies show that coral bleaching will continue in the future due to an increase in SST based on general circulation models (Hoegh-Guldberg, 1999).

Moreover, there is a sizeable latitudinal shift of species and adaptation of temperate reefs (Feary *et al.,* 2014*;* Wernberg *et al.,* 2016). As we go through several literature, we can identify coral bleaching as a result of MHWs. So far, 1998, 2010, and 2015/2016 were the three significant massive coral bleaching that occurred globally. In 1998 enormous bleaching episodes were more localized in the offshore atoll and continental shelves of Western Australian, although we do not have data during that period. The 2015 event is triggered by an extreme El Niño event and caused 3rd recorded coral bleaching in history. As per the study of Pearce *et al*. (2011) Western Australian heatwave 2010/2011 bring a massive coral bleaching in middle of January 2011, start from Ningaloo Reef and the MBI and southwardly spread into the Shark Bay, the Houtman Abrolhos Islands (HAI), Jurien Bay and lastly in waters surrounding Rottnest Island in March 2011. The stress on the coral reef may cause widespread diseases to corals and affect predation (Brandt and McManus, 2009). In addition to heat stress, the corals are also uncovered to the microbial establishment, which altogether leads to the decomposition of their shells (Leggat *et al.,* 2019).

When we talk about the MHW impact on marine organisms, it is not only confined to coral reef bleaching. There are a large number of organisms residing in the ocean. Sea grass is another remarkable fauna in the marine ecosystem because they are the source of significant carbon stock globally. Arias-Ortiz *et al.* (2018) studies show that MHW events in 2010/2011 caused the damages to above and below ground sea grass species in shark bay, where 0.7 to 2.4% of glob's sea grass occupy there. This loss was attributed to the occurrence of strong La Niña conditions and caused an

ample supply of warm water to the Western Australian coast. This disappearance of sea grass species resulted in the CO2 release. It was reported that MHW also impacted the distribution of local species of kelps, like endemic D. poha. Because of the warming trend of SST in the future, these species will experience high mortality (Thomsen *et al*., 2019). The 2014-2016 warming in the California Current System disrupted the kelp species residing there. In addition to that, it also caused the change in the species distribution in that kelp beds and invasion of new species into the ecosystem (Arafeh-Dalmau *et al*., 2019).

In the case of fish species, there are several studies reported about the poleward shift. The 2012 Northwest Atlantic MHW causes a sudden change in species distribution and fisheries. The species that respond to warming are commercially valuable like silver hake, red hake, yellowtail flounder, winter flounder, etc. (Pinsky and Fogarty, 2012). Mills *et al.* (2013) reported the effect of the 2012 Northwest Atlantic MHW on lobster fisheries. According to several studies, MHW affects the lifespan, physical and biological growth, and development of economically important species (Edwards and Richardson, 2004*;* Simpson *et al.,* 2011*;* Cheung *et al.,* 2013). Warming can directly affect the lobsters, they die off during the 1999 event, and they are affected by shell disease. Moreover, lobsters are under threat in the warming environment due to the presence of predators (Hovel and Wahle, 2010).

The 2015/2016 event in Tasmanian has widespread impacts on marine biology, such as oyster disease outbreak. Johnson *et al.* (2011) have found that there is replacing sea urchins in the kelps forest along Tasmanian. The 2011 Western Australian MHW had an impact on the blue swimmer crab (Portunus armatus) fishery and recovered once the cold temperature established (Chandra Pavan *et al.*, 2019). The fish species yellowfin whiting, which is an economically important one, showed a poleward shift

soon after the 2011 Ningaloo Niño MHW (Smith *et al.*, 2019). MHW causes widespread loss of sea cucumber in farms of northeast China. Some studies reported the impact of MHWs on the food web and show that extreme events have a general effect not confined in the marine ecosystem. During the NE Pacific MHW of 2013–2015, reported die-off of Cassin's Auklets (Ptychoramphus aleuticus), because they faced an indirect effect of MHW. These birds are primarily feeding on the zooplankton. Still, due to warm water inflow and persistence in the NE Pacific, they lost the biologically productive, oxygen-rich cold water, which ultimately led to the shift of the zooplankton population. Cassin's Auklets are already under the vulnerable category because of global warming, but due MHW events cause a massive decline in the community of this bird species. In the western South Atlantic during the 2013/2014 MHW, steers the dwindling of chlorophyll-a concentration (Rodrigues *et al*., 2019). These anomalous warm water events can affect the smooth functioning of the pelagic communities and destroy the marine ecosystem. It is reported that in the California Current ecosystem experienced replacing of the pelagic crustacean community by the gelatinous (Brodeur *et al.*, 2019). The Mediterranean Sea 2003 MHW gave rise to the sober demolition Gorgonian fan community (Garrabou *et al.,* 2009).

However, studies reported that warm water regions recognized new fish species. In the case of 2014–2018, anomalous warm water in off southern California identified the presence of 36 new fish species (Walker *et al.*, 2020).

There are studies related to how the MHWs probably evolve in the future. Oliver *et al.* (2019) warned that by the end of the 21st century, most of the Ocean would experience a perpetual condition of MHW events due to global warming. When discussing the prediction and forecast of MHWs, it is essential to make these events catastrophic for the world’s fisheries,

aquaculture, and the food chain. The Integrated Marine Observing System (IMOS) is an efficient tool for the forecast and study of MHWs. IMOS consists of data collection from the ground through in situ observation and satellite-based measurements, and models. Recently IMOS gliders provide reliable subsurface data. These collective systems efficiently fill the gaps due to the lack of real-time, functional quality datasets, and can be watched the MHWs and other Ocean extremes more precisely (Cahill *et al.*, 2020).

There are numerous studies on the topic of the potential impacts of MHW on marine organisms. However, some other implications are still unknown to the scientific communities. Again, with other oceanic basins, the studies are very less in the Indian Ocean.

2.3 Scope of the study

MHWs are less understood compared to other extreme events. There are only very few studies for the Indian Ocean, compared to other ocean basins. MHWs do not have any immediate effect but may affect humanity in many ways. MHWs have an impact on marine organisms and their ecosystems, ultimately affecting the fisheries sector severely. The northern Indian Ocean is a critical region because it supports significant marine primary productivity, and because of its role in modulating the intra-seasonal and inter-annual variability of the Indian summer monsoon.

Moreover, Roxy *et al.* (2014) have shown that the Indian Ocean has been warming over the past five decades at a rapid rate. Hence a better understanding of this extreme event in the Indian Ocean is essential for the food and water security over the Indian subcontinent. The MHW events in the Indian Ocean are not well studied; here, we are trying to find MHW events in the Indian Ocean and their probable connection with the monsoon.

CHAPTER 3
MATERIALS AND METHOD

3.1 Datasets used

For the identification of MHWs, we used the Optimum Interpolated Sea Surface Temperature (OISST) dataset at a resolution of 0.25° x 0.25° (Reynolds *et al.,* 2007). This is supplemented with the Hadley Center Sea Ice and SST (HadISST) datasets at 1° x 1° resolution from NCAR Climate Data Guide.

For studying MHW impacts on atmospheric conditions, we used the interpolated Outgoing Longwave Radiation (OLR) datasets measured from Advanced Very High-Resolution Radiometer (AVHRR) onboard NOAA polar-orbiting spacecraft (Gruber and Krueger, 1984). This data is obtained from the Climate Diagnostics Center (CDC) at a resolution of 2.5° x 2.5°. The daily wind data at 850 hPa is obtained from NCEP/NCAR reanalysis data with a resolution of 2.5° x 2.5°. Daily vertical velocity at 500 hPa data is obtained from National Center for Environmental Prediction-National Centers for Atmospheric Research (NCEP/NCAR) reanalysis dataset at a resolution of 2.5° x 2.5°. For the analysis of the rainfall variability over the Indian subcontinent, we used IMD daily rainfall at a resolution of 0.25° x 0. 25°. The daily latent heat flux, sensible heat flux, upward long wave radiation, downward solar radiation, surface net long wave radiation and surface net solar radiation are from two reanalysis products, namely National Center for Environmental Prediction-National Centers for Atmospheric Research (NCEP/NCAR) reanalysis-1 (NCEP1; Kalnay *et al*., 1996), and the European Centre for Medium-Range Weather Forecasts (ECMWF) ERA5 (Hersbach and Dee, 2016).

Ocean currents data is obtained from the Hybrid Coordinate Ocean Model (HYCOM) reanalysis (Metzger *et al.*, 2014) at a resolution of 1/12° for 1994–2015. The monthly potential temperature and salinity are obtained ORAS4 with a resolution of 1°× 1° (Balmaseda *et al.,* 2013). Apart from this, daily water temperature and salinity are obtained from HYCOM reanalysis. We also used Ocean Surface Current Analysis Real-time (OSCAR) Ocean currents on a 1/3° grid with a five-day resolution (Dohan and Maximenko, 2010) and National Centers for Environmental Prediction Global Ocean Data Assimilation System (GODAS) 0.33°×1° grid with a five day resolution (Behringer, 2007).

To explore the relationship between MHW and Indian monsoon intra-seasonal oscillation (MISO), MJO we used the RMM index (Wheeler and Hendon, 2004) and MISO index (Suhas *et al.*, 2013) for the period 1982-2018.

3.2 Detection of Marine Heatwaves

The MHWs are identified by the 90th percentile of SST, employing the definition by Hobday *et al.* (2016). Earlier studies also used the same methodology for identifying MHWs (Hobday *et al.*, 2016; Oliver *et al.*, 2014, 2017). MHWs are calculated from the OISST daily datasets, the SST must be above the 90th percentile (threshold) and should persist for at least five days. Hobday *et al.* (2016) had defined specific matrices to study and analyze MHWs, like maximum intensity, mean intensity, cumulative intensity, duration, and spatial extent, etc., that are summarized in Table: 2.1.

To study the spatial extent of the MHWs, we counted the grids where the MHW events occurred and multiplying it by the grid area.

To discover the trend in MHWs, we used the OISST data from 1982 to 2018 and applied the heatwave detection function in each grid then fit a linear trend model. Since we are looking into the impact of MHWs on the convection during the summer monsoon, we restricted the trend analysis to these events from June to September.

Further, we did a composite analysis of wind, SST, latent heat flux, sensible heat flux, upward longwave radiation, downward solar radiation, rainfall, vertically integrated moisture flux, and specific humidity during seven days before and after the starting date of MHW days, This provides us with a comprehensive picture of the lifecycle of MHWs, and also helps us in answering what the actual driver of MHW in a particular region is.

To study the MHW and monsoon interaction, we plotted the mean picture of SST, wind (at 850 hPa), OLR, and omega (at 500 hPa), and rainfall over India during MHW days (June to September).

Table 3.1: Marine Heat waves characteristics (Hobday *et al*., 2016)

MHW statistics	Description	Unit
Climatology	It is the mean value of temperature, calculated over a period.	Degree Celsius [°C]
Threshold	Threshold means the 90th percentile of Sea Surface Temperature data	Degree Celsius [°C]
Starting and ending date	Start date: is the date where Sea Surface Temperature is above the threshold values End date: where the threshold is greater than SST	
Duration	It is the days between the start and end date. It should be >= 5 days with no more than 2 gaps.	Days
Mean and Maximum intensity	Mean intensity: it is the average temperature anomaly along with the duration of MHW Maximum intensity: it is the maximum temperature anomaly during the MHW days.	Degree Celsius [°C]
Rate of onset and decline	Rate of onset: it is the rate of temperature rise from the start of MHW to the maximum intensity. Rate of decline: rate of temperature change from the maximum intensity to end of the MHW	Degree Celsius per day [°C/day]

Cumulative intensity	It is the sum of daily anomalies for the entire duration of MHW	Degree Celsius day [°C day]
Area	It is the area of ocean where MHWs have occurred	km^2

3.3 Mixed Layer Heat Budget

To study the local factors influencing the genesis of MHWs, we calculate the mixed layer heat budget using the temperature tendency equation. The temperature tendency equation gives us a comprehensive picture of factors that lead to the change in the ocean surface temperature. According to Rodrigues *et al*. (2019), the temperature tendency equation is given by

$$\partial T_m/\partial t = -v.\nabla T + Q_0/\rho C_p H_m + Res$$

Where, ρ is the density of seawater (1,026 kg m^{-3}) and C_p is the specific heat of seawater (3902 J kg^{-1} K^{-1}). While T_m is the mixed layer temperature, here we used the SST as mixed layer temperature, because earlier studies also agreed with this (Lee *et al*., 2004). '$\partial T_m/\partial t$' represents the rate of change of mixed layer temperature. The term '-v.∇T' indicates the advection and 'v' indicate the horizontal velocity vector (v at 15m depth using OSCAR Ocean currents and considered as vertically averaged over the mixed layer). H_m means the mixed layer depth (MLD) in meters. Using the monthly potential temperature and salinity data of ORAS4 and by applying a criterion that the density (0.07 kg m^{-3}) increases from a depth of 5m, we calculated the monthly MLD. Later the monthly MLD is

interpolated in to daily to estimate the heat flux terms (Rodrigues *et al*., 2019).

$$Q_0 = Q_s + Q_b + Q_e + Q_h$$

Q_0 is the net surface heat flux (w/m^2), which includes latent heat flux (Q_e) and sensible heat flux (Q_h) released from the ocean mixed layer, and the net solar radiation received (Q_s), net long wave radiation released (Q_b). Finally, the 'Res' include the remaining unresolved process such as vertical diffusion, entrainment.

The heat budget analysis is also verified with HYCOM and GODAS datasets.

All the heat budget terms are calculated from 1994-2015 for the two study regions and averaged over that region. Anomalies are also calculated from the 1994-2015 daily climatology. Then we estimate the heat budget terms for the 5 days before the start date of MHWs in the selected regions.

CHAPTER 4
RESULT AND DISCUSSION

4.1. Marine Heat Waves in the Indian Ocean and their Trend Analysis

MHWs are the extreme temperature events in the ocean that result in numerous detrimental impacts on the marine ecosystem. The effects of MHWs, especially on the atmospheric circulation, are mostly unknown. Here we investigate the magnitude and extent of MHWs in the Indian Ocean, how their activity is changing over time, and its impact on the Indian monsoon.

To examine the changes in MHWs over time, we calculated the trend, based on the peak date of MHW events (where the SST anomaly is maximum during a particular MHW event). The trend is calculated for the period 1982-2018, as shown in fig: 4.1(a). Applied the heatwave detection function in each grid then fit a linear trend model then find out the slope and significance. From the trend analysis, it is clear that the western Indian Ocean shows a positive trend especially in the Somali region (41°E –56°E–8°S–8°N). The Somali region has an increasing trend of 12 events in 100 years and 1 event in 10 years. The northern Arabian Sea is also showing a similar increasing trend. While in the eastern Indian Ocean and central equatorial Indian Ocean, the trend is 4 to 8 events in 100 years at each grid.

Since we are focusing on the impacts of these events on the convection and monsoon, we examined the MHWs during the summer monsoon season (June–September). The Indian summer monsoon plays a key role in every sector of human life in the Indian subcontinent, regulating the socio-economic balance over the region. The trend of MHWs for the period of 1982-2018 is shown in the figure: 4.1(b).

We could see that there are two regions where MHWs activities are high, one is in the Somali region similar to the annual trend and the second one is in the northern Bay of Bengal (85°E– 93°E–15°N–23°N). From figure 4.1(b) we can see that both the Somali region and north Bay of Bengal have a high number of MHW with a count of more than 5 events in 100 years at each grid point. The northeastern Arabian Sea also shows a similar increasing trend.

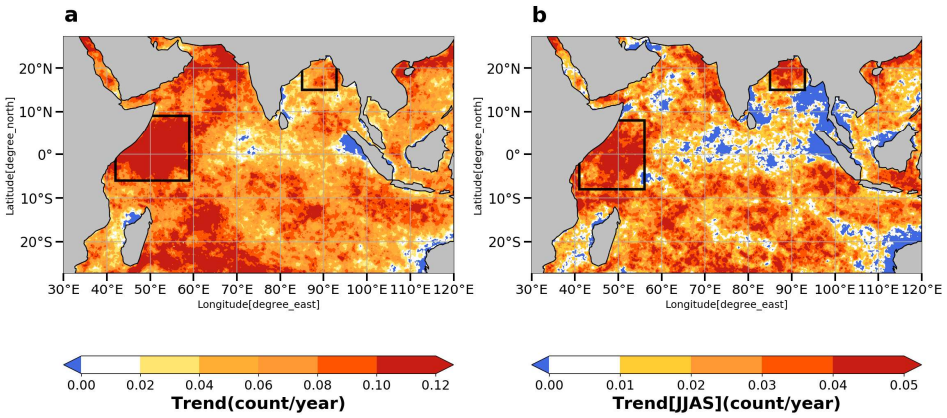

Figure 4.1: Trend map of MHW frequency a) annual (count/year), b) during JJAS (count/year) from 1982-2018 in the Indian Ocean using NOAA OISST dataset.

4.1.1 Somali Region (41°E–56°E–8°S–8°N)

From the trend analysis, it is clear that both during annual and JJAS time, this region has a large number of MHW activities. Thus the anomalous warming in this region might have a link with summer Monsoon over Indian landmass, and also Somali region is an important place because of the upwelling process. In the tropical ocean, the El Niño Southern Oscillation (ENSO) and Indian Ocean Dipole (IOD) are the causes of warm SST (Holbrook NJ, *et al.*, 2019). The 1997/98 warming event occurred in the Indian Ocean (Seychelles region) is because of the weakened trade wind which prevents the ocean-atmosphere interaction by blocking the heat transport from ocean to atmosphere (Saji NH, *et al.,*1999). Moreover, in the equatorial ocean relaxation of wind drives the reduced evaporation cooling, and the Kelvin and Rossby planetary waves further make significant warming (Spencer T, *et al.,* 2000).

Figure 4.2 indicates that the time series of MHW frequency during annual (a) and JJAS period (b). It can be derived from the figure that annually the number of MHWs in the Somali region has increased by a total of 5 events over the 36 years (from 1982-2018), while for JJAS it is 1.33 events.

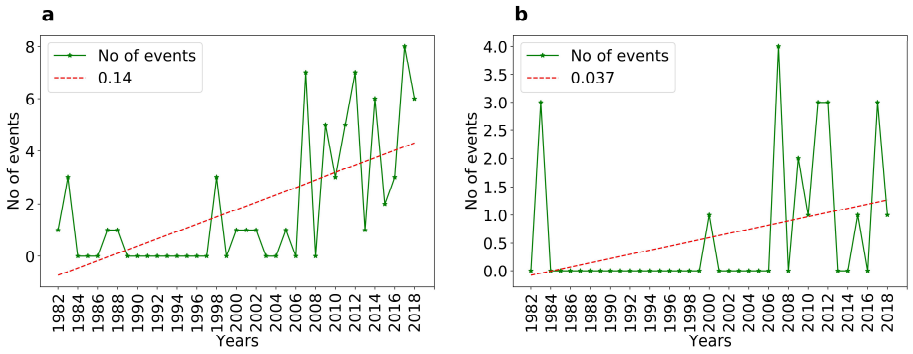

Figure 4.2: Time series of the number of MHW events a) annual and b) during JJAS, from 1982-2018 in the Somali (41°E–56°E–8°S–8°N) region.

Figure 4.2 also conveys an interesting fact that the MHW events are increasing after 1997 in the Somali region. On an annual basis, the MHWs numbers are increasing with a slope value of 0.14. On the other hand during JJAS it is 0.037, also have an increasing trend.

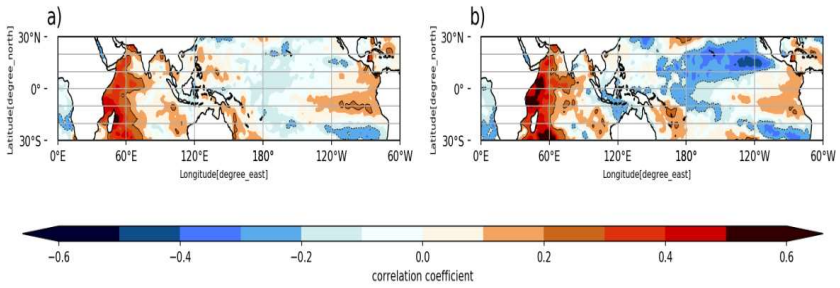

Figure 4.3: Correlation map of global SST (using HAdISST dataset) anomalies and the number of MHW events in the Somali (41°E–56°E–8°S–8°N), in each grid points a) annual, b) during JJAS, for the period 1982-2018.

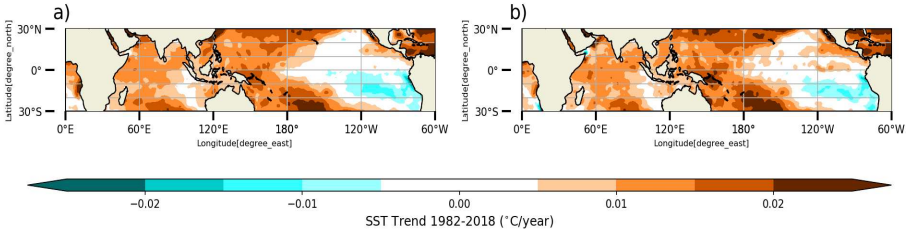

Figure 4.4: The global SST trend map (using HAdISST dataset) a) annual, b) during JJAS for the period 1982-2018.

We carry out a correlation between the global SST and the number of MHW events in the Somali region for both annually and during the JJAS period (figure 4.3). We could see that there is a signal of El Niño s and positive IOD, that is El Niño s and positive IOD are the major drivers of MHWs in the Somali. This correlation pattern is obtained when we removed the trend of the SST and the signal, but this picture is different when we do not remove the trend. Later we carry out a pattern correlation between the correlation map (figure 4.3) and the SST trend map (figure 4.4) for the tropics. It is interesting that when we do the pattern correlation between SST trend map and correlation map (without removing the trend), we obtain high correlation values, that is for Somali annual r=0.9 and during the June-September, r= 0.5. But the pattern correlation values become less when we do the same analysis by removing the trend of the time series. This may be due to the warming trend in the SST, which drives the MHW events generally when we remove the trend, and then we obtain fewer correlation values. Moreover, after removing the trend in the time series we got the El Niño and positive IOD pattern, which is apart from the global warming El Niño s are the primary driver of the MHWs in the Somali. In a nutshell, the Somali region's MHWs are driven by El Niño s, positive IOD, and the warming trend of SST.

Along with ENSO and IOD, Madden-Julian Oscillation (MJO) also plays an important role in the genesis of MHWs, and the 2017 Southwestern Atlantic shelf MHW had a connection with MJO (Manta *et al.,* 2018). According to Maloney and Kiehl (2009), MJO and monsoon variability can cause warming in the tropical oceans, by affecting the interaction between atmosphere and Ocean.

When we plot the probability distribution of MJO 8 phases during the MHW days as shown in the figure, we can see that (figure: 4.5) annually 1, 2 phase of MJO is associated with the MHWs in the Somali region, that means during the 1, 2 phases MJO stays in the Indian Ocean and moving eastward direction, which might have some relationship with the MHWs in the Somali region.

Now, it is clear that Somali is an important MHW prone area in the Indian Ocean. This region experienced a total number of 66 events from 1982 to 2018, out of 66 events 21 events that occurred during the summer monsoon season.

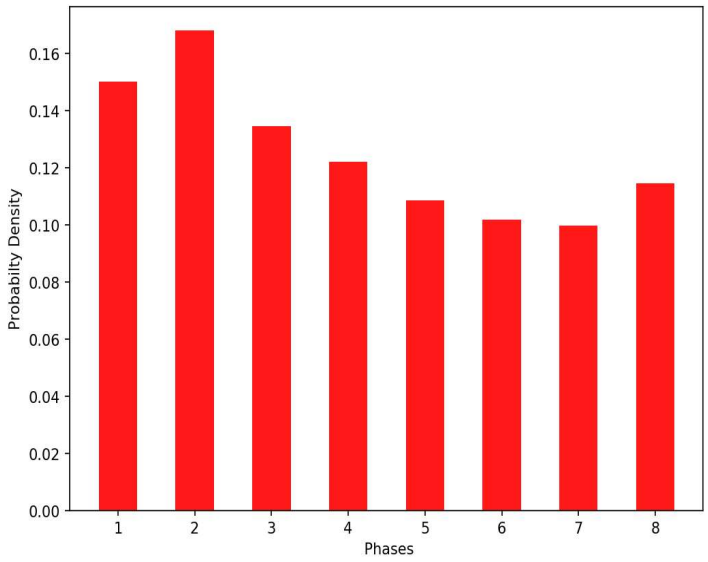

Figure 4.5: The probability distribution of the MJO (RMM) phases during the MHW days (annually) in the Somali (41°E–56°E–8°S–8°N) region from 1982-2018.

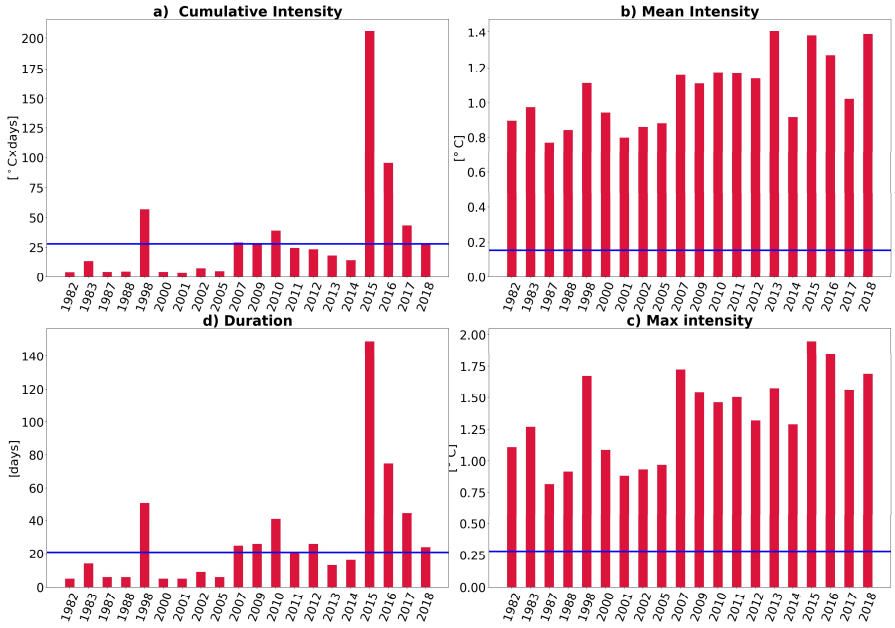

Figure 4.6: MHW metrics (calculated annually) for the Somali region (41°E–56°E–8°S–8°N), the blue line represents the standard deviation. a) Cumulative intensity (°C days), b) Mean intensity (°C), c) Maximum intensity (°C), d) Duration (days), for the period 1982-2018.

From fig 4.6 represents the MHW metrics calculated annually, we can see that in the case of duration and cumulative intensity, certain events are above the standard deviation line. As in the case of maximum and mean intensity for all events, it is above the standard deviation line. It can be worth to note that the largest event in the Somali region lasted for 149 days and had a cumulative intensity of 206°C days.

Table 4.7 represents the largest five events (based on the duration of MHW events) in the Somali region from 1982 to 2018. The Somali region experienced anomalous warming extending 149 days during 2015. Among the metrics of MHW cumulative intensity is something very important because it is usually used for the identification of the largest MHW.

Cumulative intensity means the integral of temperature anomaly for the duration of an MHW event, and it is similar to the Degree of Heating Days used for the coral bleaching studies (Fordyce *et al.,* 2019).

Table 4.7: Largest five (duration wise) events in the Somali (41°E–56°E–8°S–8°N) region.

Start Date	End Date	Peak Date	No of Days (days)	Mean intensity (°C)	Maximum intensity (°C)	Cumulative intensity (°C day)
2015-08-01	2015-12-27	2015-09-13	149	1.38	1.95	205.72
2016-02-26	2016-05-10	2016-03-18	75	1.27	1.85	95.34
1998-02-13	1998-04-04	1998-02-20	51	1.11	1.57	56.77
1997-12-26	1998-02-09	1998-02-02	46	1.11	1.67	51.04
2017-04-19	2017-06-02	2017-05-30	45	0.97	1.56	43.68

The largest event in the Somali region had a duration of 149 days with a cumulative intensity of 206 °C days, which is the largest event in the Somali, lasted almost four months. This is important because it probably had an impact on the marine environment. Several kinds of literature are

discussing the ecological impact of the largest MHWs in the other Ocean basins. However, other Ocean basins also reported the largest events like a blob in the northeast pacific lasted for 17 months (Bond *et al.,* 2015).

Until now, we are aware of the MHW events in this region, and we did not have any information about the seasonal climatology of these metrics. That is how their behavior is varying with different months. To get the seasonal climatology of MHW metrics, we selected each of these metrics based on the peak date and also plotted the standard deviation as an error bar. In addition to the four MHW statistics, we added two more metrics, which are the area of MHW events and the number of events. From figure 4.8; we could see that the cumulative intensity and duration have almost the same pattern even though the values are different. In the Somali region, all the MHW metrics except the number of events shows a double peak in the seasonal climatology signal. They all are peak during March and September months. As in the case of the number of events, it shows an increasing trend, and the maximum number shows during October month (8 events). Overall, during the JJAS period, all of this shows a significant pattern, that is why we obtained a trend during the JJAS period. So this is important to study how the MHWs activities during JJAS and how this will relate to southwest monsoon rainfall over the Indian subcontinent.

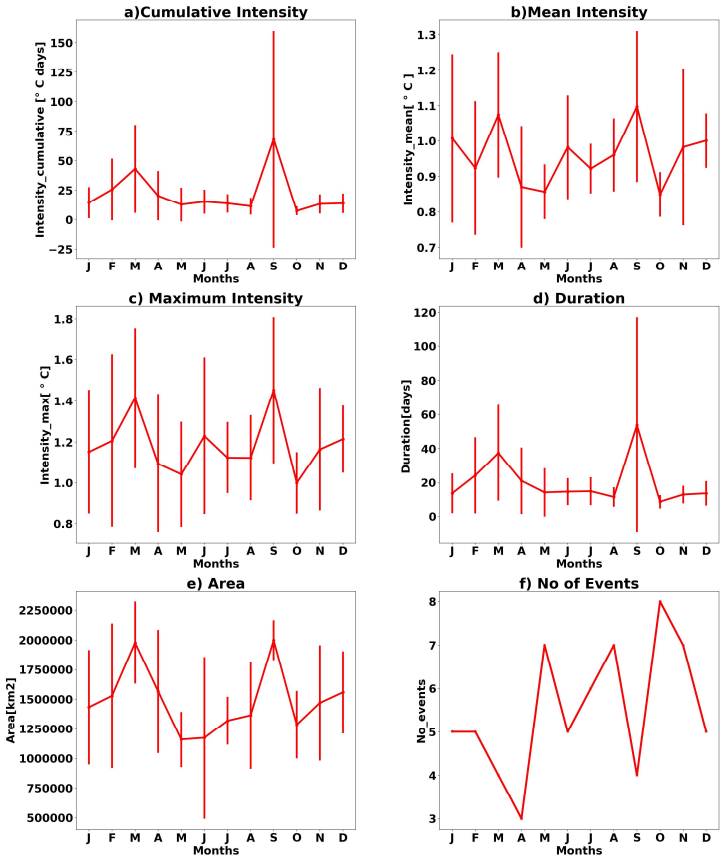

Figure 4.8: Climatology of MHW metrics for the Somali (41°E–56°E–8°S–8°N) region, error bar represents the standard deviation. a) Cumulative intensity (°C days), b) Mean intensity (°C), c) Duration (days) , d) Maximum intensity(°C) , e) area (km^2), f) Number of events, for the period 1982-2018.

Figure 4.9 represents the mean area of MHW events in the Somali region. The 2015 event has the largest area (2.25 million km^2), both for the annual and also for JJAS. Now we have to concentrate on each of these events, so for that plotted three largest and three smallest events in the region during the JJAS period. Figure 4.10 illustrates the SSTA and wind during the peak date of the largest 3 MHW events (based on area) in the Somali region. From fig 4.10 we can see that during the largest events the southwest monsoon winds are weak.

On the other hand, the smallest event does not show the relaxation of south-westerlies (fig 4.11). Therefore we can assume that there must be a connection between MHW events and monsoon circulation.

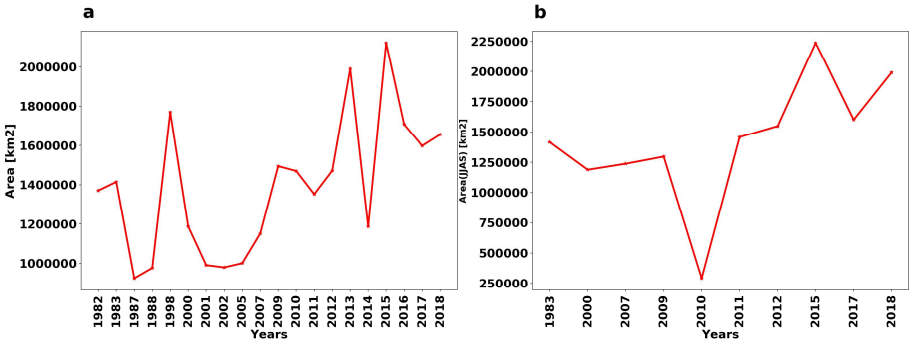

Figure 4.9: Mean area of MHW events during the peak date in the Somali (41°E–56°E–8°S–8°N) region, a) annual, b) JJAS for the period 1982-2018.

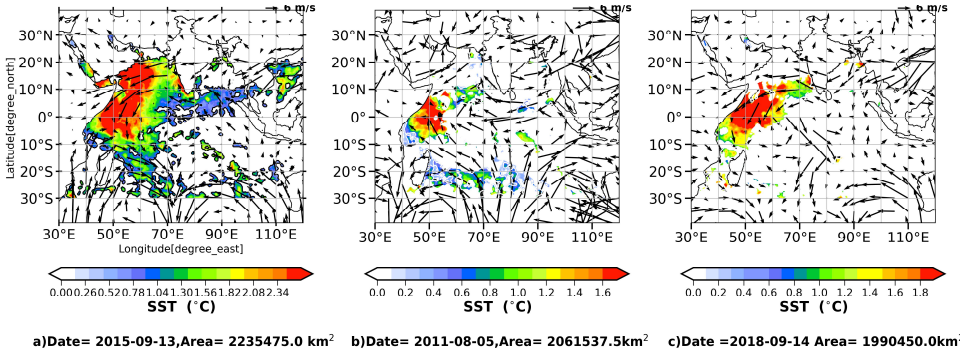

a)Date= 2015-09-13,Area= 2235475.0 km^2 b)Date= 2011-08-05,Area= 2061537.5km^2 c)Date =2018-09-14 Area= 1990450.0km^2

Figure 4.10: Spatial plot of SSTA and wind at 850 hPa during the peak date of largest 3 MHW events (area wise) in the Somali (41°E–56°E–8°S–8°N) region.

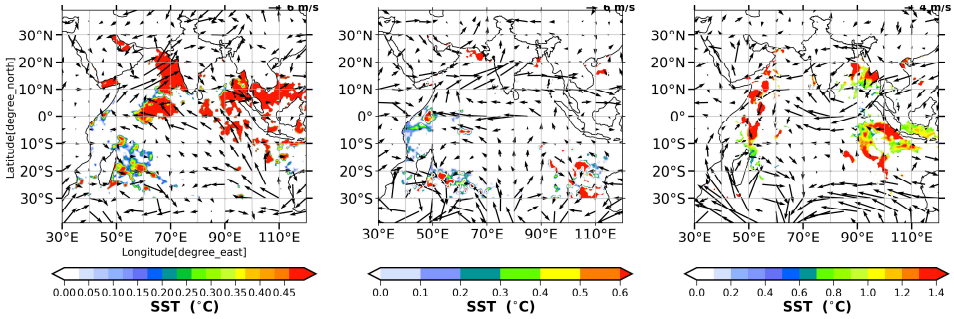

a)Date= 2010-06-05,Area= 291912.50 km^2 b)Date= 2011-06-11,Area= 728268.75 km^2 c) Date =2009-08-25,Area= 757006.25 km^2

Figure 4.11: Spatial the plot of SSTA and wind at 850 hPa during the peak date of smallest 3 MHW events (area wise) in the Somali (41°E –56°E–8°S–8°N) region.

4.1.2 North Bay of Bengal (85°E–93°E–15°N–23°N)

The north Bay of Bengal region is another important MHW prone area in the Indian Ocean, even though it is not visible in the annual trend MHW. But this region gains importance because this shows a trend during the summer monsoon season. This region experienced a total of 94 events from 1982 to 2018 and out of 94 events, 34 events have occurred during the June-September period.

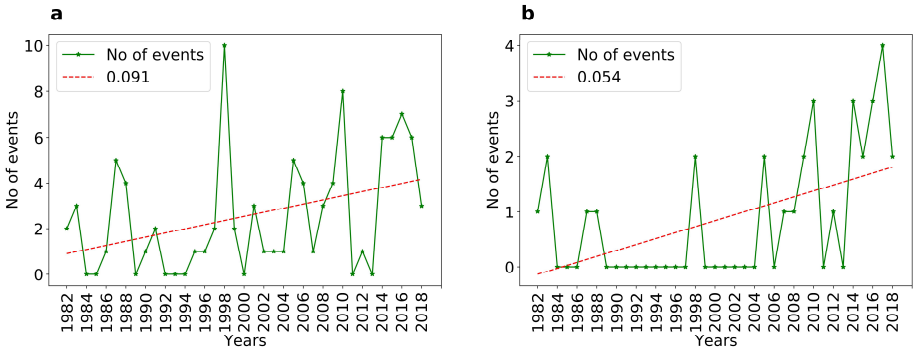

Figure 4.12: Time series of the number of MHW events a) annual and b) during JJAS, from 1982-2018 in the north Bay of Bengal (85°E–93°E–15°N–23°N) region.

Holbrook *et al*. (2019) had suggested that the warming and coral bleaching events recorded in the Bay of Bengal (Andaman Sea) happened before or after extreme El Niño events in the Pacific and also led by the warming of the Indian Ocean Basin and the negative Indian Ocean Dipole. There are kinds of literature documenting the devastating coral bleaching in the Bay of Bengal, the Andaman Sea in 1998, 2002, 2005, and 2010, among them the most extreme coral bleaching occurred in April – May 2010 (Krishnan *et al.,* 2011).

Figure 4.12 shows the time series of the number of MHW events during the summer monsoon period, similar to the Somali region; this region also experienced more number of MHWs after 1997. In the North Bay of Bengal during 1982-2018 periods the MHW events are increased by 3 events annually, while during JJAS it is 1.94 events. From the slope values, it is clear that during the summer monsoon period the Bay of Bengal region experienced more heat waves than the Somali region. On the other hand, on an annual basis, Somali has the most number of MHWs.

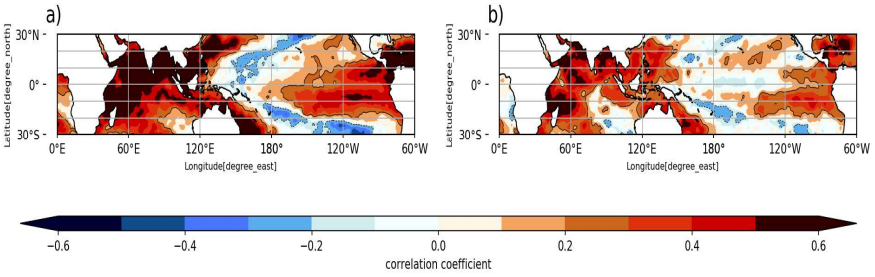

Figure 4.13: Correlation of the number of MHW events in the north Bay of Bengal (85°E–93°E–15°N–23°N) and global SST (using HAdISST dataset) anomalies, a) annual, b) during JJAS, for the period 1982-2018.

Earlier for the Somali region, we had done a correlation between the global SST and the number of MHW events, similarly, when we did it for the Bay of Bengal region (figure 4.13). We obtained the signal of El Niño that is El Niño is the primary driver of MHWs in the north Bay of Bengal too. This correlation pattern is obtained when we removed the trend of the SST and the signal, but this picture is different when we do not remove the trend. After that, we carry out a pattern correlation between the correlation map (figure 4.13) and the SST trend map (Figure 4.4) for the tropics.

It is interesting that when we do the pattern correlation between SST trend map and correlation map (without removing the trend), obtained high correlation values, that is for Bay of Bengal annual r=0.3 and during the June-September r=0.5. However, when we do the same analysis by removing the trend of time series, the values become less. This may be due to the warming trend in the SST, which drives the MHW events generally when we remove the trend, and then we obtain fewer correlation values. Moreover, after removing the trend in the time series we got the El Niño pattern, which is apart from the global warming El Niño s are the primary driver of the MHWs in the Bay of Bengal region. From figure 4.13, we can see that the Indian Ocean basin warming also contributes to MHW events in the north Bay of Bengal region.

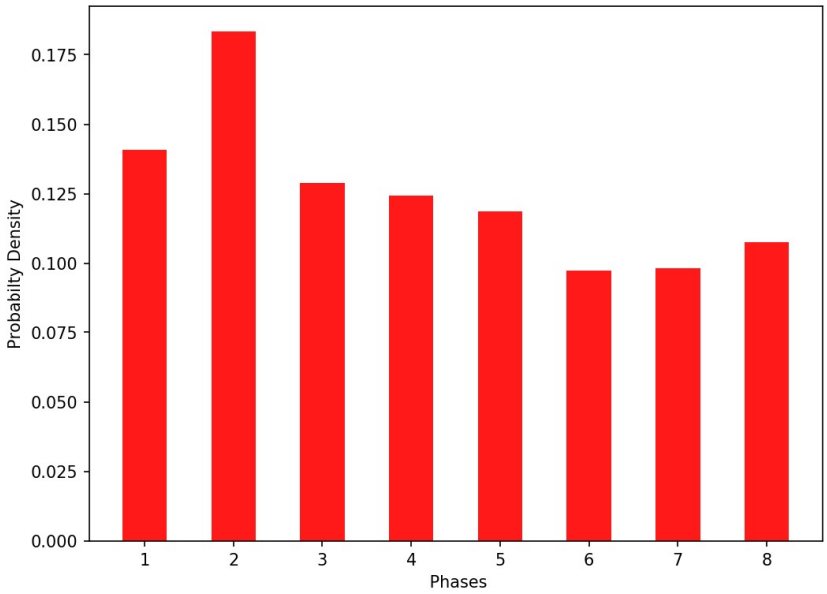

Figure 4.14: The probability distribution of the MJO (RMM) phases during the MHW days (annual) in the north Bay of Bengal (85°E–93°E–15°N–23°N) region from 1982-2018.

Similar to the Somali region MHWs days, in the north Bay of Bengal are also related to the MJO 1 and 2 phases (figure: 4.14).

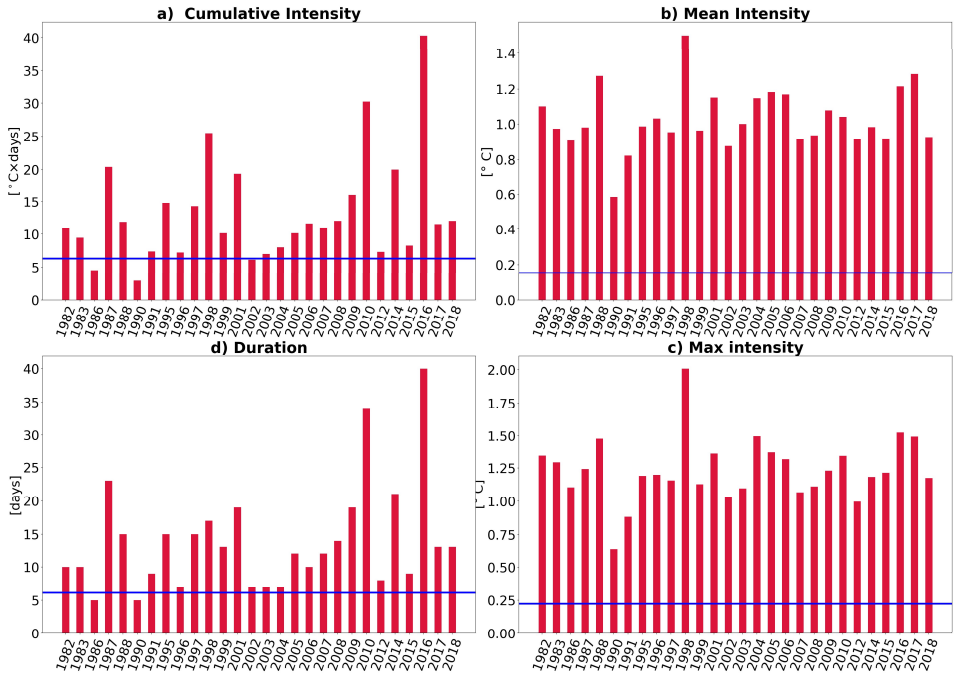

Figure 4.15: MHW metrics (calculated annually) for the north Bay of Bengal (85°E–93°E–15°N–23°N) region, the blue line represents the standard deviation. a) Cumulative intensity (°C days), b) mean intensity (°C), c) maximum intensity (°C), d) duration (days) for the period 1982-2018.

Figure 4.15 illustrates the MHW metrics calculated annually and the blue line represents the standard deviation line. It is interesting to note that there are more MHW events in the north Bay of Bengal region compared to the Somali. Also the number of events above the standard deviation line is more in this particular region. However, the cumulative intensity or duration is less compared to the Somali.

The largest event in the north Bay of Bengal region only lasts for 40 days and has a cumulative intensity of 40.31 °C days (table 4.16). The largest event in the north Bay of Bengal occurred during 2016.

Table 4.16: Largest five events (duration wise) in the north Bay of Bengal (85°E–93°E–15°N–23°N) region.

Start Date	End Date	Peak Date	No of Days [day]	Mean intensity [°C]	Maximum intensity [°C]	Cumulative intensity [°C day]
2016-02-10	2016-03-20	2016-02-20	40	1	1.32	40.3
2010-06-26	2010-07-29	2010-07-20	34	0.89	1.31	30.22
2010-08-08	2010-09-05	2010-08-23	29	0.99	1.34	29
1987-12-03	1987-12-25	1987-12-07	23	0.89	1.21	20.4
2014-06-05	2014-06-25	2014-06-16	21	0.95	1.12	20

Figure 4.17 shows the seasonal climatology of MHW metrics in the north Bay of Bengal region. In this, the cumulative intensity and duration have a peak during February, while area, mean intensity, and during May and October months (ranging from 12-14 events). The seasonal signal of MHW metrics in the north Bay of Bengal maximum intensity is in May. Further, the number of events has a prominent double peak, which is

occurring shows peak values either in February or May, which is they show maximum values during the summer season.

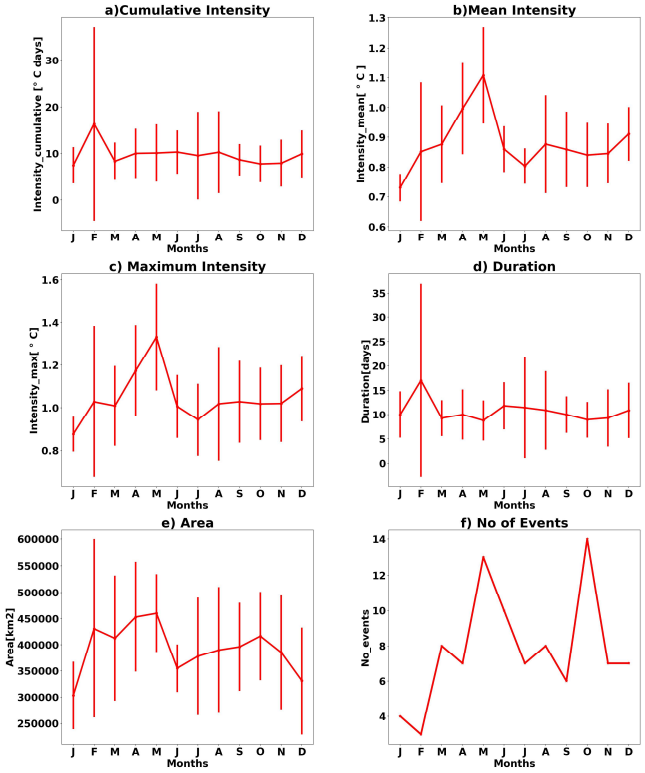

Figure 4.17: Climatology of MHW metrics for the north Bay of Bengal (85°E–93°E–15°N–23°N) region, error bar represents the standard deviation. a) Cumulative intensity (°C days), b) mean intensity (°C), c) duration (days), d) maximum intensity (°C), e) area (km^2), f) number of events, from 1982-2018.

In the north Bay of Bengal region, the area is fluctuating between 0.25 million - 0.5 million km^2. Figure 4.18 shows the mean area of MHW events during the peak date. When we analyze the spatial extent for the annual, 1995 event had the largest area (0.511 million km^2), while during the JJAS 2008 event (0.5 million km^2) had the largest area.

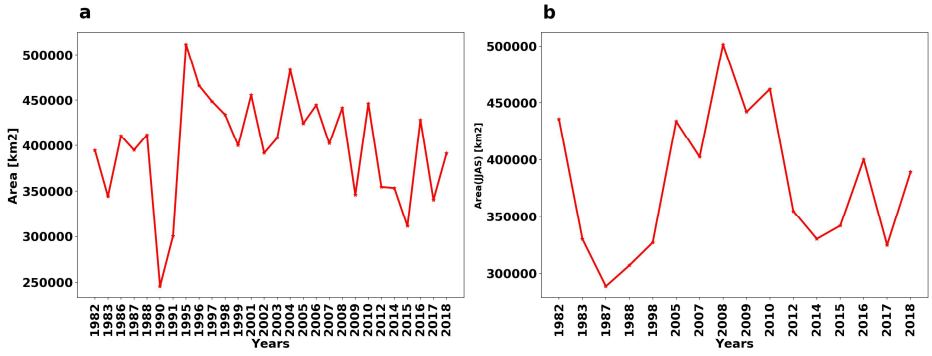

Figure 4.18: Mean area (km^2) of MHWs during the peak date a) annually, b) during JJAS, from 1982-2018 in the north Bay of Bengal (85°E–93°E–15°N–23°N) region.

Fig 4.19 and 4.20 show the three largest and smallest (area wise) events in the north Bay of Bengal region during the summer monsoon. There is a convergence of winds over the Indian subcontinent. In most of the cases, there is a prominent pattern of northeasterly winds over the north Bay of Bengal region.

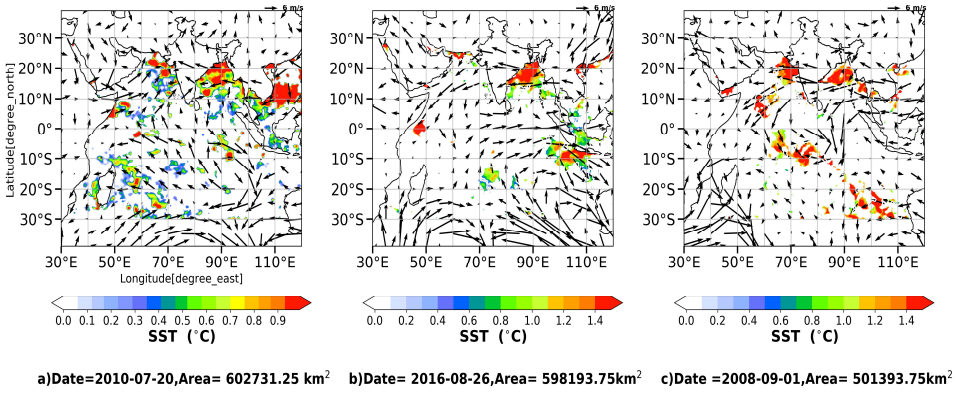

Figure 4.19: Spatial plot of SSTA and wind at 850 hPa during the peak date of largest 3 MHW events (area wise) in the north Bay of Bengal region (85°E–93°E–15°N–23°N).

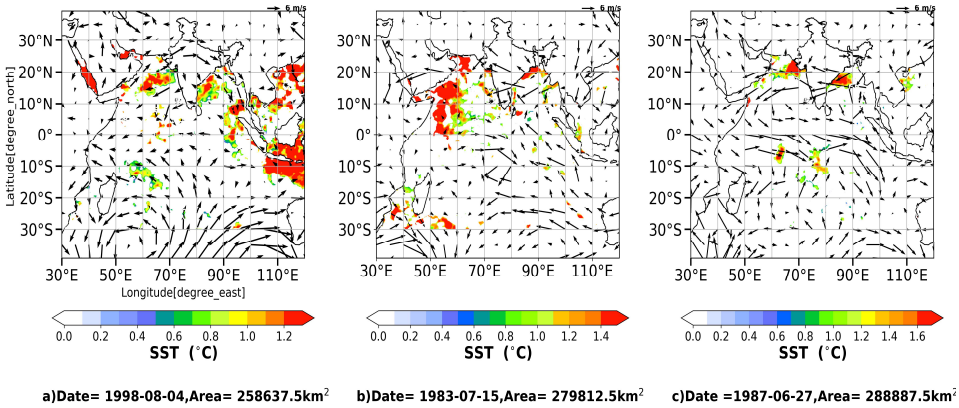

Figure 4.20: Spatial plot of SSTA and wind at 850 hPa during the peak date of smallest 3 MHW events (area wise) in the north Bay of Bengal region (85°E–93°E–15°N–23°N).

4.2. The Lifecycle of Marine Heat Waves

MHWs, the anomalous warm water events called the monster of the warming Ocean. Earlier, we familiarized with the trend of MHW events in the Indian Ocean and discussed the seasonal climatology of different statistics of MHW events in the two selected regions. Now we know that there is anomalous warming occurring in the Indian Ocean, but not aware of the conditions that lead to the formation of these events or how the atmospheric condition changes with these monstrous events. According to the study of western South Atlantic MHW in 2013/14, the increased solar radiation and the weak wind itself mainspring the manifestation of MHWs (Rodrigues *et al.,* 2019). As in the case of North Pacific 2014–2016, MHW was attributed by the tranquillity of local winds along with the mid-level atmospheric blocking (Fewings and Brown, 2019). While the MHWs delineated in China's marginal seas and adjacent offshore waters also have similar reasons like the increased shortwave radiation, reduced heat swaps between the Ocean and atmosphere and the moderate wind speed accompanied with the presence of western boundary current, Kuroshio and the warm phase of ENSO (Yao *et al.*, 2020).

Here we are going to do a composite analysis of SST, wind [850 hpa], latent heat flux, downward solar radiation, upward longwave radiation, sensible heat flux & OLR anomalies of the 45 days before and after the starting date of MHW in both regions. This would light up our understanding of the entire situation of atmosphere during the lifespan of MHW and may provide us what the cause of a sudden increase in temperature in these particular regions is. Let us examine the two MHW regions in the Indian Ocean separately.

4.2.1. The life cycle of Marine Heat Waves in the Somali region (41°E –56°E–8°S–8°N)

The Somali region is the most important MHW prone area, which has significant MHW activity both during the entire year and during the Summer Monsoon season. Here we are doing a composite analysis of SST (blue line), wind (red line) (850 hpa) & OLR (Outgoing Longwave Radiation) (magenta line) anomalies of the 45 Days Before and After the Starting Date of MHW. Figure 4.21 gives an overall picture of atmospheric parameters 45 days before and after the MHW starting day. From the figure zero-day implies the starting day of MHW events, it is visible that almost 20 days before the starting day, wind anomaly drops below zero, SST is low, 0.5 °C and OLR just started to rise, together we can infer that 20 days before the starting date the atmosphere looks like calm, clear sky and probably have subsidence of air. This condition extends up to five days before the starting day, we can see 5 days before the onset of MHW the wind anomaly decreased, and it is below zero, the SST started increasing slowly. The OLR anomaly remained above zero expected a clear sky condition. As in the case of fluxes (figure 4.22) 5 days before the onset of MHWs. We can see that the latent (yellow line) and sensible heat fluxes (green line) are negative, and continue to decrease, while the downward solar radiation (purple line) and the upward long wave radiation (black line) are showing an increase. That is the five days before the MHW, the wind speed is low, and the latent and sensible heat is negative, that there is no heat transport is occurring between the ocean and atmosphere. Moreover the solar radiation is more in this region.

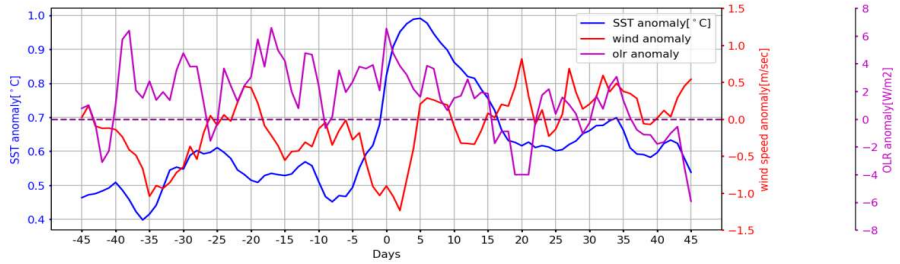

Figure 4.21: Composite of SST(blue line), wind (red line) (850 hPa) & OLR(magenta line) anomalies of the 45 days before and after the starting date of MHW in the Somali (41°E–56°E–8°S–8°N) region for the period 1982-2018 .

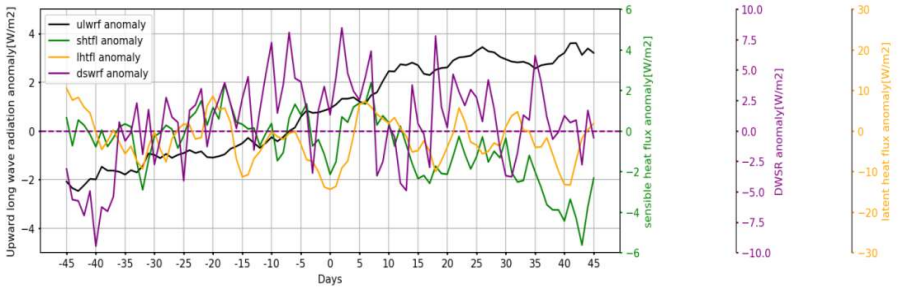

Figure 4.22: Composite of latent heat flux (yellow line), sensible heat flux (green line), downward solar radiation (purple line), and upward long wave radiation (black line) anomalies of the 45 days before and after the starting date of MHW in the Somali (41°E –56°E–8°S–8°N) region (using NCEP datasets from 1982-2018).

During the starting day of MHW we can see that the wind is around its minimum, SST anomaly increased to 0.9°C, and OLR anomaly is a positive, besides, the latent and sensible heat is in its minimum, so we can refer a clear sky with anomalous warm water in the Ocean. The 3rd day after the starting date of MHW, wind anomaly shows a minimum value. In contrast, SST anomaly reached the maximum value above 1°C, OLR remains above zero, besides the latent and sensible heat is started to increase, we can expect there to be more heat storage. That is after the onset of MHWs, almost four days onwards there is heat transport initiated from the Ocean probably due to the increase of wind speed in the particular region. After ten days of the MHW initiation, the situation changed, the wind anomaly increased, SST anomaly showing a decrease. The OLR, downward solar radiation, latent, and sensible heat flux anomalies are also decreased. All these lead to the fact that in that area convection is occurring, and clouds may form. When we take a look at the 20 days after the MHW, it also has a similar situation as the $+10^{th}$ day had. The one thing that is interesting here is that the atmospheric conditions brought out by the MHW events are staying in the Somali region for a comparatively longer time.

Even Though we have the composite picture of atmospheric parameters on 45 days before and after the start date of MHW events, it is not enough to say which parameter is causing the SST rise in the particular region. So we have to go for another analysis. Thus figure 4.23 shows the lead-lag correlation between SST and wind (red line), latent heat flux (yellow line), downward solar radiation (purple line), OLR (blue line), sensible heat flux (green line) and upward longwave radiation (black line) in the Somali region.

From the picture, we can see that the negative wind anomaly leads SST by ~3 days and positive latent heat flux anomaly lags SST by ~5 days. In other words, the drop in the wind speed happens first and after 3 days the SST anomaly rises, that is the weakening of the southwest winds has an impact on the MHW (r=-0.24) than the other way (r=0.1). The MHW in the Northeast Pacific during 2014–16, was also driven by the weak wind anomalies; they added that the weakening of the wind in that area lasted for 2 weeks (Fewings and Brown, 2019). In the case of latent heat flux, it increases after the SST increases by 5 days, and there is also a peak of latent heat flux in the lead 3 days, but it is not that significant because the correlation coefficient value is very low (r=-0.12).

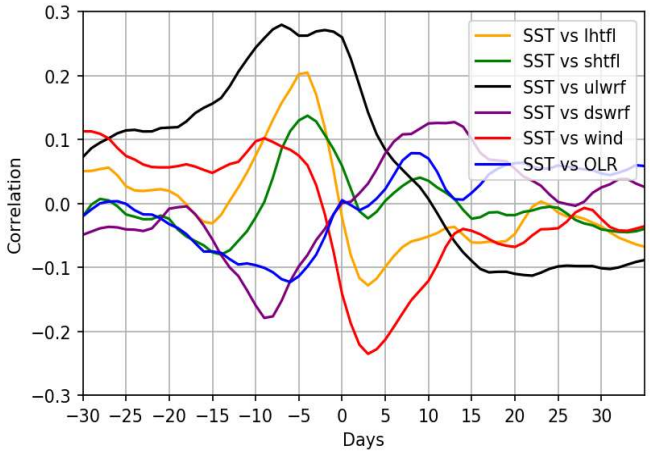

Figure 4.23: The lead-lag correlation between SST and wind (red line), latent heat flux (orange line), sensible heat flux (green line), upward long wave radiation (black line), OLR (blue line) in the Somali (41°E–56°E–8°S–8°N) region. Estimated from the 30 days before and 30 days after the start date of MHW events, from 1982-2018.

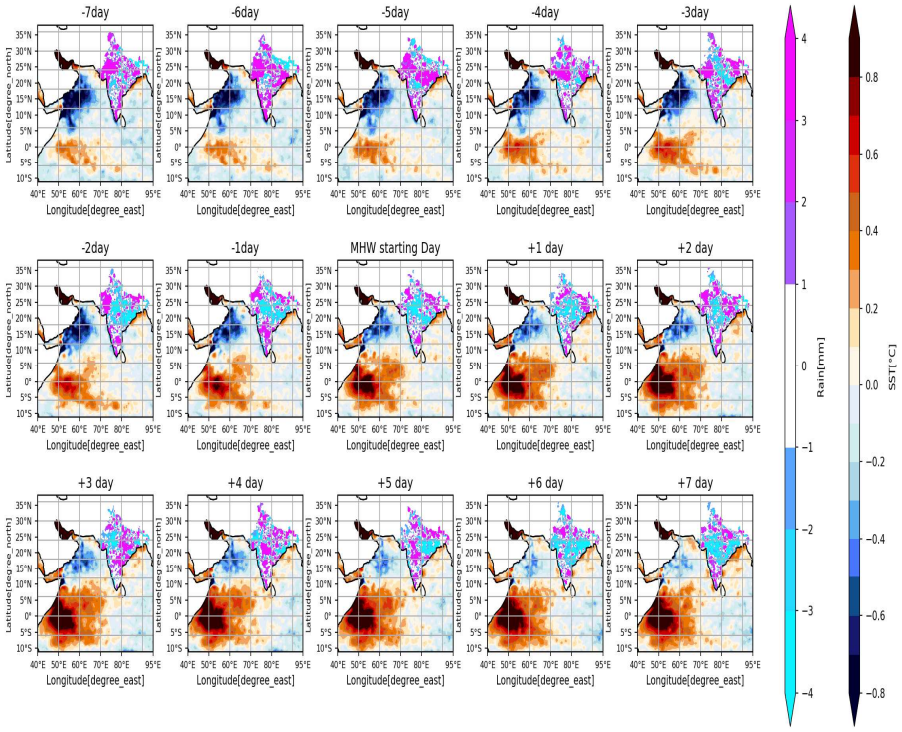

Figure 4.24:The spatial plot of the composite of rainfall anomalies over India and SST anomalies of the 7 days before and after the starting date of MHW in the Somali (41°E–56°E–8°S–8°N) region, using OISST and IMD rainfall datasets from 1982-2018.

When we take the SST- OLR and SST-downward solar radiation, we can see that both the OLR and DSWRF are leading the SST by ~10 days that is the increase in the OLR and downward solar radiation occurring first, they have a contribution to the SST increase in the Somali region.

This relation is different in the case of sensible and upward long wave radiation, in the case of sensible heat flux, it is lagging SST by ~ 5 days, and for the upward long wave radiation, it is at zero lag. That is the sensible heat flux is going out from the Ocean 5 days after the onset of MHW in the Somali region and upward longwave radiation release from the Ocean and the SST rise co-occurring.

From figure 4.24, we can see the evolution of the SST in the Somali region. We can see a cold SST region above the study region. Figure 4.25 also gives a more detailed picture of what is happening in the Somali region and how the wind speed is affecting the SST changes in the Somali. We can see that before the 7^{th} day of the onset of MHW, the wind is in the southwest direction, and it is showing a weakening pattern -4 days onwards. From the figure 4.25, we can deduce a dipole nature of wind, that the wind speed is high in the southern side of Somali, at the same time wind speed is very low in the north side, along with that we can see a negative latent heat flux forming in the north side. In the Somali region, we can assume that the Ocean current system is usually transporting the heat due to the strong southwest monsoon winds. But before the onset of MHWs, these winds are weakened, which may be ended up with the deficient transport of heat by the ocean currents, and this may be the reason for the triggering of SST rise in this region.

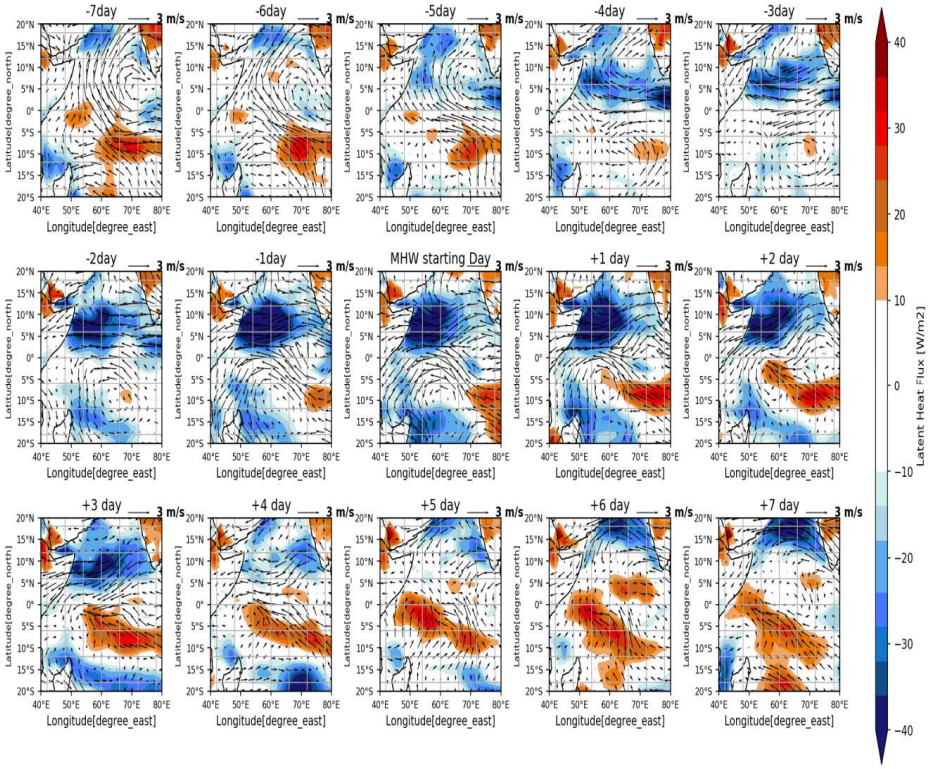

Figure 4.25: The spatial plot of the composite of wind (850 hPa) & Latent heat flux anomalies of the 7 days before and after the starting date of MHW in the Somali (41°E –56°E–8°S–8°N) region, using NCEP/NCAR datasets from 1982 to 2018.

Along with the wind and latent heat flux, the OLR and the downward solar radiation also play an important role in the Somali for setting the MHW condition. From the lead-lag analysis, we already saw that the OLR and downward solar radiation is heating the Ocean surface before the onset of the MHWs. This relation is much more visible through the spatial composite map (figure 4.26).

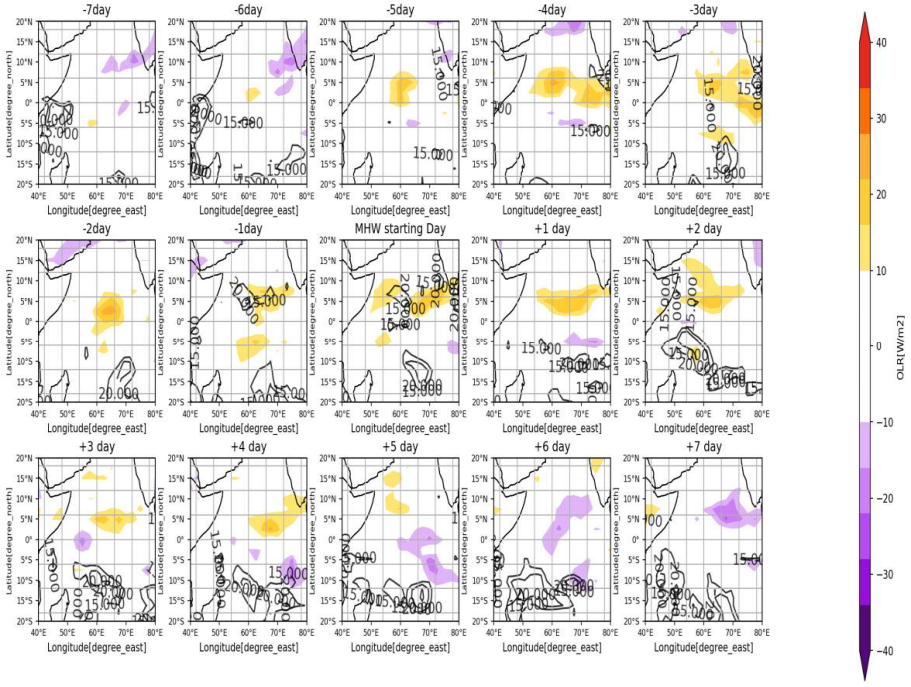

Figure 4.26: The spatial plot of the composite of OLR & downward solar radiation anomalies of the 7 days before and after the starting date of MHW in the Somali (41°E –56°E–8°S–8°N) region, using NCEP/NCAR datasets from 1982 to 2018. The colour represents the OLR and contours as downward solar radiation.

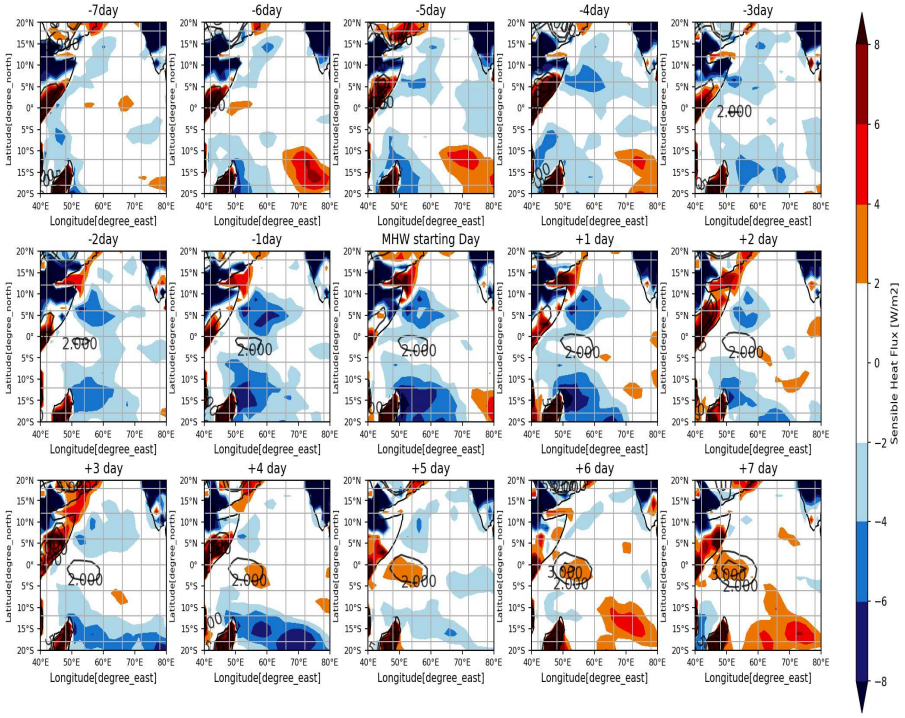

Figure 4.27: The spatial plot of the composite of sensible heat flux and upward longwave radiation anomalies of the 7 days before and after the starting date of MHW in the Somali (41°E –56°E–8°S–8°N) region, using NCEP/NCAR datasets from 1982 to 2018. The colour represents the sensible heat and contours as upward longwave radiation.

As illustrated in the lead-lag analysis, sensible and upward long wave are released from the Somali region after the outset of MHWs, it is also detectable in figure 4.27. We can see that sensible and upward long wave radiation is increasing +4 days onwards. Figure 4.28 gives us the overall picture that we have discussed so far.

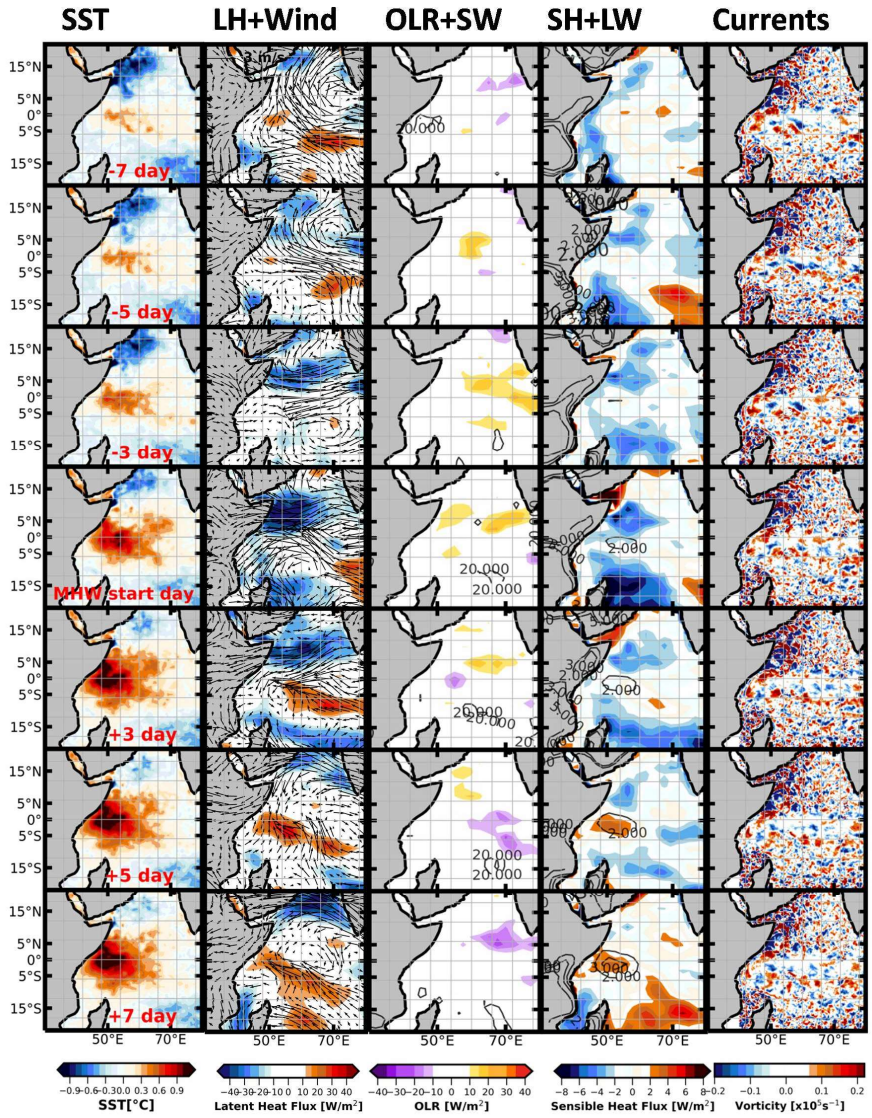

Figure 4.28: Flowchart of Marine Heat Wave in the Somali (41°E–56°E–8°S–8°N) region.

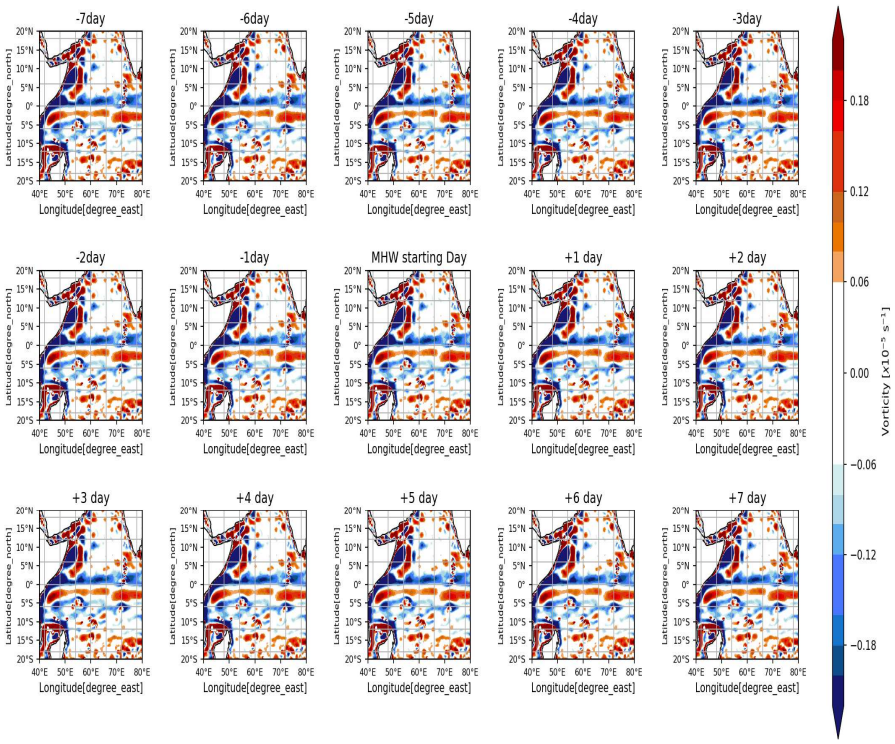

Figure 4.29: The JJAS mean of Ocean current vorticity anomalies in the Somali (41°E–56°E–8°S–8°N) region, using the HYCOM reanalysis datasets from 1994 to 2015.

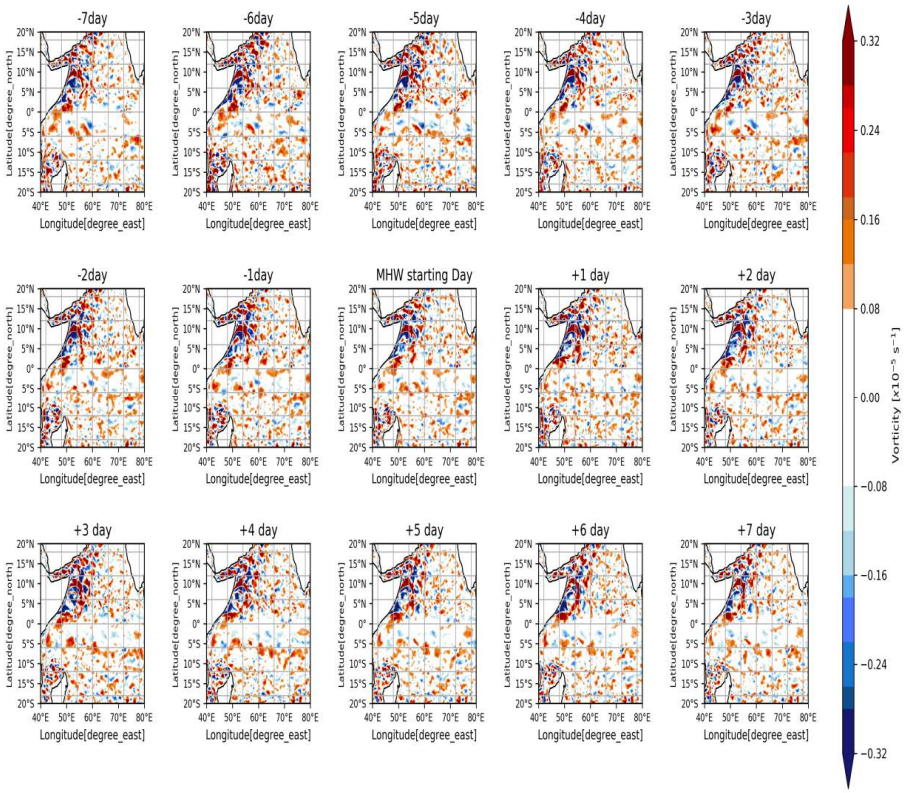

Figure 4.30: The spatial plot of the composite of ocean current vorticity anomalies of the 7 days before and after the starting date of MHW in the Somali (41°E–56°E–8°S–8°N) region, using the HYCOM reanalysis datasets from 1994 to 2015.

Apart from the changes in the air-sea fluxes and weak wind speed, the Ocean circulation also plays a role in the manifestation of MHWs (A. Schaeffer *et al.,* 2017; Oliver *et al*., 2014). Oliver *et al*. (2014) also found out that Ocean eddy activities simulate the MHWs.

Moreover, in the western Tasman Sea, MHWs occurring in the subsurface layers has a relation with the Ocean eddies, which usually transports the warm water (Elzahaby and Schaeffer, 2019). The Somali region is a dynamically active and also an important western boundary current region; because of this, we can expect the role of ocean currents in the genesis of MHWs in the Somali region. To check the possibility of ocean currents, we plotted the ocean current vorticity anomalies in the Somali region. Figure 4.29 represents the June to September composite of vorticity anomaly in the Somali region. We can see that in the Somali region, there are two anticyclonic circulations during the monsoon period. When we look into figure 4.30, it is evident that the anticyclonic circulation in the south of the Somali is strong. At the same time, the north anticyclone is not that strong, and it is relatively weak also. Earlier we saw that the wind is showing a dipole pattern, that is the high wind speed in the south of Somali, while low wind speed in the north side. All this lead to the fact that the high wind speed in the south transport the heat into the north, while in the north wind is weak and finally heat is trapped in that place.

All the things that we have discussed so far give us a rough picture of factors favourable for the genesis of MHWs. That is the weak wind restrict the transport of heat by the ocean currents that are ocean current is persisted in the Somali region. Also, the sun is heating the ocean surface; all this make the piling up of heat in this particular region and finally favouring the MHW.

Until now, we have the factors that might contribute to the MHW condition. But the problem is that here all the correlation coefficient is very low, and it is difficult to single out the factors leading to the genesis. If we have to quantify the role of the different factors leading to the temperature change in this region, we have to do the ocean mixed layer heat budget analysis. Figure 4.31 illustrates the composite of heat budget factors, representing the five days before the onset of MHWs in the Somali region, from 1994-2015. Figure 4.31(a) shows that the rate of change in temperature in the Somali region influences the advection and heat flux term. In the advection term, the zonal advection is dominant. Along with the advection term, the heat flux term also has a contribution to the temperature change. We can see that in the net heat flux, the net solar radiation received in the mixed layer and the latent heat is the major contributors. That is the increased solar radiation and decreased latent heat release from the ocean contributes the MHW genesis in the Somali region.

$$\partial T_{SST}/\partial t = -v_{(at\ 15m\ depth)} \bullet \nabla T_{SST} + Q_{0(ERA5)}/\rho C_p H_{m(ORAS4)} + Res$$

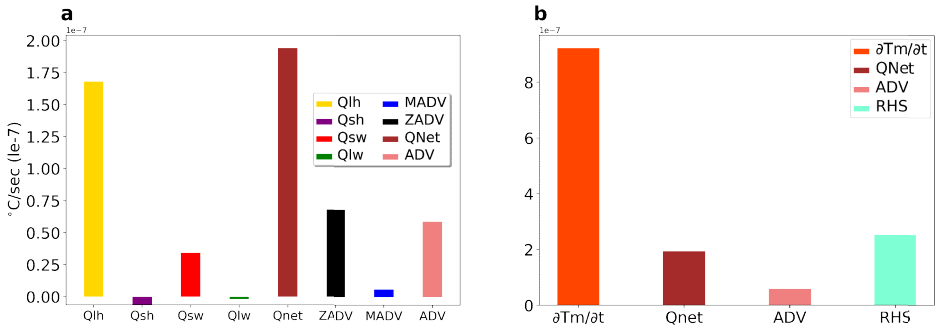

Figure 4.31: The heat budget terms calculated for the 5 days before the starting date of MHW in the Somali (41°E –56°E–8°S–8°N) region, a) terms in the right-hand side of the temperature tendency equation, b) terms in both side of the temperature tendency equation, using the OSCAR datasets and NCEP/NCAR fluxes from 1994 to 2015.

As a whole, we can say that the MHWs in the Somali region is formed due to the influence of the dipole nature of wind in the area which further influences the transport of heat by the ocean currents. The solar insulation in a particular region also affects the genesis of MHWs. These results are well agreeing with the other studies too.

Now we know that the Somali region has an unusual SST rise attributed to the changes in the wind, ocean currents, and air-sea fluxes, during the summer monsoon period. The next question is how this anomalous warming influences the monsoon rainfall over India? Or is there any change in the rainfall pattern during the lifecycle of MHW in the Somali region?

We already have an answer to that question. From figure 4.24, we could have a primary understanding of this topic. There is monsoon rainfall over India before the onset of MHWs in the Somali region, but after the beginning of MHW, it is showing that rainfall over India is decreasing. We can see an apparent decrease in rainfall on 6th day after the start date of MHWs in the Somali region. For confirming the result, we also plotted the omega at 500 hPa, vertically integrated moisture flux convergence, and specific humidity during seven days before and after the start date of MHW.

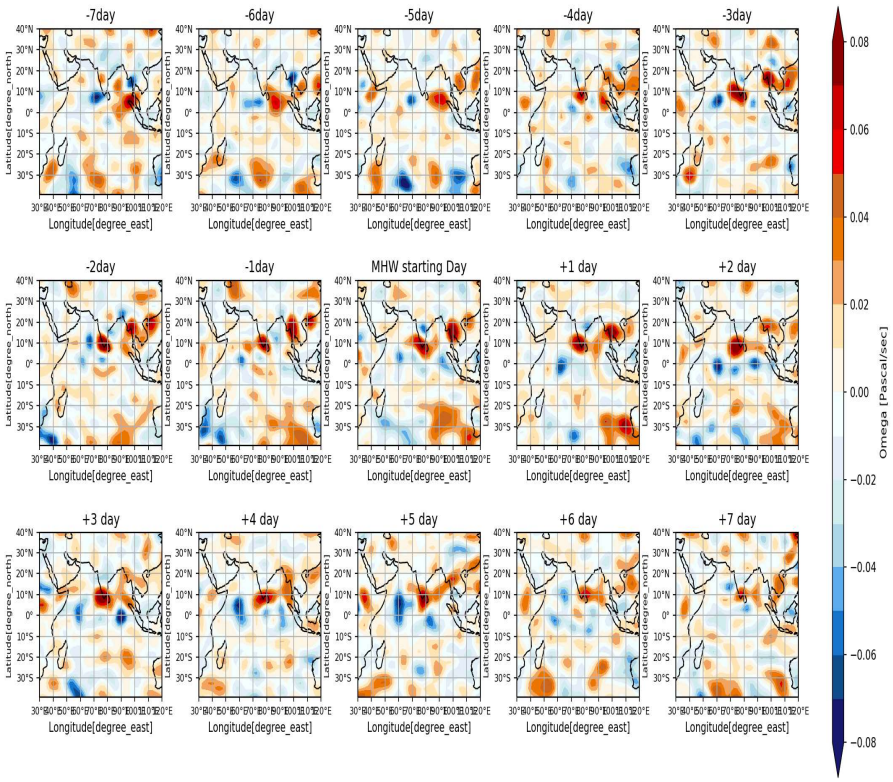

Figure 4.32: The spatial plot of the composite of Omega (at 500 hPa) anomalies of the 7 days before and after the starting date of MHW in the Somali (41°E–56°E–8°S–8°N) region using NCEP/NCAR datasets from 1982-2018.

The composite of omega at 500 hPa (figure 4.32) shows that after the initiation of MHW in the Somali region over the south India subsidence is occurring, while over the Somali region we can see negative vertical velocity that is convection is occurring.

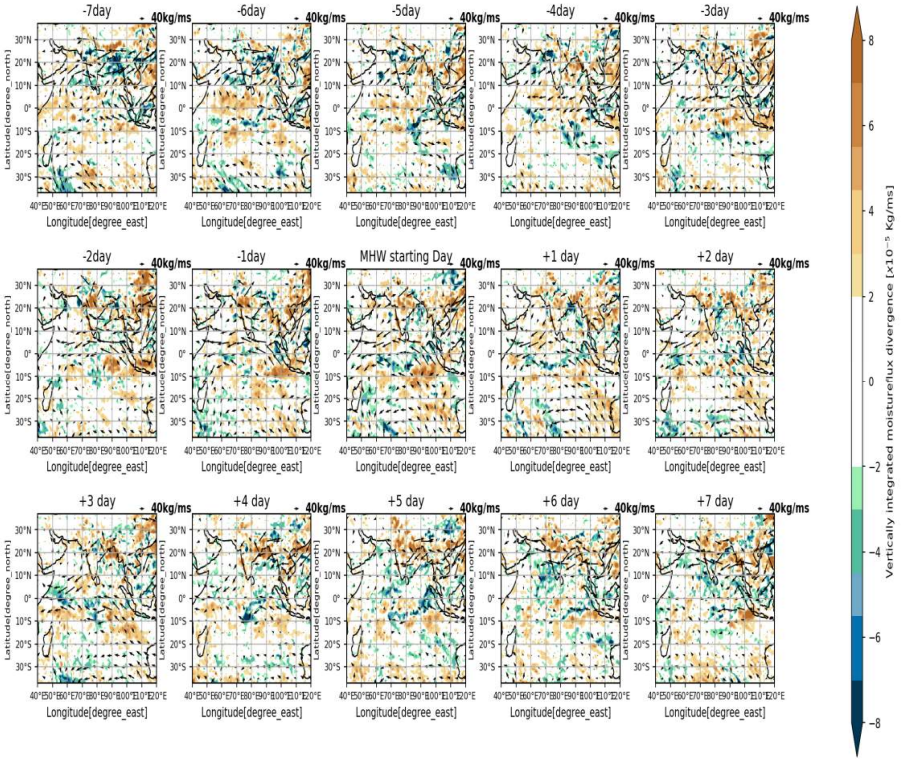

Figure 4.33: The spatial plot of the composite of vertically integrated moisture flux divergence anomalies of the 7 days before and after the starting date of MHW in the Somali (41°E–56°E–8°S–8°N) region, using ERA5 moisture flux convergence datasets from 1982-2018.

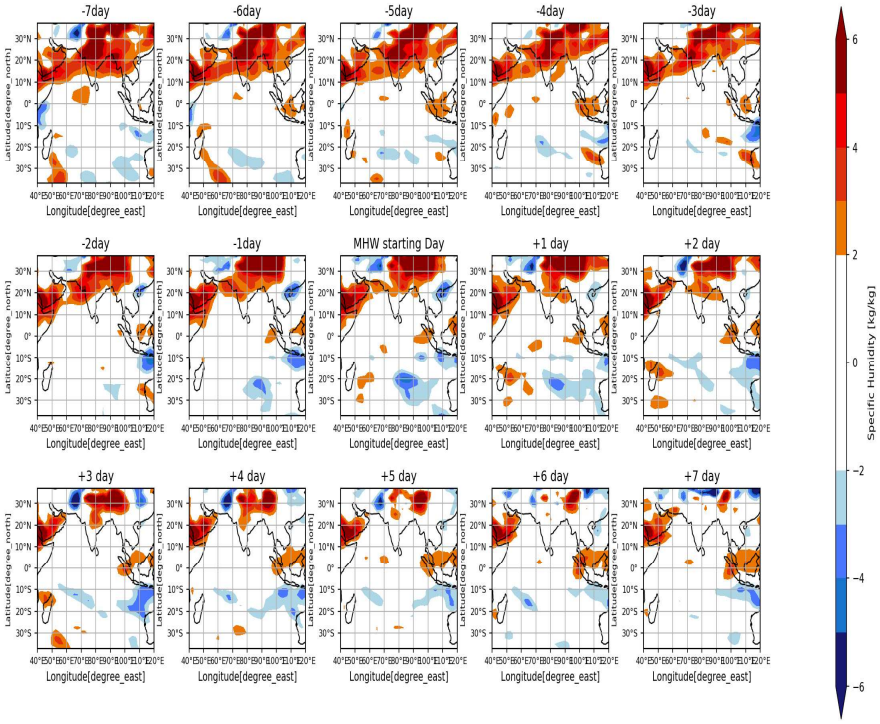

Figure 4.34: The spatial plot of the composite of vertically integrated specific humidity anomalies of the 7 days before and after the starting date of MHW in the Somali (41°E–56°E–8°S–8°N) region, using NCEP/NCAR specific humidity datasets for the period 1982-2018.

From figure 4.33 and 4.34, we can say that before the starting date of MHW, there is some amount of moisture convergence that is south-westerlies are carrying moisture to the landmass. Also, there is high specific humidity over the Indian continent. But after the starting date of MHWs, there is a visible reduction in the moisture and the specific humidity over the subcontinent. After the 6th day, we can see a moisture flux divergence and almost no specific humidity over entire India. It appears that the rainfall over India shows a reduction after the onset of MHW in the Somali region.

4.2.2. The Life cycle of Marine Heat Waves in the North Bay of Bengal Region (85°E–93°E–15°N–23°N)

We have seen the lifecycle of MHWs in the Somali region, and realize the synoptic condition before and after the MHW events. Here we are going to do a similar analysis for the north Bay of Bengal, figure 4.35 and 4.36 show an overall picture of atmospheric parameters 45 days before and after the MHW starting day. As we know, the zero-day in the figure implies the starting date of MHW events. It is clear that almost 20 days before the starting day, wind speed (red line) is above zero, SST (blue line) is low, 0.35°C and OLR (magenta line) anomaly is negative, latent heat flux (yellow line) is positive. But the sensible (green line), upward long wave (black line) and solar radiation downward (purple line) all are low; similar to the Somali region this region also experienced clear sky and subsidence. During the six days before the starting day, the wind anomaly started to decrease, and the downward solar radiation is increasing while latent heat and sensible heat flux are low along with SST and the OLR anomaly started to rise, showing a clear sky condition.

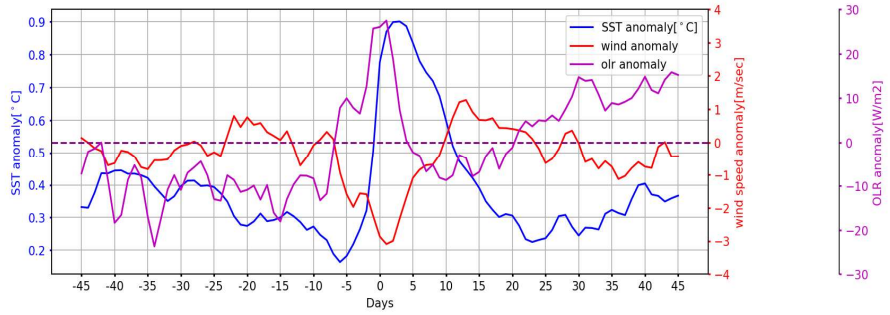

Figure 4.35: Composite of SST(blue line), wind(red line) [850 hpa] & OLR (magenta line) anomalies of the 45 days before and after the starting date of MHW in the north Bay of Bengal (85°E–93°E–15°N–23°N) region, from 1982-2018.

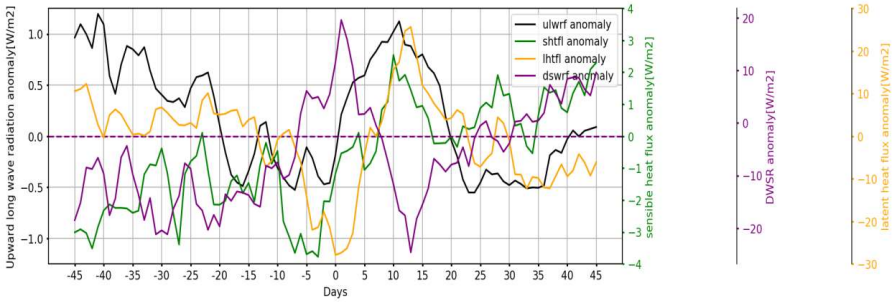

Figure 4.36: Composite of latent heat flux (yellow line), sensible heat flux (green line), downward solar radiation (purple line) and upward long wave radiation (black line) anomalies of the 45 days before and after the starting date of MHW in the north Bay of Bengal (85°E–93°E–15°N–23°N) region (using NCEP/NCAR datasets from 1982-2018).

When MHW initiated, it is clear that the wind is at its minimum, SST anomaly has crossed the threshold value, but the latent heat flux is at its minimum. Sensible heat flux is low, while the OLR and downward solar radiation are at its maximum, again there may be a clear sky situation. On the 4^{th} day after the starting date of MHW, now wind anomaly is below zero, while SST anomaly reached the maximum value of 0.9°C, OLR anomaly decreased. Moreover, the latent heat flux, upward longwave radiation, and sensible heat flux are started to increase, and we can assume that the warm Ocean will slowly begin to release the heat energy. On the 10^{th} day after MHW initiation, the situation has changed, the wind speed increased, SST showing a decrease and OLR, downward solar radiation is negative, in addition to that we can see that the sensible heat flux, latent heat flux, and the upward longwave radiation are increased, which means the wind is causing the evaporation cooling of the ocean surface along with the loss of heat as sensible heat and longwave. Thus we can expect, convection is occurring and clouds will form. After the 25 days, the atmosphere and Ocean are probably back to the normal condition that the SST anomaly decreased, wind anomaly is negative, and OLR is positive, and may have a clear sky condition. Apart from the Somali region's MHW, the north Bay of Bengal region has MHW with a comparatively shorter life span (fig 4.35). The Bay of Bengal is recovering relatively faster rate from the MHW condition than the Somali region.

To get a better picture of which parameter is causing the anomalous warming, we have done a lead-lag correlation between SST and wind (red line), latent heat flux (orange line), sensible heat flux (green line), upward longwave radiation (purple line) and OLR (blue line) in the north Bay of Bengal region. From figure 4.37, we can see that negative wind anomaly leads SST by ~2 days, while the latent heat flux also shows a similar relationship with the SST. For latent heat, it is leading the SST by ~ 3 days.

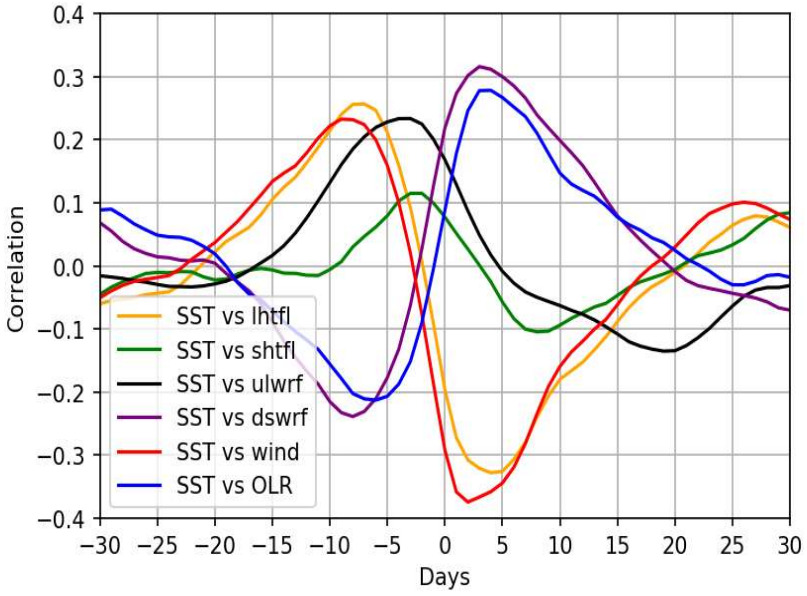

Figure 4.37: The lead-lag correlation between SST and wind (red line), latent heat flux (orange line), sensible heat flux (green line), upward long wave radiation (black line), OLR (blue line) in the north Bay of Bengal (85°E–93°E–15°N–23°N) region. Estimated from the 30 days before and 30 days after the start date of MHW events (using NCEP/NCAR reanalysis datasets from 1982-2018).

That is wind anomaly becomes negative ~ two days before the starting date of MHW. Then SST rises (r=-0.38), more clearly we can say that the weakened wind causing the less evaporation cooling over the ocean surface, which is generating the negative latent heat in the ocean, that is

making the storage of heat in the ocean itself further increased SST. In the case of OLR and downward solar radiation showing an almost similar relation with the SST, positive OLR and downward solar radiation leads SST by ~ 4 days with r values 0.28 and 0.31 respectively. This means that the OLR and solar insulation are high before the onset of MHWs in the north Bay of Bengal region. When we take the sensible and upward longwave radiation, they are lagging the SST by almost ~ 3 days (r=0.12 and 0.23 respectively). In the north Bay of Bengal region, sensible heat flux and upward longwave radiation are started to release from the ocean after three days of the onset of the MHWs. Studies are agreeing on the results, according to them the changes in the air temperature, wind speed and subsequent reduction in the exchange of heat between the ocean and atmosphere can lead to the genesis of MHWs in a particular region (Bond *et al.,* 2015; Chen *et al.,* 2015).

Now we know from the composite and lead-lag analysis SST is increasing in the north Bay of Bengal region. Figure 4.38 will give us the more exact picture of the SST rise in the north Bay of Bengal region. When we draw a similar composite map for latent heat flux and the wind in the particular region, we can deduce that wind speed is decreasing in the region three days before the onset of MHW, at the same time the latent heat flux is showing a negative anomaly that is latent heat flux is decreasing. So from figure 4.39, we can conclude that the decrease in the wind speed causes the heat storage in the ocean by the decreased evaporation cooling in the ocean. And it is also evident from the figure that, after the onset of MHW, almost 4, 5 days the heat is released from the ocean.

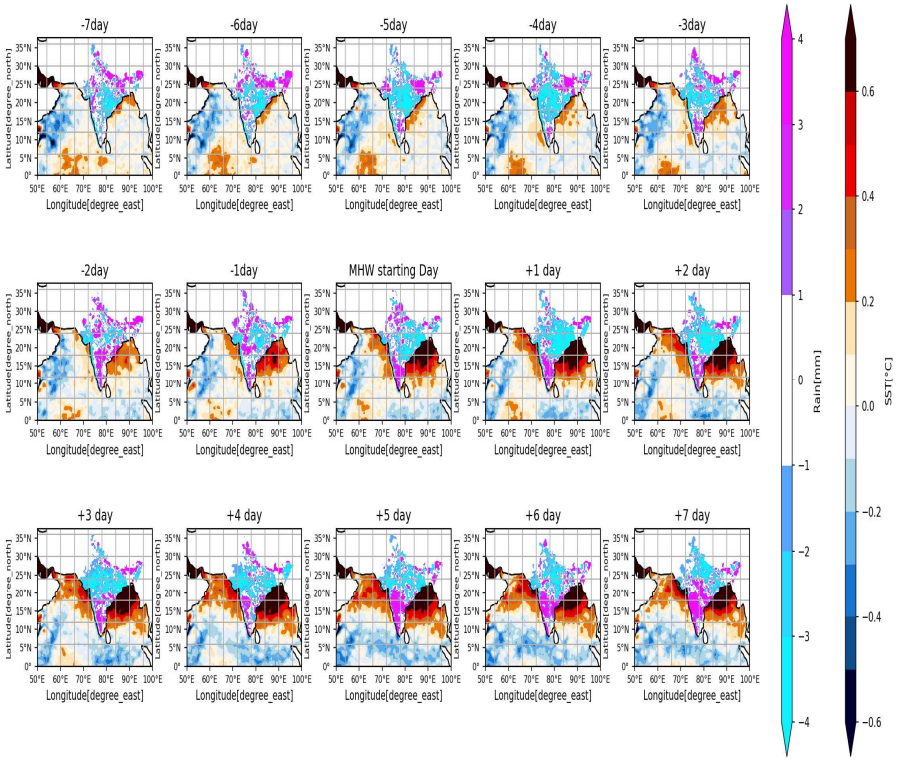

Figure 4.38: The spatial plot of the composite of rainfall anomalies over India and SST anomalies of the 7 days before and after the starting date of MHW in the north Bay of Bengal (85°E–93°E–15°N–23°N) region, using OISST and IMD rainfall datasets from 1982-2018.

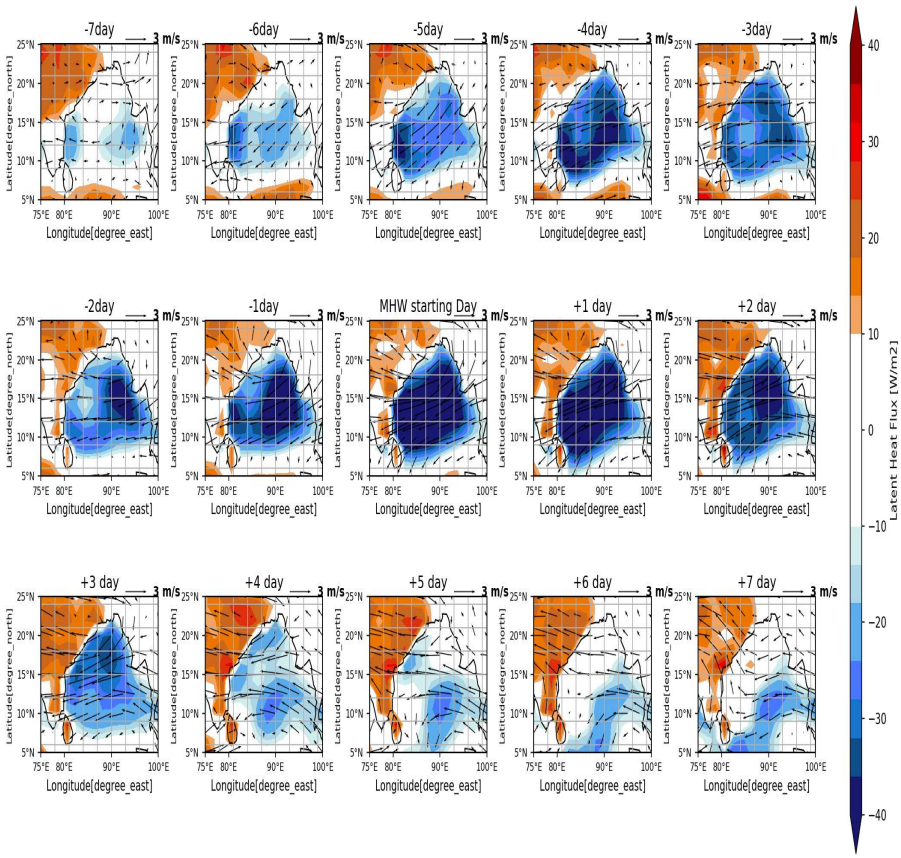

Figure 4.39: The spatial plot of the composite of wind (850 hPa) & latent heat flux anomalies of the 7 days before and after the starting date of MHW in the north Bay of Bengal (85°E–93°E–15°N–23°N) region, using NCEP/NCAR datasets from 1982-2018.

In the case of OLR and downward solar radiation, we already saw that it is increasing before the onset of MHW, and have a contribution to the SST increase in the north Bay of Bengal region.

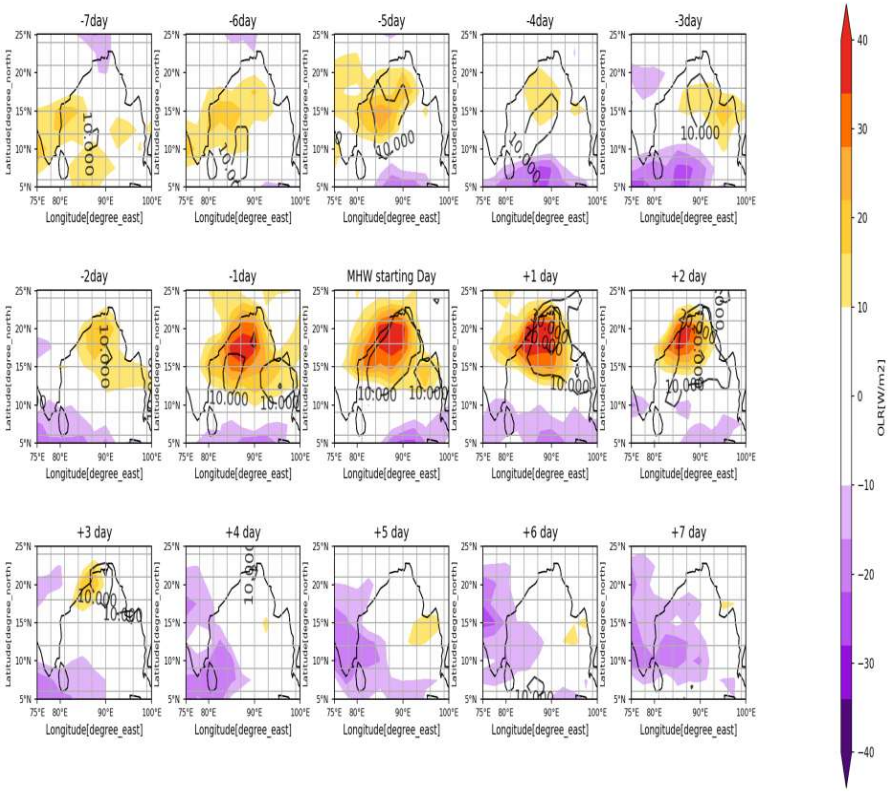

Figure 4.40: The spatial plot of the composite of OLR & downward solar radiation anomalies of the 7 days before and after the starting date of MHW in the north Bay of Bengal (85°E–93°E–15°N–23°N) region. The colour bar represents the OLR and contours as downward solar radiation, using NCEP/NCAR datasets from 1982-2018.

It can be evident in figure 4.40; OLR and downward solar radiation are decreasing after the onset of MHWs. That is there might be more convection and cloud formation after the MHW initiation.

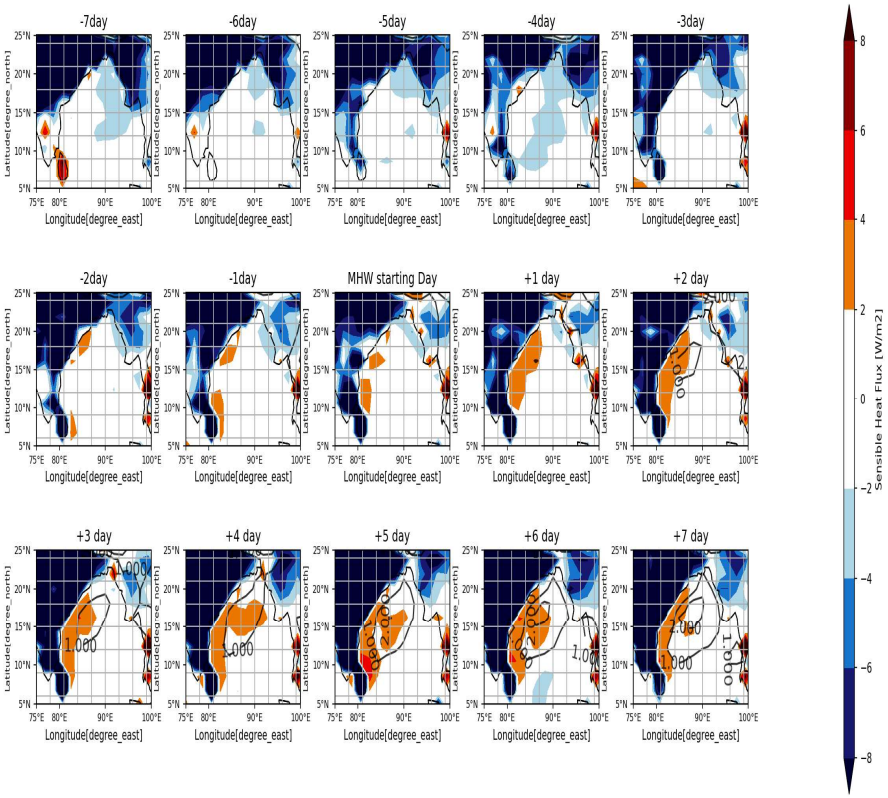

.

Figure 4.41: The spatial plot of the composite of sensible heat flux and upward long wave radiation anomalies of the 7 days before and after the starting date of MHW north Bay of Bengal (85°E–93°E–15°N–23°N) region, using NCEP/NCAR Sensible heat flux and upward long wave radiation datasets from 1982-2018. The colours indicate the sensible heat flux anomalies and contours are the upward long wave radiation anomalies.

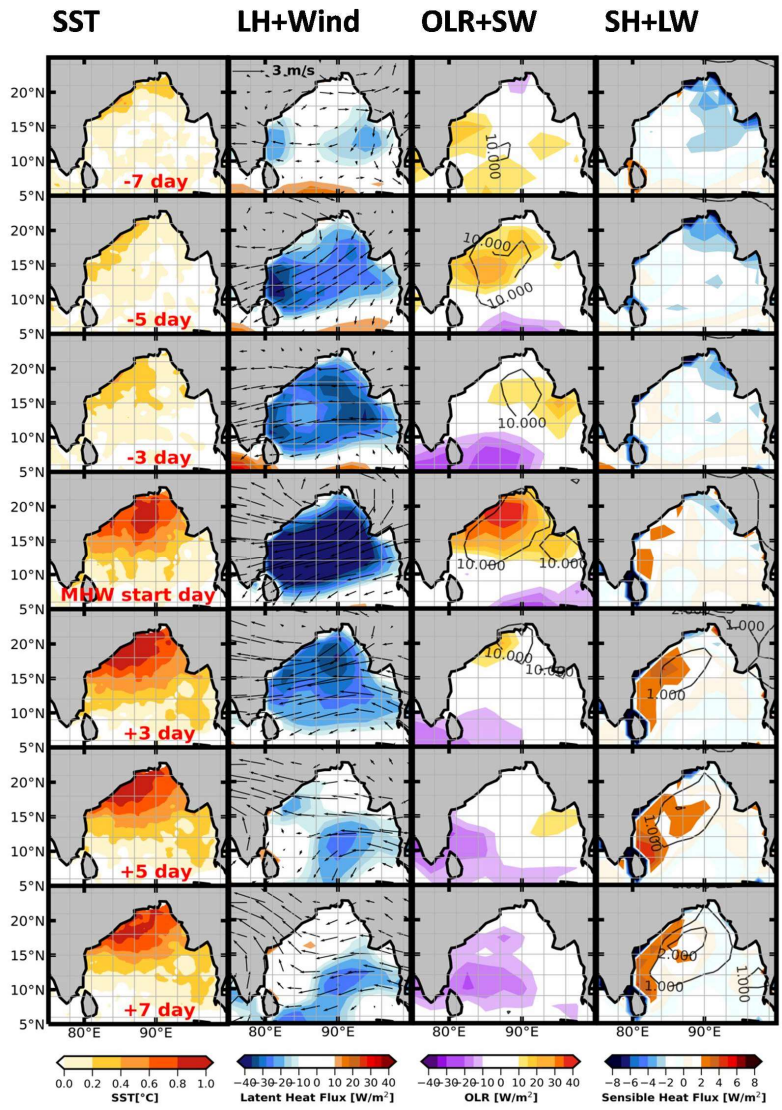

Figure 4.42: Flowchart of MHW events in the north Bay of Bengal (85°E–93°E–15°N–23°N) region.

We have already seen that the sensible and upward longwave radiation is going from the ocean after 4, 5 days. This is portrayed in figure 4.41. We can see a gradual increase of sensible and upward longwave radiation after the four days of onset of MHW in the north Bay of Bengal. The flowchart (fig.4.42) will give us the general picture of air-sea fluxes and wind contributions to the SST rise in the north Bay of Bengal region.

So far we know that in the north Bay of Bengal region, the MHWs are caused by the weakening of wind and the changes in the air-sea fluxes. To quantify the contribution of these factors, we have done a heat budget analysis, and the figure 4.43 shows the composite of heat budget factors, representing the five days before the onset of MHWs. This could light up the role of different factors in the rate of change of temperature in the north Bay of Bengal region. Heat budget of the mixed layer is calculated from 1994-2015. As we have said earlier, in the north Bay of Bengal, the temperature change is attributed by the net heat flux.

$$\partial T_{SST}/\partial t = -v_{(at\ 15m\ depth)} \bullet \nabla T_{SST} + Q_{0(ERA5)}/\rho C_p H_{m(ORAS4)} + Res$$

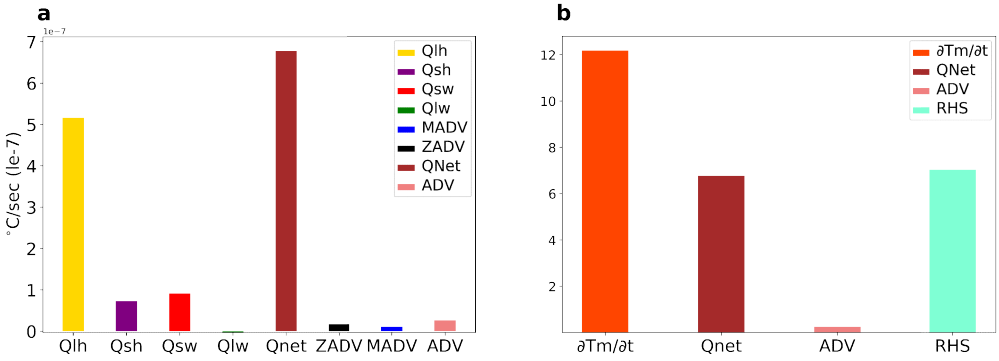

Figure 4.43: The heat budget terms calculated for the 5 days before the starting date of MHW in the north Bay of Bengal (85°E–93°E–15°N–23°N) region, a) terms in the right-hand side of the temperature tendency equation, b) terms in both side of the temperature tendency equation, using the OSCAR datasets and NCEP/NCAR fluxes from 1994 to 2015.

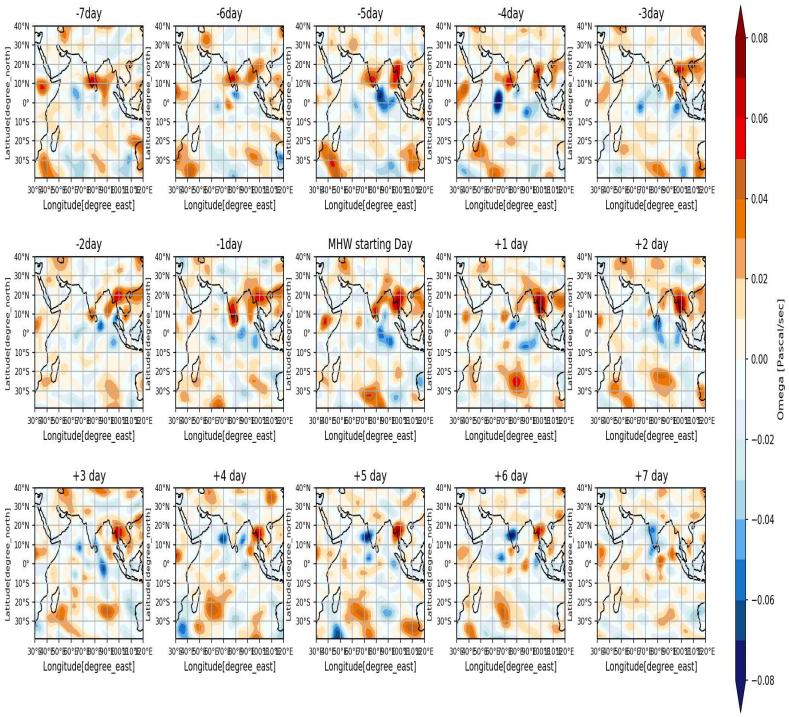

Figure 4.44: The spatial plot of the composite of Omega (at 500 hPa) anomalies of the 7 days before and after the starting date of MHW in the north Bay of Bengal (85°E–93°E–15°N–23°N) region, using NCEP/NCAR omega datasets from 1982-2018.

Among the heat flux terms, the latent heat and net solar radiation have a prominent role. Here we only have a small role of advection terms. In a nutshell, we can say that the weakening wind and the changes in the air-sea flux exchange play a role in the genesis of MHWs in the north Bay of Bengal region. The role of advection is very small compared with the heat flux terms.

Now we have to check how the rainfall over India is changing with the genesis of MHWs in the north Bay of Bengal. From figure 4.45, we can see that there is no much rainfall over the Indian subcontinent before the onset of MHW. But after the outset of MHWs, rainfall is increasing in South India. On the $+6^{th}$ day, there is rainfall over the Indian landmass. For more clarity, we have plotted the vertical velocity for seven days before and after the start date of MHW. It is clear from figure 4.44 that before the onset of MHW, there is a subsidence of air in the Indian landmass, but after that around the 6^{th} day, we can see a negative omega over south India, that is convective activities over that region.

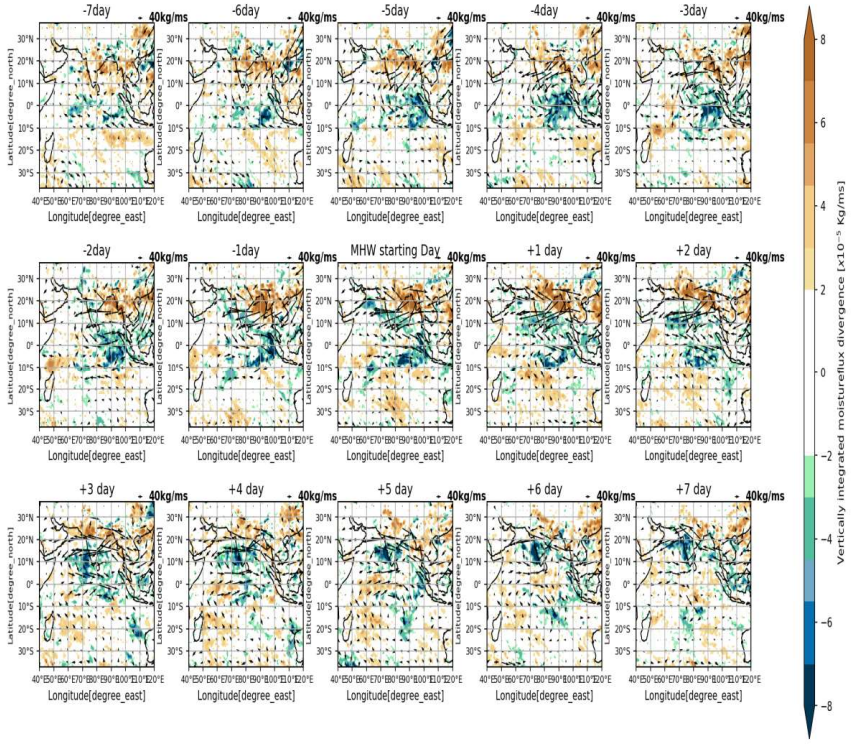

Figure 4.45: The spatial plot of the composite of vertically integrated moisture flux divergence anomalies of the 7 days before and after the starting date of MHW in the North Bay of Bengal (85°E–93°E–15°N–23°N) region, using ERA5 moisture flux convergence datasets from 1982-2018.

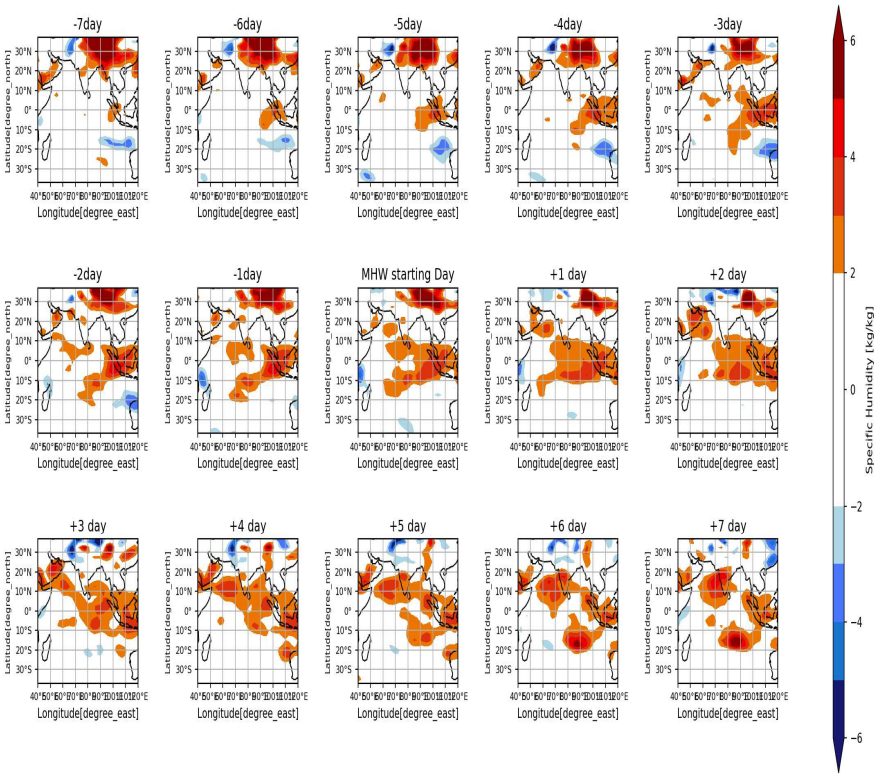

Figure 4.46: The spatial plot of the composite of vertically integrated specific humidity anomalies of the 7 days before and after the starting date of MHW in the North Bay of Bengal (85°E–93°E–15°N–23°N) region, using NCEP/NCAR specific humidity datasets from 1982-2018.

From figures 4.45 and 4.46 are given more information about moisture transport and specific humidity. In the case of moisture flux convergence, we can see that before the onset of MHW, there is no moisture transport. But after the start date of MHW, five days onwards over south India there is moisture transport and convergence. The northeasterly winds mainly carry the moisture. The vertically integrated specific humidity also agrees with the results.

4.3. Impacts of Marine Heat Waves events on Indian summer monsoon

So far, we are discussing various features of MHWs in the Indian Ocean and the factors leading to the emergence of MHWs in the Indian Ocean. Now in this chapter, we have to look into the main research question. Is there any relation with MHWs and southwest monsoon?

The North Bay of Bengal region experienced more number of events (94) during the period 1982-2018 than the Somali region (it has only 66 events). We know that the Indian Ocean has two regions, where the MHW activity is high during the Southwest Monsoon season. Both regions may have different signatures because of their position in the Indian Ocean. We have seen that the Somali region experienced 149 days long and 206°C days cumulative intensity MHW event, while North Bay of Bengal has the largest event of 40 days. From these statistics, it is clear that the Somali region experienced intense warming caused by so-called MHWs. Moreover, we realized that the weakening of wind is the common culprit for the anomalous warming events in the Indian Ocean.

Southwest monsoon over Indian landmass is very important because it provides water security over the subcontinent and holds the agricultural sector, ultimately providing food security. There are so many questions like; do these monstrous events have any impact on the monsoon rainfall distribution over the Indian subcontinent? If so, how will it be?

To answer all these questions regarding the relation of these events with the Southwest Monsoon, we have to carry out a detailed analysis of atmospheric parameters during MHW days (during the summer monsoon period).

4.3.1. Composite Analysis of Atmospheric Parameters in the Somali region (41°E–56°E–8°S–8°N) During Summer Monsoon period (June-September)

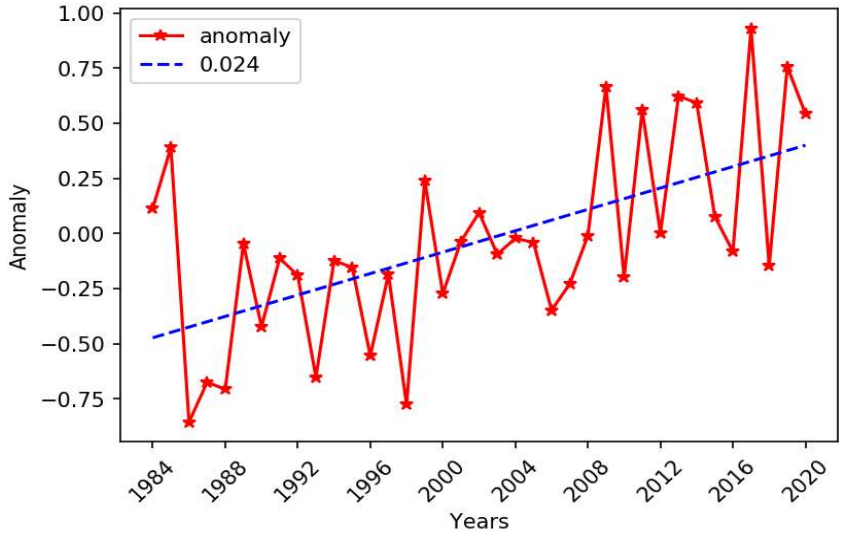

Figure 4.47: Time series of Sea Surface Temperature Anomaly (SSTA) during JJAS (in Somali (41°E–56°E–8°S–8°N) region) from 1982-2018.

Several studies warning about the temperature rise, the Indian Ocean also experiencing warming. From figure 4.47, it is clear that the Sea Surface Temperature Anomaly in the Somali region during the summer monsoon period is increasing monotonically with a slope value of 0.022.

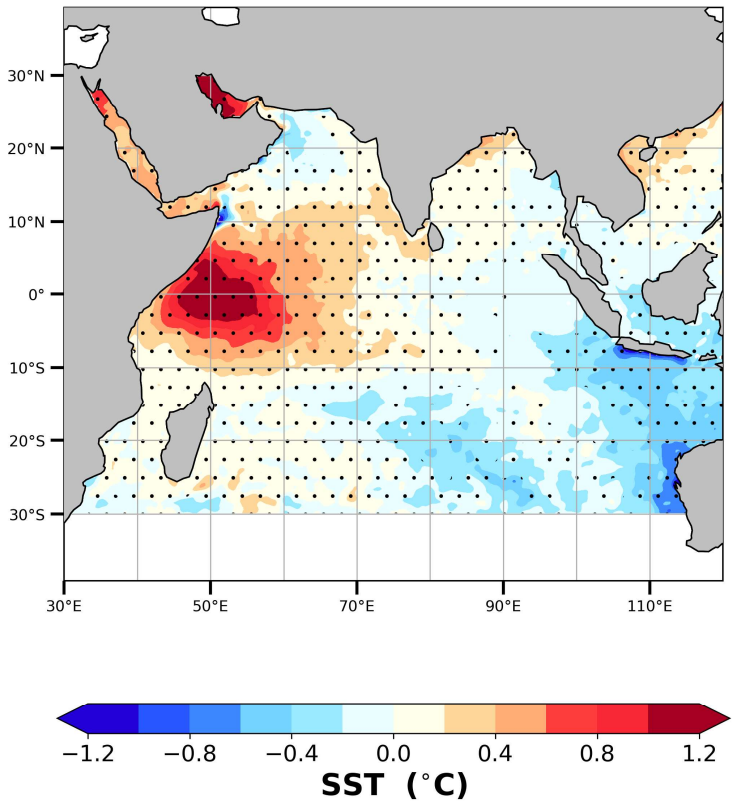

Figure 4.48: Composite of daily Sea Surface Temperature Anomalies (SSTA) for MHW days during JJAS over the Somali (41°E–56°E–8°S–8°N) region (in °C) using OISST datasets from 1982-2018. Dots represent 95% significance.

When we analyze the SST anomaly composite of MHW days during the Summer Monsoon period over the Somali region (figure 4.48), It clearly shows a warm pool area, with temperature anomaly varying from 0.9 to 1.2 °C in the Somali region. The Somali region has high SST during the MHW days, and the negative omega values (ranging from -0.02 to -0.05 Pascal/sec), from figure 4.49 together show more convective activities in this region.

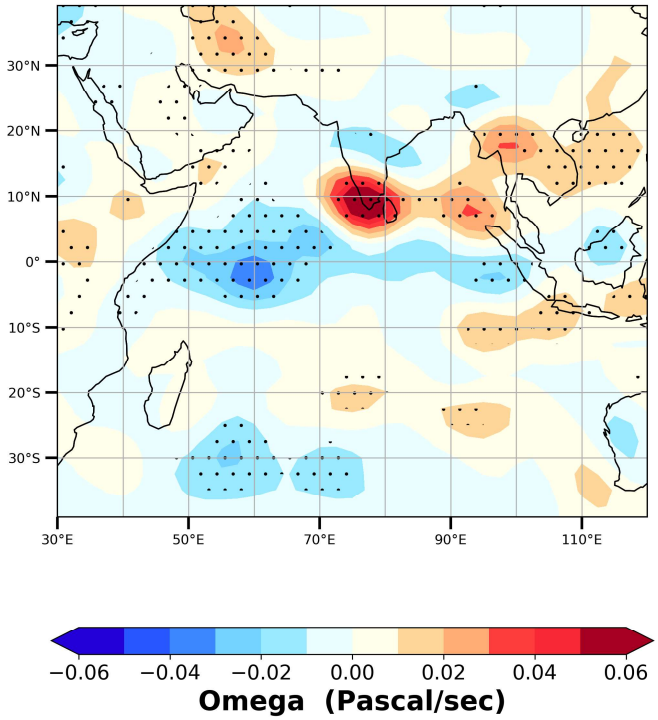

Figure 4.49: Composite of daily vertical velocity anomalies (omega) (in Pascal/sec) (at 500 hPa) for MHW days during JJAS over the Somali (41°E–56°E–8°S–8°N) region using NCEP/NCAR reanalysis datasets from 1982-2018. Dots represent 95% significance.

The negative anomaly of omega means more vertical motion, which is due to the warm SST area probably having accelerated evaporation to the atmosphere, which results in the ascending motion of air, and more convective activity.

From figure 4.50, negative OLR values (around -6 W/m^2) are observed in the Somali region, suggesting more clouds and more convective activity in this region. The wind anomaly at 850 hPa indicates the weak south-westerlies.

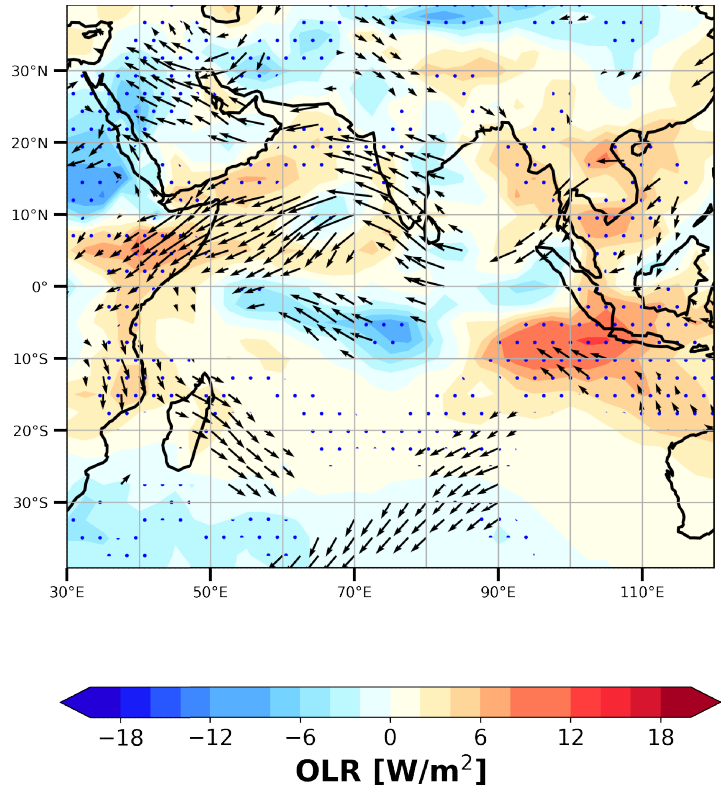

Figure 4.50: Composite of daily circulation anomalies at 850 hPa (in m/s $^{-2}$) and Outgoing Long wave Radiation(OLR) anomalies(in W /m ^{2}) for MHW days during JJAS over Somali (41°E–56°E–8°S–8°N) region using NCEP/NCAR reanalysis datasets from 1982-2018. Dots represent 95% significance.

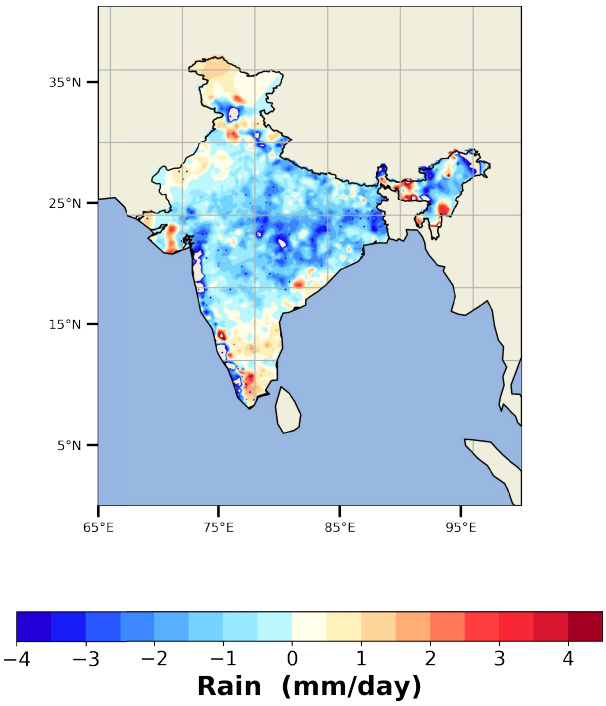

Figure 4.51: Composite of daily rainfall (in mm/day) for MHW days (in Somali (41°E–56°E–8°S–8°N) region) during JJAS over the Indian subcontinent using IMD daily rainfall datasets from 1982-2018. Dots represent 95% significance.

The unusual warming in this particular region caused by the weak winds and may further weaken the monsoon winds. Moreover, the rainfall pattern during MHW days over the Indian landmass strengthens the fact that the (figure 4.51) MHW events in the Somali region are triggering high SST that will intensify the convection, and making a low-pressure region, which attracts the wind. This leading to the weakening of the Summer Monsoon winds and could not reach into the Indian land mass. From figure 4.52, it is clear that there are only a few regions that show a correlation between the number of MHW events in the Somali and rainfall in the Indian landmass.

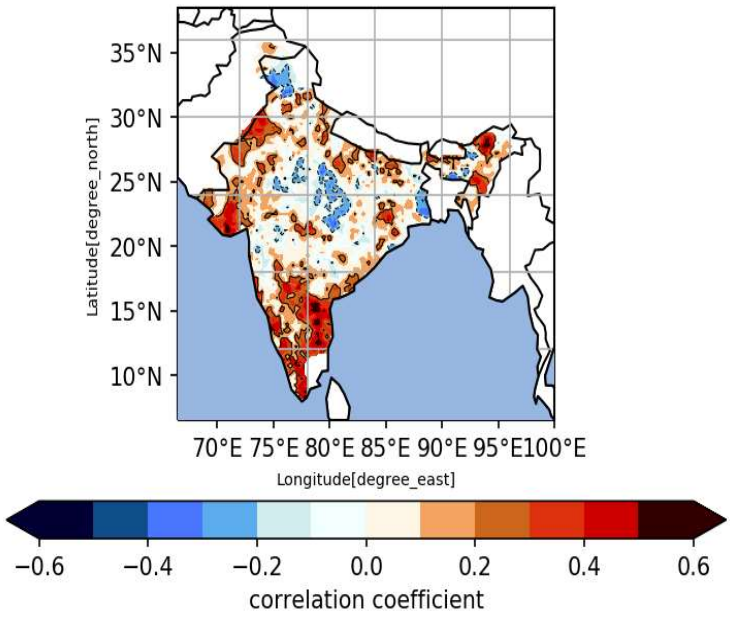

Figure 4.52: Correlation map between precipitation (IMD-daily dataset) anomalies (in mm/day) in the Indian landmass and the number of MHW events in the Somali (41°E–56°E–8°S–8°N) during JJAS from 1982-2018.

Figure 4.53 shows the mean meridional circulation over 41-100 °E for the Somali region MHW days during the JJAS for the period 1982-2018. From the picture, the equator has increased convection (negative omega values for entire levels) during MHW days. Moreover, there is a suppressed convection (positive vertical velocity values for entire levels) in the Indian subcontinent, which means a suppressed rainfall over the landmass during the MHW days.

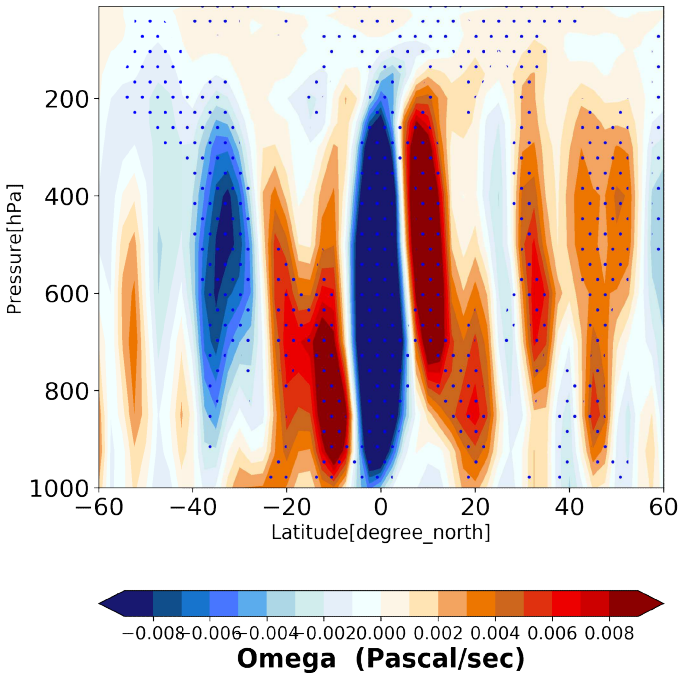

Figure 4.53: Mean meridional circulation over 41-100 °E (vertical velocity in Pascal/sec) for MHW days (in Somali (41°E–56°E–8°S–8°N) region) during JJAS using NCEP/NCAR reanalysis daily datasets from 1982-2018. Dots represent 95% significance.

McPhaden, M, J. (1999) reported that the El Nino is the key contributor of MHW events in the tropical Ocean because El Nino events always cause the weakening of walker circulation and leading to the piling-up of warm water. According to Holbrook NJ, et al. (2019), MHWs in the western Indian Ocean are mainly due to the climatic modes and teleconnections which make the weakening of the monsoon winds. These things may lead to positive feedback in the Somali region that the weakening monsoon winds may lose the strength and affect the upwelling process in the Somali, ultimately induce the warm water accumulation leading to the genesis of more MHW events. However in the western Indian Ocean, there is another study also discussing the same kind of result according to them, the warming in the western equatorial Indian Ocean region (45-60 °E and 10 °S-10 °N) is due to the zonal advection and this warming causes weak monsoon over India (Fathrio *et al.,* 2018).

Hence we can conclude that the MHW activities in Somali during Summer Monsoon may suppress the Indian Subcontinent's southwest monsoon rainfall. Roxy *et al*. (2015) point out that the warming in the Indian Ocean weakens the summer monsoon's main driver, which is the land-sea thermal contrast and leads to the monsoon circulation weakening and drying of the central Indian subcontinent. It also concluded that on a longer time scale the warmer ocean has a major impact on the weakening of monsoon because of the high seasonal variation in this area and the short-term continuity of atmospheric shifts. Thus the MHWs in the Somali region cause abnormal heating and probably have wind convergence and enhanced convection, ultimately weakening the monsoon over the Indian subcontinent.

4.3.2. Composite Analysis of Atmospheric Parameters in the North Bay of Bengal region (85°E–93°E–15°S–23°N) During Summer Monsoon period [June-September]

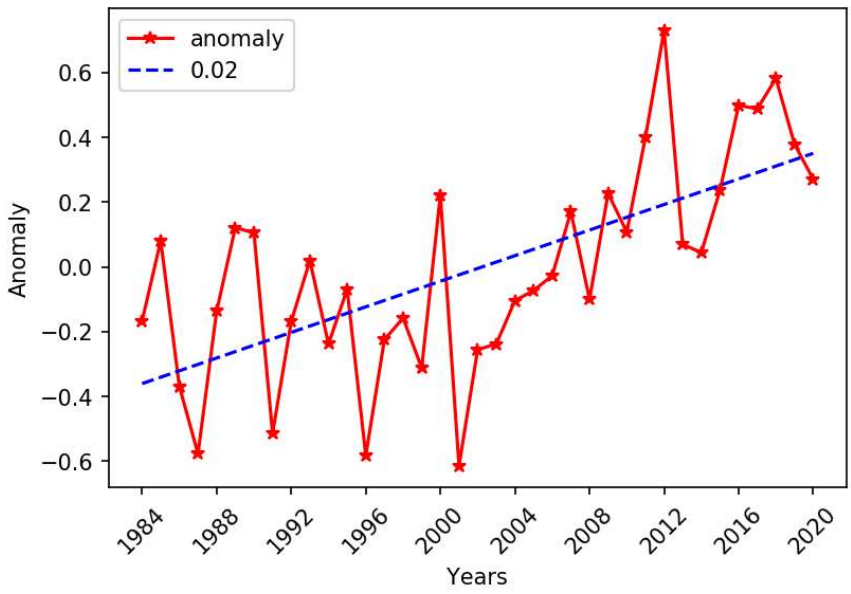

Figure 4.54: Time series of Sea Surface Temperature Anomaly (SSTA) during JJAS from 1982-2018 for the north Bay of Bengal (85°E–93°E–15°N–23°N) region.

From figure 4.54, similar to the Somali region north Bay of Bengal region also has an increasing trend of Sea Surface Temperature. When we look into the SST anomalies during June-September, it is increasing monotonically with a slope value of 0.02.

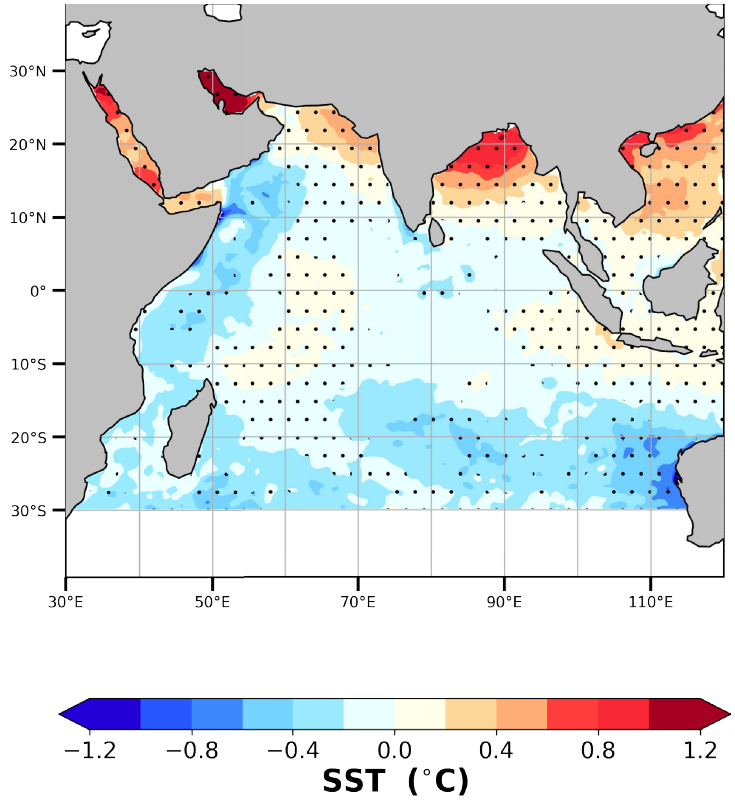

Figure 4.55: Composite of daily Sea Surface Temperature Anomalies (SSTA) for MHW days during the JJAS, over north Bay of Bengal (85°E–93°E–15°N–23°N) region (in °C) using OISST datasets from 1982-2018. Dots represent 95% significance.

That is during the period 1982-2018; SST in the north Bay of Bengal region is increasing.

The picture (fig 4.55) illustrates the higher SST in the north Bay of Bengal region during the June-September MHW days. It causes higher vertical velocity, but the positive OLR values imply the absence of cloud cover in this region (clear sky during strong MHW events). However, negative OLR values (around -6 W/m^2) in figure 4.57 and omega (500 hPa level) (figure 4.56) over the western Indian Ocean and the Indian subcontinent (southern India) suggest more convergence and strong ascending motion in this region.

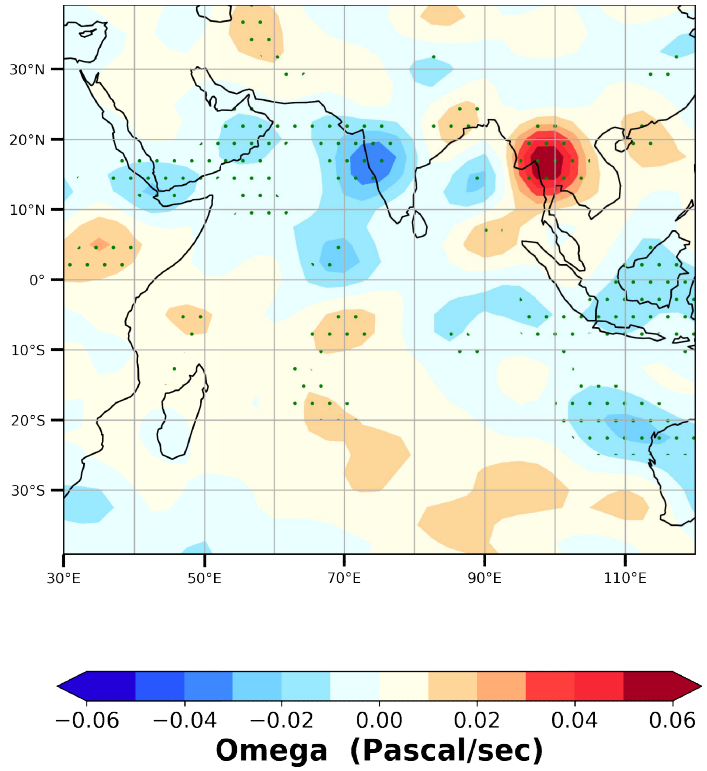

Figure 4.56: Composite of daily vertical velocity anomalies (omega in Pascal/sec) (at 500 hPa) for MHW days during JJAS over north Bay of Bengal (85°E–93°E–15°N–23°N) region using NCEP/NCAR reanalysis datasets from 1982-2018. Dots represent 95% significance.

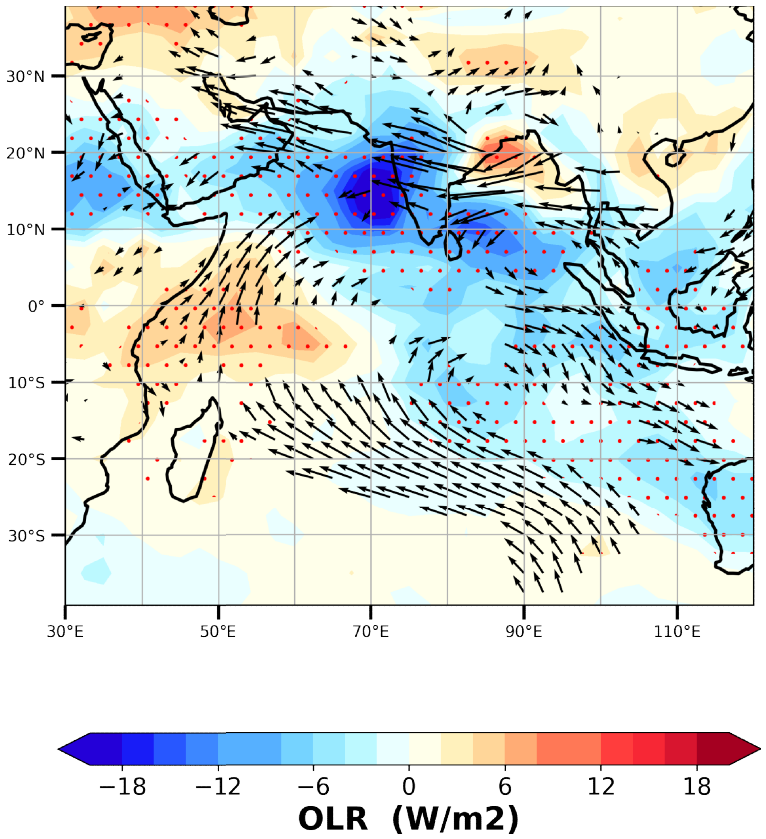

Figure 4.57: Composite of daily circulation anomalies at 850 hPa (in m/s $^{-2}$) and Outgoing Long wave Radiation(OLR) anomalies(in W /m ^{2}) for MHW days during JJAS over north Bay of Bengal region (85°E–93°E–15°N–23°N) using NCEP/NCAR reanalysis datasets from 1982-2018. Dots represent 95% significance.

The wind anomaly at 850 hPa (figure 4.57) indicates a convergence of the wind in the same region where the OLR and omega are negative. The distribution of precipitation (figure 4.58) during MHW days (JJAS) together shows that the MHW events in the north Bay of Bengal region are triggering convergence of winds and precipitation in south India. Moreover suppressed cloudiness and positive OLR values in the north Bay of Bengal region (probably due to strong MHW events in that region).

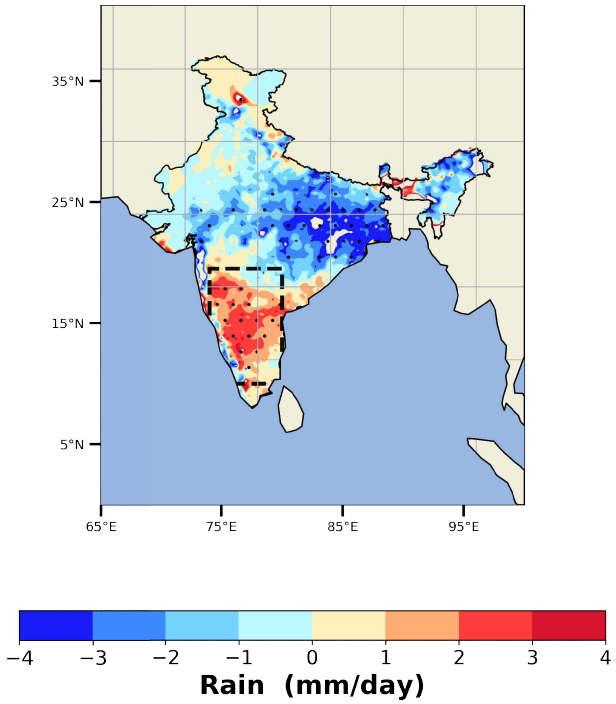

Figure 4.58: Composite of daily rainfall (in mm/day) for MHW days (in north Bay of Bengal region (85°E–93°E–15°N–23°N)) during JJAS over the Indian subcontinent using IMD datasets from 1982-2018. Dots represent 95% significance.

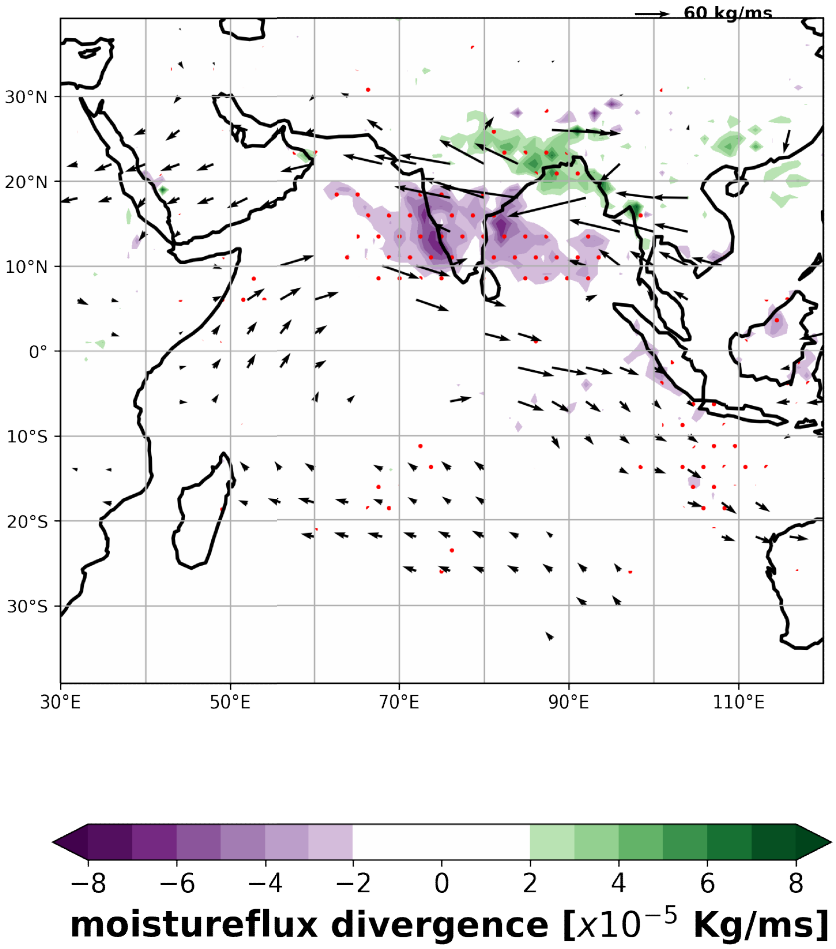

Figure 4.59: Composite of daily moisture flux convergence (in kg/ms) for MHW days (in north Bay of Bengal (85°E–93°E–15°N–23°N) region) during JJAS over the Indian subcontinent using ERA5 moisture flux divergence datasets from 1982-2018.

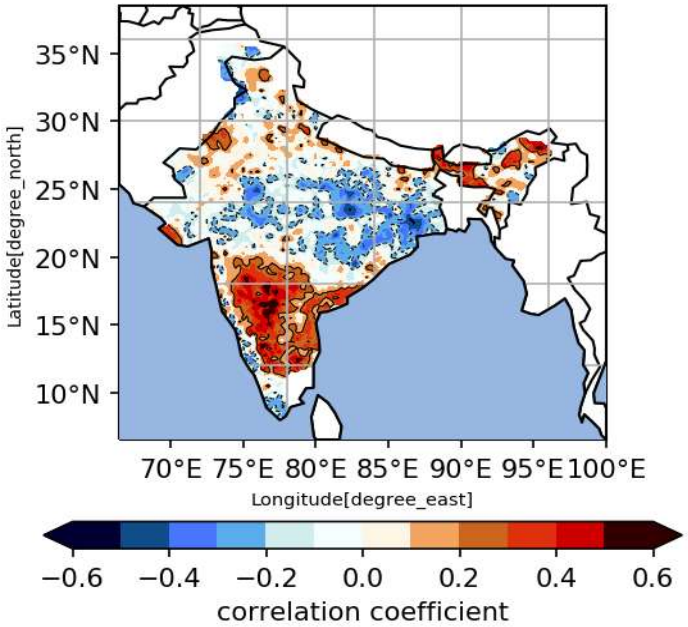

Figure 4.60: Correlation map between the rainfall (IMD-daily dataset) anomalies in the Indian landmass and the number of MHW events in the north Bay of the Bengal (85°E–93°E–15°N–23°N) region during JJAS, for the period 1982-2018.

The composite of moisture flux convergence over the Indian landmass gives us a pretty good idea about the rainfall pattern. Here in figure 4.59 during MHW days, there is moisture transport by the easterlies and convergence over the South Indian region. Besides, we can see the moisture flux divergence over the north Bay of Bengal region during the MHW days. As a whole, there is a relation between the MHWs in the north Bay of Bengal and summer monsoon rainfall over south India.

Figure 4.60 strengthens the results that we can see in south India, showing a high correlation between the number of MHW events in the Bay of Bengal and summer rainfall.

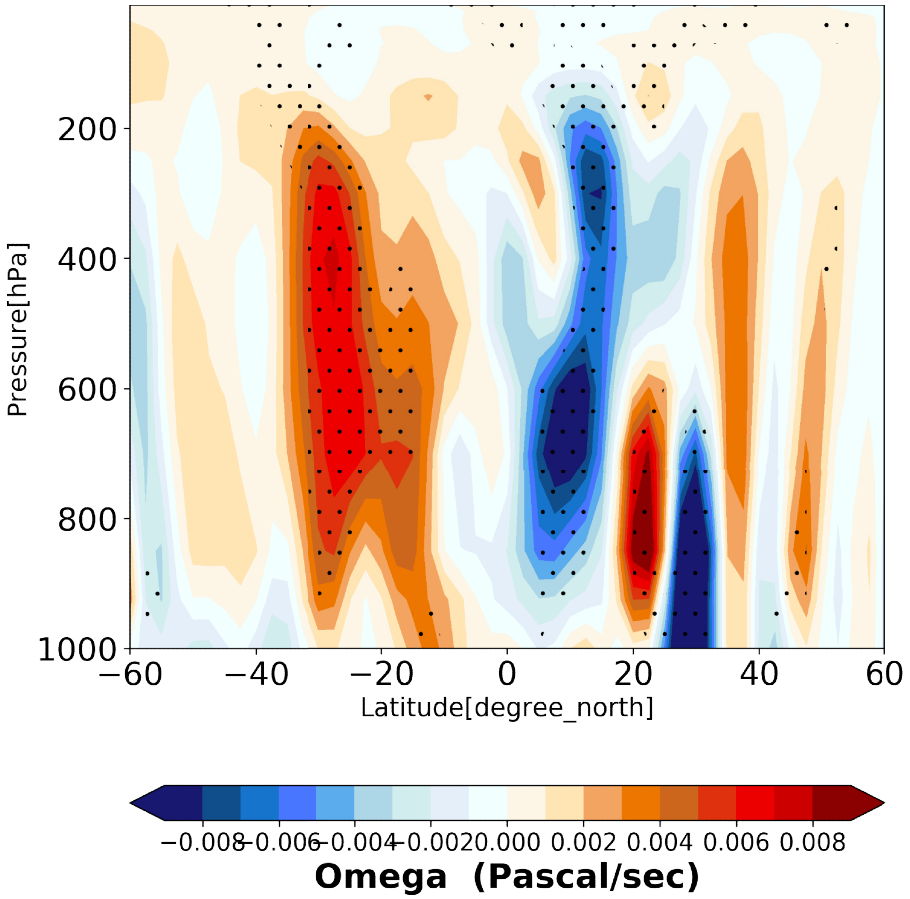

Figure 4.61: Mean meridional circulation over 41-100 °E (vertical velocity at 500 hPa) for MHW days [in north Bay of Bengal (85°E–93°E–15°N–23°N) region] during JJAS in (Pascal/sec), using NCEP/NCAR reanalysis daily omega datasets from 1982-2018. Dots represent 95% significance.

Figure 4.61 shows mean meridional circulation over 41-100 °E for the north Bay of Bengal region during the JJAS MHW days for the period 1982-2018. From the picture, equator and landmass (also 30-degree lat) have increased convection during MHW days, supporting the previous results, while there is a suppressed convection in the 20-degree latitude.

Moreover, Mishra *et, al* (2012) showed that the warming in the Bay of Bengal region triggers high monsoon rainfall over south India, this is generally a lagged response of ENSO and which causing monsoon variability over India. Hence the MHW activities in the north Bay of Bengal region during JJAS may have an association with the summer rainfall over Indian Subcontinent (particularly in southern India).

4.3.3. Marine Heat Waves (MHWs) interaction with Madden-Julian Oscillation (MJO) and Indian Monsoon Intra seasonal Oscillation (MISO)

In the previous discussion, we have found out that there is a connection between Madden-Julian Oscillation (MJO) and MHWs in both selected regions. That is in both areas MHWs are related to the MJO 1, 2 phases. MJO is an oscillation of 40-50 days, propagating eastward direction along the tropics, which is associated with suppressed (enhanced) convective activities. Likewise, there is another oscillation of 30-60 days over the southwest monsoon domain called as Indian Monsoon Intraseasonal Oscillation (MISO). But compared to MJO, it has propagation in the eastward and northward direction (Krishnamurti and Subrahmanyam, 1982; Lau and Chan, 1986). So this is a complex oscillation and also affects the summer monsoon over the Indian region.

We have done the probability distribution of MHW days during the summer monsoon with MJO and MISO phases. Figure 4.62 shows the results, the left column is for the Somali region and right column is for the north Bay of Bengal region, the first row represents the probability density with the MJO phases for both the selected region, while in the second row represents MISO. In the first row, the green bar represents the probability density of the MJO phase in the seven days before the start date of MHW. In contrast, the blue bar is the probability distribution of MJO phases during the entire MHWs days in the JJAS period. In the case of MJO, both the region is associated with the 1 and 2 phases. We could see that the Somali region MHWs have more probability with the 1, 2 phase of MJO, both for the pre-condition of MHW and for the entire MHW days.

In the second raw yellow bar represents the probability density of the MISO phase with the pre-condition of MHWs (7 days before the onset of MHWs). In contrast, the red bar represents the probability distribution of

MISO phases during the entire MHWs days in the JJAS period. In the case of the Somali region, MISO phase 4 is dominant during the pre-condition of MHW, while during the MHW days there is no marked relation with MISO. So we can assume that MHWs in the Somali region are more connected with MJO 1 and 2 phases because this region is situated in the equator. During 1, 2 phases of MJO is in the Indian Ocean.

The north Bay of Bengal region MHWs is associated with MISO. During the pre-condition of MHWs, MISO 1 and 2 phases have a dominant pattern (almost 50%). Figure 4.63 a and b shows the composite of 20-50 days filtered wind at 850 hPa and OLR anomalies during 1 and 2 phase of MISO. We can see that there are easterlies over the Bay of Bengal region during these phases, which means there are weak south-westerlies (may have a contribution to the genesis of MHWs, due to the relaxation of wind). On the other hand, during the entire JJAS MHW days, 3 and 4 phases (almost 40%) are dominant. According to Konda and Vissa, (2019) the phase 3, in the northern Indian Ocean has the presence of both eastward and northward ISO. They also added that phase 1-3 has the eastward-moving signal of ISO.

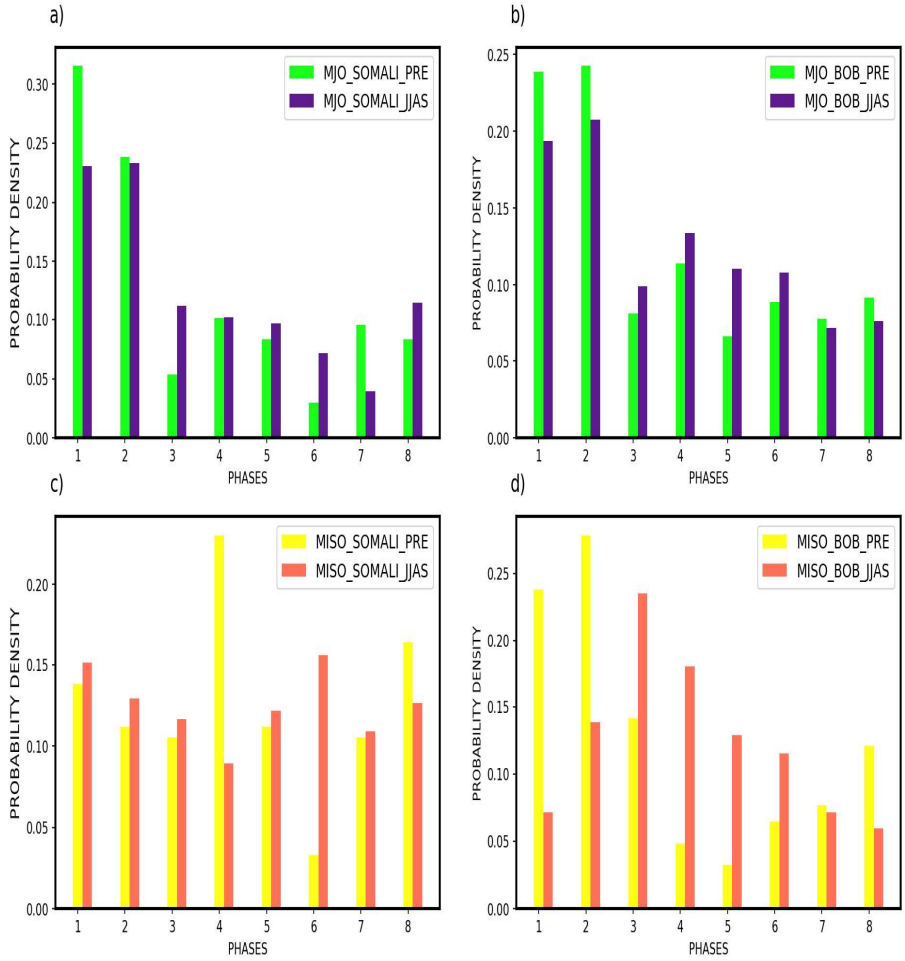

Figure 4.62: a) Probability distribution of MJO index phases during and before 7 days of the start date of MHW days during the summer monsoon period in the Somali (41°E–56°E–8°S–8°N) region (1982-2018). b) Probability distribution of MJO index phases during and before 7 days of the start date of MHW days during the summer monsoon period in the north Bay of Bengal region (1982-2018). c) Probability distribution of MISO index phases during and before 7 days of the start date of MHW days during the summer monsoon period in the Somali region (1982-2018). d) Probability distribution of MISO index phases during and before 7 days of the start date of MHW days during the summer monsoon period in the north Bay of Bengal region (85°E–93°E–15°N–23°N) from 1982-2018.

Moreover, phase 4 and 5 has the active monsoon, while phases 1, 2, and 7, 8 have weak monsoon activities. In the north Bay of Bengal, the MHW days are related to the MISO, and we can see that phase 3, 4 is dominant. From the earlier results, we know that the north Bay of Bengal MHWs can be related to the rainfall over south India, and these interactions with the MISO are also strengthening our previous results. Figure 4.63 c and d indicate the composite of 3 and 4 phases of MISO, with 20-50 days filtered wind anomalies at 850 hPa and OLR anomalies. We can see an anticyclonic circulation over the northwest pacific, called western North Pacific subtropical high (WNPSH) and strong north easterlies over the north Bay of Bengal. Moreover, the moisture flux convergence over the north Bay of Bengal in the lead-lag and composite plot also shows the presence of north easterlies.

To cut a long story short, the north Bay of Bengal MHWs and MISO phases 1, 2, 3, and 4 have a relationship. Before the onset of MHWs over the north Bay of Bengal, 1 and 2 phases are prominent and also have northeasterly winds over the Indian Ocean. In comparison, during the entire MHW days, the 3 and 4 phases dominate. In addition to these, we saw that MHWs in the north Bay of Bengal are associated with increased rainfall over south India (MISO 3 and 4 phase have increased monsoon activity over Indian landmass). Contrarily in the Somali region, MHWs are coinciding with the MJO 1 and 2 phases and do not have a strong relation with MISO phases.

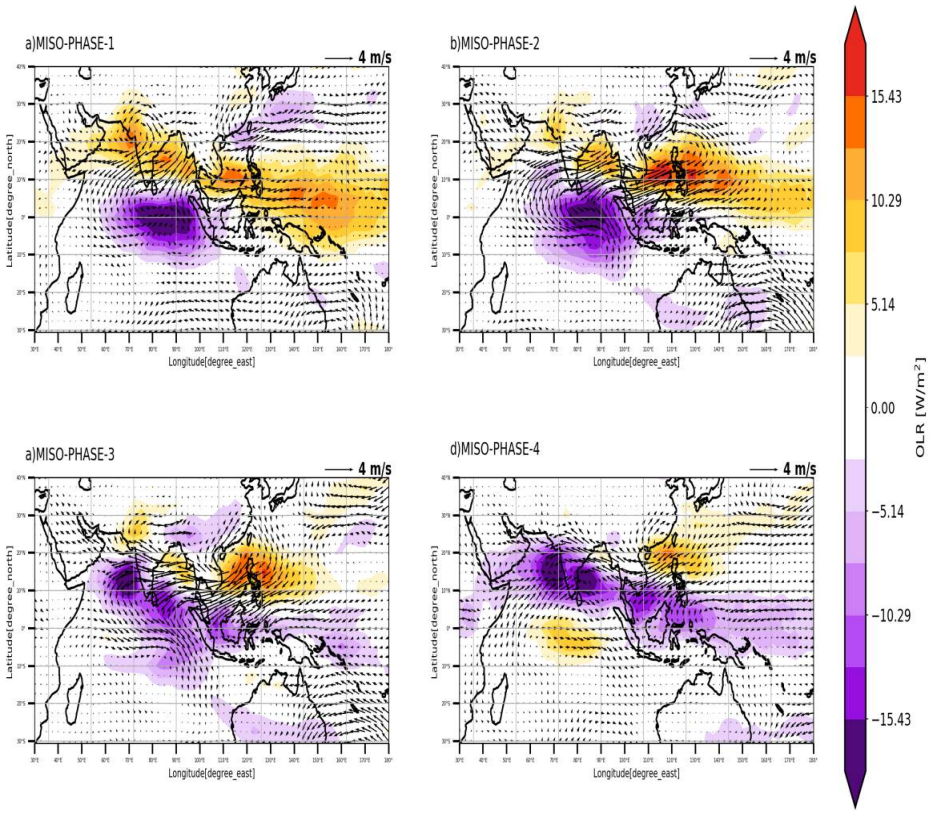

Figure 4.63: a) Composite of 20-50-day filtered wind anomaly at 850 hPa and OLR anomaly during the 1st phase of ISO (1982-2018). b) Composite of 20-50-day filtered wind anomaly at 850 hPa and OLR anomaly during the 2nd phase of ISO (1982-2018). c) Composite of 20-50-day filtered wind anomaly at 850 hPa and OLR anomaly during the 3rd phase of ISO (1982-2018). d) Composite of 20-50-day filtered wind anomaly at 850 hPa and OLR anomaly during the 4th phase of ISO (1982-2018), using NCEP/NCAR wind datasets.

CHAPTER 5
SUMMARY AND CONCLUSION

This study did a robust analysis of the MHWs in the Indian Ocean, and their impact on the convection and monsoon. A trend analysis of MHWs in the Indian Ocean shows that the Somali region experienced the largest number of MHW events, on an annual basis. When we consider the June-September trend of MHWs, along with the Somali, the north Bay of Bengal also experienced a significantly large number of MHWs. From 1982 to 2018, the Somali region witnessed 66 events, and out of these, 21events occurred in the summer monsoon period. On the other hand, the North Bay of Bengal had 94 events and out these, 34 events were in the southwest monsoon period.

From the analysis of seasonal climatology of the MHW metrics, it was found in the Somali region that all the MHW metrics except the number of events show a double peak in the seasonal climatology signal. They all are peak during March and September months. As in the case of the number of events, it shows an increasing trend, and the maximum number shows during October month (8 events). Whereas in the North Bay of Bengal region the cumulative intensity and duration have a peak during February, while area, mean intensity, and maximum intensity is in May. Further, the number of events has a prominent double peak, which is occurring during May and October months (ranging from 12-14 events). The seasonal signal of MHW metrics in the north Bay of Bengal shows peak values either in February or May, that is they show maximum values during the summer season.

The time series of the number of MHW events in the Somali region for both during the annual and summer monsoon period have shown that the numbers of MHW events are increasing after 1997, with slope values of

0.14 (annually), 0.037 (during June-September). Similarly, in the north Bay of Bengal region, it appears that the number of MHWs increased after 1997 and had the slope values of 0.091 (annually), 0.054 (during June-September).

Later we did a correlation analysis between the global SST distribution and number of MHW events for both regions. Interestingly, both the correlation maps showed an El Niño -like pattern. Moreover, from the pattern correlation between the SST trend map and the correlation map, there are high correlation values for both regions. This indicates that global ocean warming has a major role in driving the MHWs in both regions. In the Somali region, along with El Niño, positive IOD has contributed to the MHW events. While the North Bay of Bengal does not show the IOD pattern, except had a warming pattern in the Indian Ocean basin.

Apart from the IOD, ENSO, and the global warming trend, the MJO might play a role in the manifestation of MHWs in the Indian Ocean. It turned out that, from the probability distribution of MJO phases during the MHW days annually and during the summer monsoon, for both regions Somali and north Bay of Bengal there is relation with the MJO 1, 2 phases. Hence, there might be a connection between the MJO with MHWs in both regions.

From the area analysis of MHW events, it emerged that in the Somali region, the size of MHWs is varying from 1 million km^2- 2 million km^2 for both annually and summer monsoon. Moreover, the 2015 event has the largest area (2.25 million km^2). Contrastingly in the north Bay of Bengal region, the size of MHW is varying from 0.25 million km^2 - 0.5 million km^2. On an annual basis, the 1995 event has the largest area (0.51 million km2). Additionally, during the summer monsoon period, the size of MHW

is varying from 0.3 million km^2 - 0.5 million km^2 and the 2008 (0.5 million km^2) events hold the largest area.

It has become evident that week monsoon winds follow the largest MHW events in the Somali region. Though, the smallest events do not have a similar pattern. On the contrary, over the north Bay of Bengal region, there is north easterlies over the north Indian Ocean and a wind convergence over the Indian landmass.

The factors that lead to the genesis of MHWs in both regions are also explored. We did a lead-lag correlation between SST and wind, latent heat flux, sensible heat flux, upward longwave radiation, downward solar radiation, and OLR. From all of these, it is clear that during the MHW days for both regions, the wind anomalies first dropped, and later after 2 or 4 days, SST started to rise. It is also found that both regions have different factors affecting the genesis of MHWs. In the case of the Somali region from the heat budget analysis, it is revealed that heat transport by the ocean currents has a major role in the formation of MHWs. As in the case of heat fluxes, the downward solar radiation and OLR are high before the onset of MHWs. In the case of sensible and upward longwave radiation is started to release from the ocean after the outset of MHWs. It can be concluded that the weakening of wind in the Somali region restricts the ocean currents to transport heat from the equator to northwards. In addition to that, the increased solar radiation and decreased evaporation cooling heat the ocean surface which together leads to the manifestation of anomalously warm water in the Somali region. In the case of rainfall, it has very small correlation values. From the spatial plots of precipitation, vertically integrated moisture flux, and the vertically integrated specific humidity, it turns out that, the rainfall over India shows a decreasing pattern coincides with the onset of MHWs in the Somali region.

For the MHW initiation in the North Bay of Bengal, it is found from the lead-lag analysis that the wind speed is decreasing first almost three days before the SST increase, while latent heat release is decreasing. That is, in the north Bay of Bengal region, the solar radiation is heating the ocean surface. At the same time, the tranquility in the wind decreases the evaporation cooling, leading to the piling up of warm water in this region. After 5/6 days the heat is released from the ocean as latent heat, sensible heat, and upward longwave radiation.

The heat budget analysis also agrees with the current results, from the heat budget in the North Bay of Bengal region the temperature change is attributed by the net heat flux changes, especially the latent heat flux and solar radiation downward. In the case of rainfall, there will be an increase in rainfall over India (particularly over south India) after the onset of MHWs in the north Bay of Bengal (on $+6^{th}$ day). Vertically integrated moisture flux anomaly composite shows that the moisture is transported to the North Bay of Bengal region by the north easterlies.

Afterwards, we concentrated on the main research topic, which is the interaction between MHWs and Indian summer monsoon. It is fascinating that both regions in the Indian Ocean have different signatures. Firstly, in the Somali region, from composite analysis of SST, OLR, wind (at 850 hPa) anomalies, and rainfall anomalies over India. It is revealed that the onset of MHWs in the Somali affects the wind that is it shows weak southwest winds. It may be due to the intense warming in the Somali region where this intense warm pool area creates low pressure and drags the wind into this region. Ultimately, this prevents the establishment of strong southwest monsoon winds in the Indian Ocean.

On the other hand, the North Bay of Bengal MHWs influences monsoon in another way. It has been discovered that the north Bay of

Bengal there is a convergence of winds. Moreover, the composite of vertically integrated moisture flux anomalies during MHW days unfold that north easterlies are transporting the moisture towards the Indian landmass, and there is moisture divergence over the north Bay of Bengal. Figures 5.1 and 5.2 give the overall picture of MHWs in the Indian Ocean.

In this study, we also examine the relation between MISO and MHWs in the Indian Ocean. It is perceived that the MHWs in the north Bay of Bengal is associated with MISO phases 1, 2, 3 and 4. During the precondition of MHWs, it is related to 1 and 2 phases, while for the entire MHW days (June-September), MISO phase 3 and 4 dominate. On the other side, the Somali MHWs did not have any noticeable relation with MISO, but they are more related to MJO 1 and 2 phases.

We have seen that the MHWs in the Indian Ocean lasted for a more extended period, as in the case of Somali, the largest event had a duration of 149 days, and on the other hand the north Bay of Bengal had 40 days. These two MHWs had cumulative intensities of 206 °C days and 40 °C days each. From these results, we can assume that it will probably affect the marine biodiversity in that particular region.

Apart from the two regions discussed here, there are other regions in the Indian Ocean where MHWs are maybe occurring at a smaller scale. From the trend plot of MHW frequency, we can see that in the northeastern Arabian Sea, there are patches of MHW prominent regions. This is important in the sense that there may be impacts on the marine ecosystem and the atmospheric conditions too. These MHWs and their consequences need to be explored in the future.

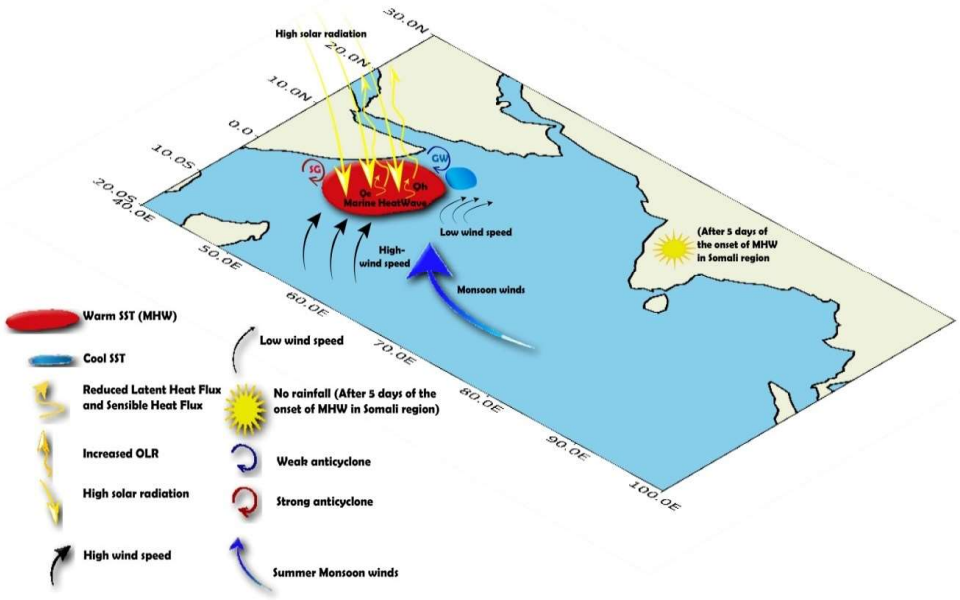

Figure 5.1: Schematic representation of MHWs in the Somali region (41°E–56°E–8°S–8°N).

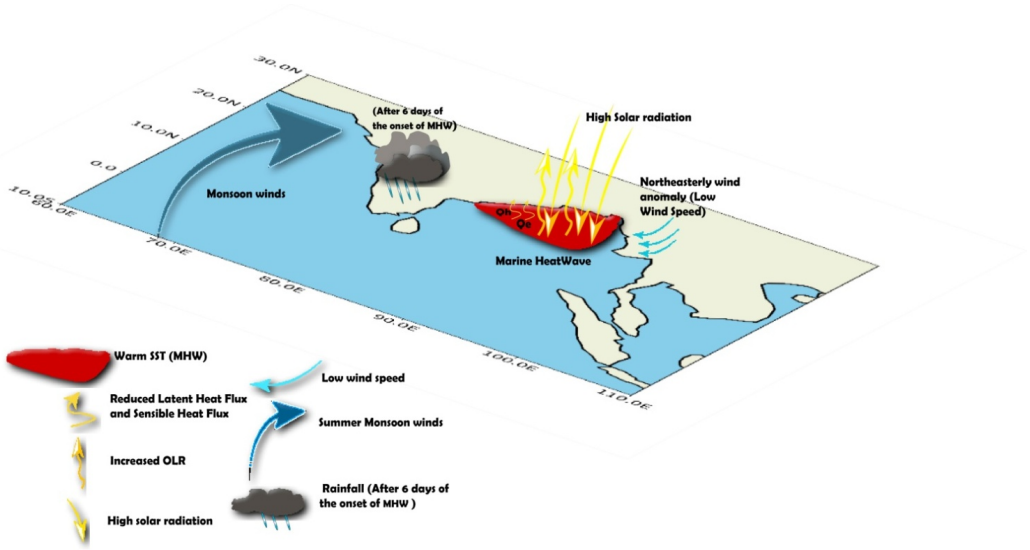

Figure 5.2: Schematic representation of MHWs in the North Bay of Bengal (85°E–93°E–15°N–23°N) region.

CHAPTER 6
SUPPLEMENTARY INFORMATION

6.1. Composite analysis using ERA5 datasets in the Somali Region (41°E–56°E–8°S–8°N).

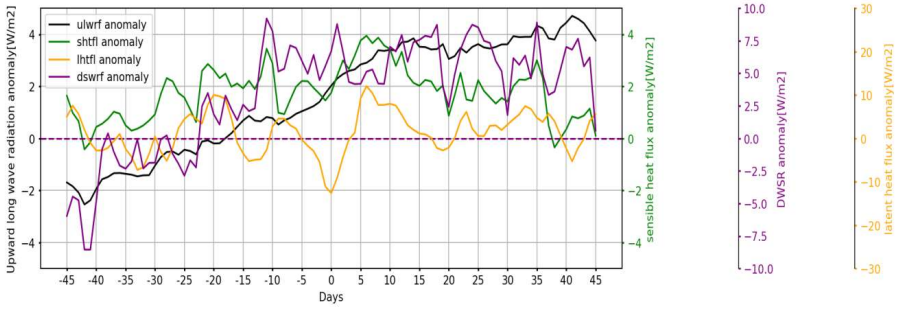

Figure 6.S1: Composite of latent heat flux (yellow line), sensible heat flux (green line), downward solar radiation (purple line), and upward long wave radiation (black line) anomalies of the 45 days before and after the starting date of MHW in the Somali (41°E–56°E–8°S–8°N) region (using ERA5 datasets from 1982-2018).

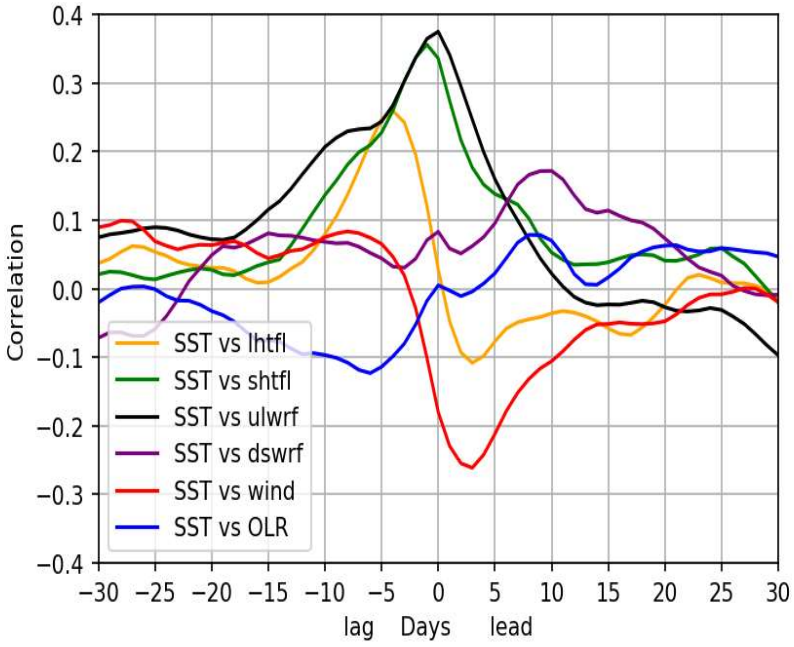

Figure 6.S2: The lead-lag correlation between SST and wind (red line), latent heat flux (orange line), sensible heat flux (green line), upward long wave radiation (black line), OLR (blue line) in the Somali (41°E–56°E–8°S–8°N) region. Estimated from the 30 days before and 30 days after the start date of MHW events (using ERA5 flux datasets from 1982-2018).

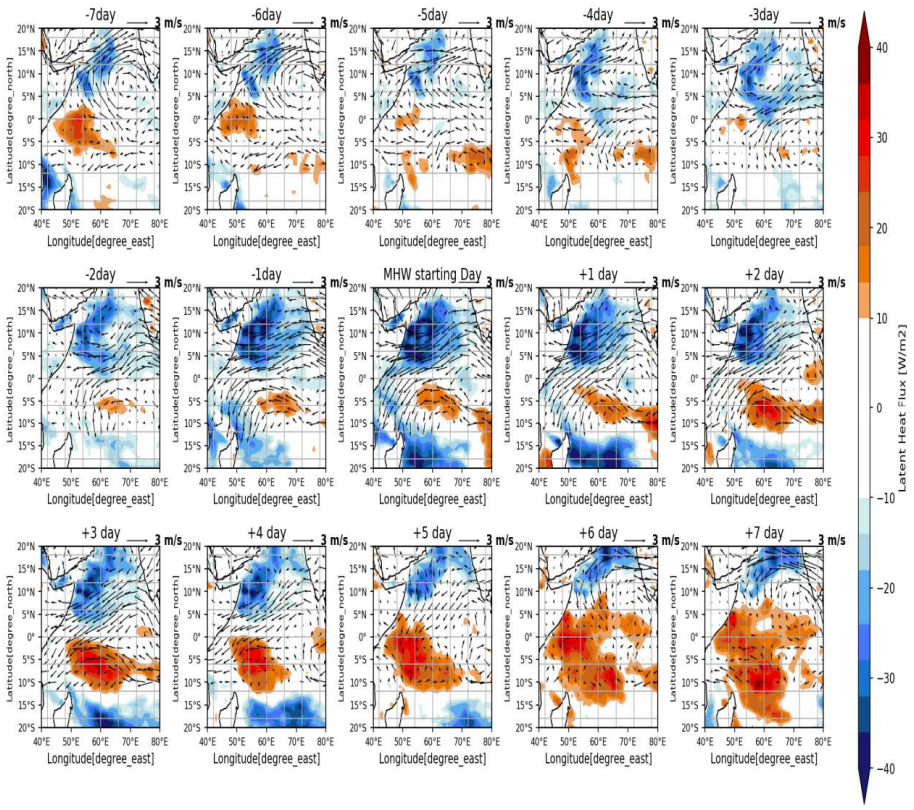

Figure 6.S3: The spatial plot of the composite of wind (at 850 hPa) & latent heat flux anomalies of the 7 days before and after the starting date of MHW in the Somali (41°E–56°E–8°S–8°N) region (using ERA5 datasets) from 1982-2018.

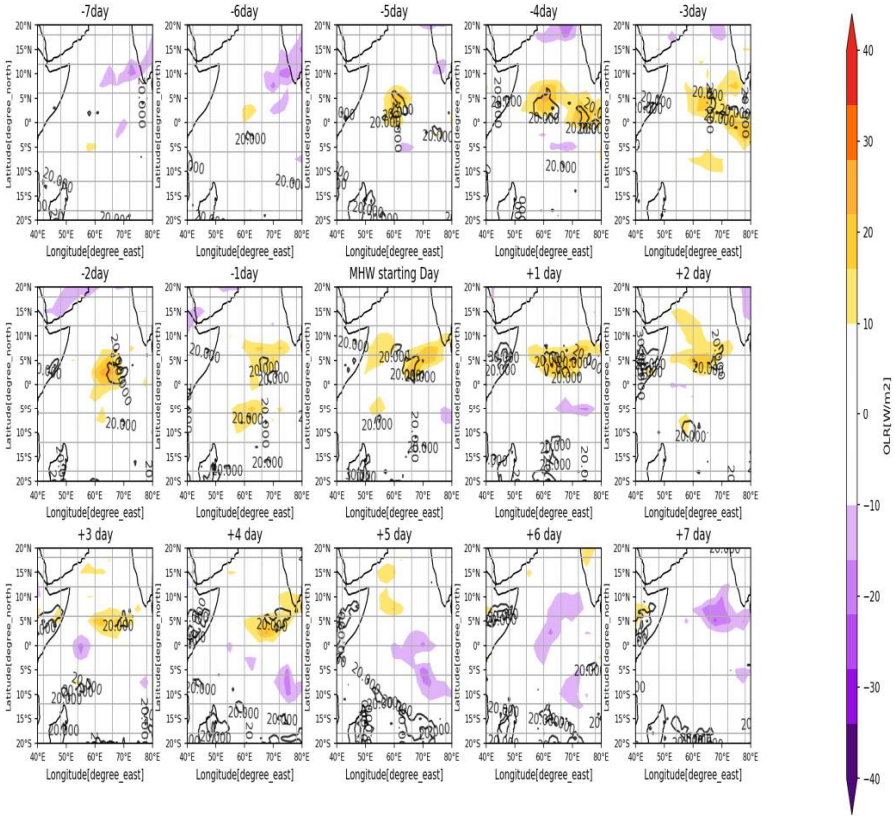

Figure 6.S4: The spatial plot of the composite of OLR & downward solar radiation anomalies of the 7 days before and after the starting date of MHW in Somali (41°E–56°E–8°S–8°N) region (using ERA5 datasets) from 1982-2018.

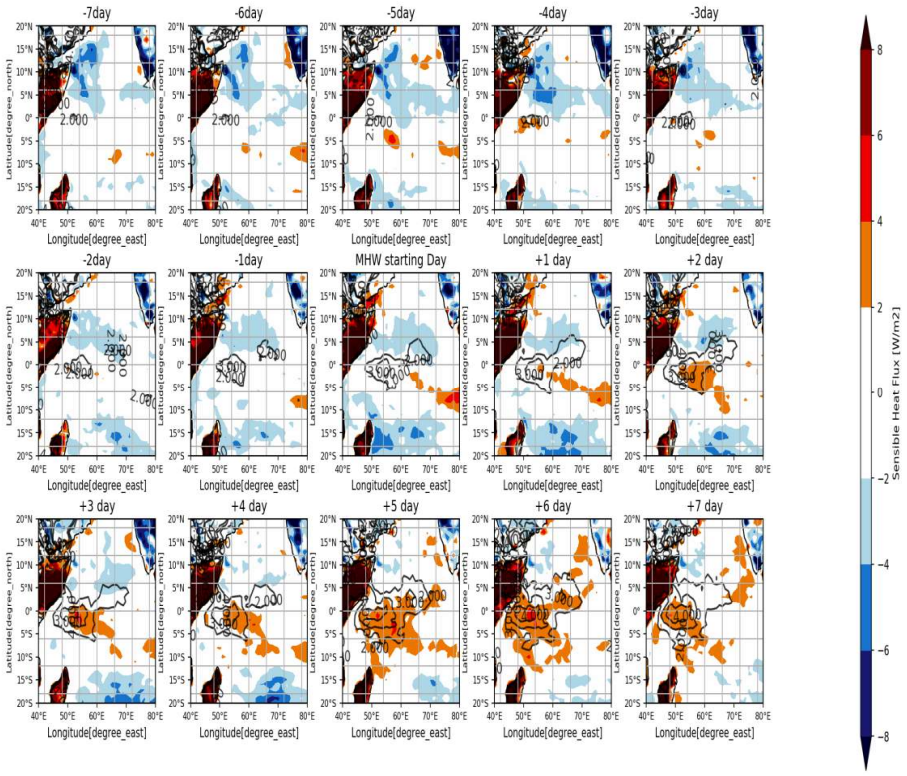

Figure 6.S5: The spatial plot of the composite of sensible heat flux and upward long wave radiation anomalies of the 7 days before and after the starting date of MHW in the Somali (41°E–56°E–8°S–8°N) region (using ERA5 datasets) from 1982-2018.

6.1.2. Ocean mixed layer heat budget analysis using HYCOM Ocean current datasets in the Somali Region (41°E–56°E–8°S–8°N).

$$\partial T_{SST}/\partial t = -v_{(\text{vertically averaged over mld})} \bullet \nabla T_{SST} + Q_{0(ERA5)}/\rho C_p H_{m(hycom)} + Res$$

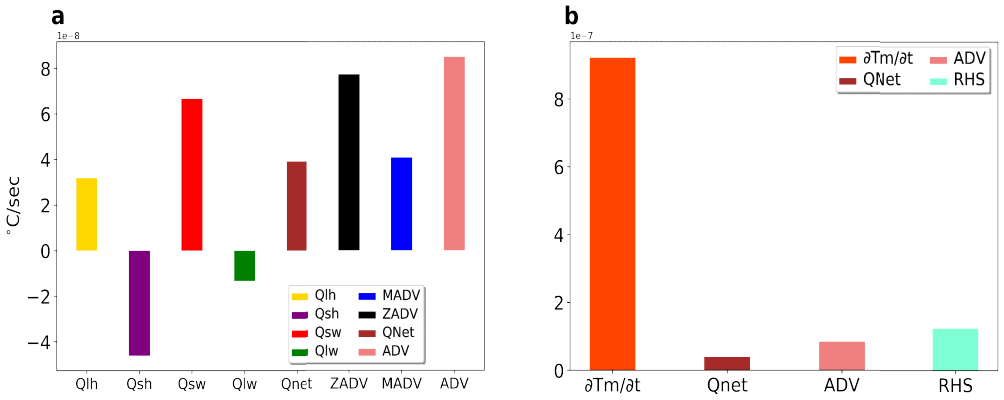

Figure 6.S6: The heat budget terms calculated for the 5 days before the starting date of MHW in the Somali (41°E–56°E–8°S–8°N) region, a) terms in the right-hand side of the temperature tendency equation, b) terms in both side of the temperature tendency equation, using the HYCOM Ocean current datasets and ERA5 fluxes from 1994 to 2015.

6.1.3. Ocean mixed layer heat budget analysis using GODAS Ocean current datasets in the Somali Region (41°E–56°E–8°S–8°N).

$$\partial T_{SST}/\partial t = -v_{(\text{vertically averaged over mld})} \bullet \nabla T_{SST} + Q_{0(ERA5)}/\rho C_p H_{m(GODAS)} + Res$$

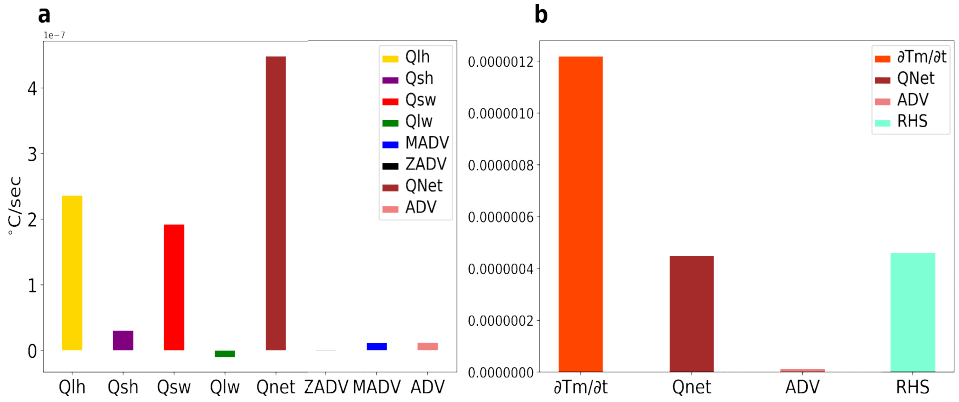

Figure 6.S7: The heat budget terms calculated for the 5 days before the starting date of MHW in the Somali (41°E–56°E–8°S–8°N) region, a) terms in the right-hand side of the temperature tendency equation, b) terms in both side of the temperature tendency equation, using the GODAS Ocean current datasets and ERA5 fluxes from 1994 to 2015.

6.2.1. Composite analysis using ERA5 datasets in the North Bay of Bengal Region (85°E–93°E–15°N–23°N).

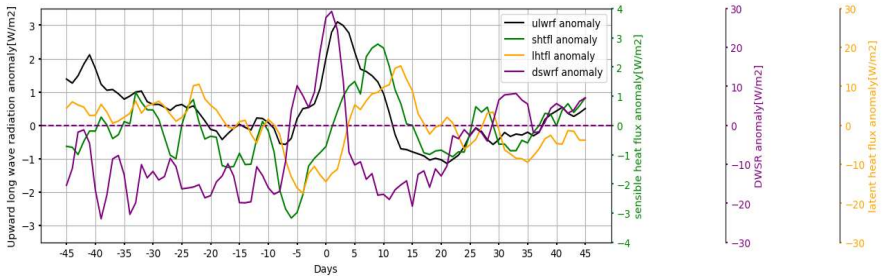

Figure 6.S8: Composite of latent heat flux (yellow line), sensible heat flux (green line), downward solar radiation (purple line), and upward long wave radiation (black line) anomalies of the 45 days before and after the starting date of MHW in the north Bay of Bengal (85°E–93°E–15°N–23°N) region (using ERA5 datasets from 1982-2018).

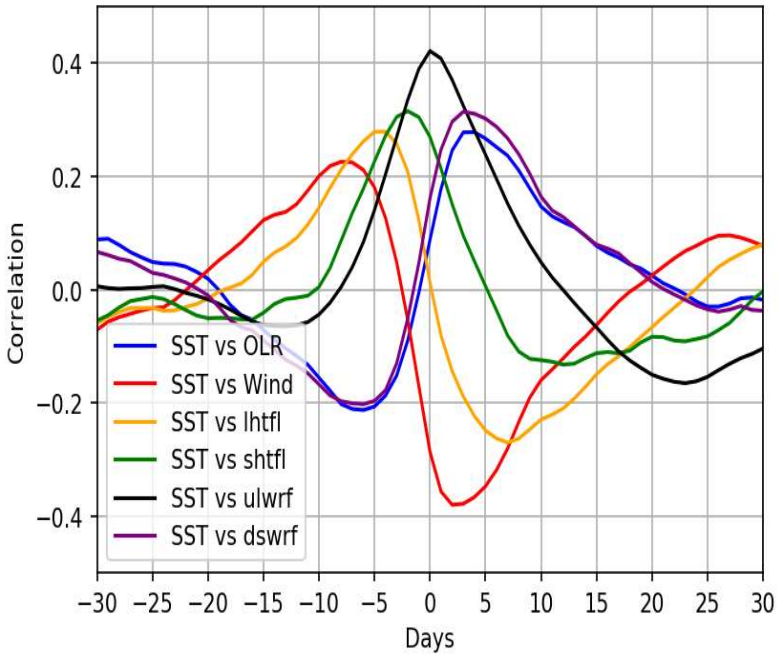

Figure 6.S9: The lead-lag correlation between SST and wind (red line), latent heat flux (orange line), sensible heat flux (green line), upward long wave radiation (black line), OLR (blue line) in the north Bay of Bengal (85°E–93°E–15°N–23°N) region. Estimated from the 30 days before and 30 days after the start date of MHW events using ERA5 reanalysis datasets from 1982-2018.

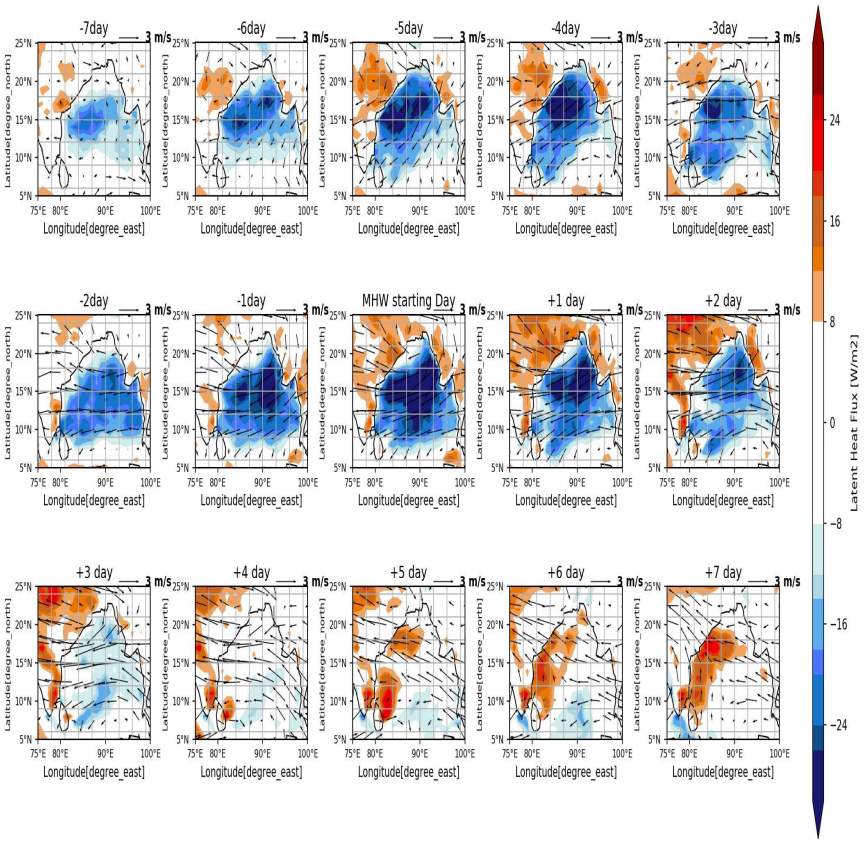

Figure 6.S10: The spatial plot of the composite of wind (850 hPa) & latent heat flux anomalies of the 7 days before and after the starting date of MHW in the north Bay of Bengal (85°E–93°E–15°N–23°N) region (using ERA5 datasets from 1982-2018).

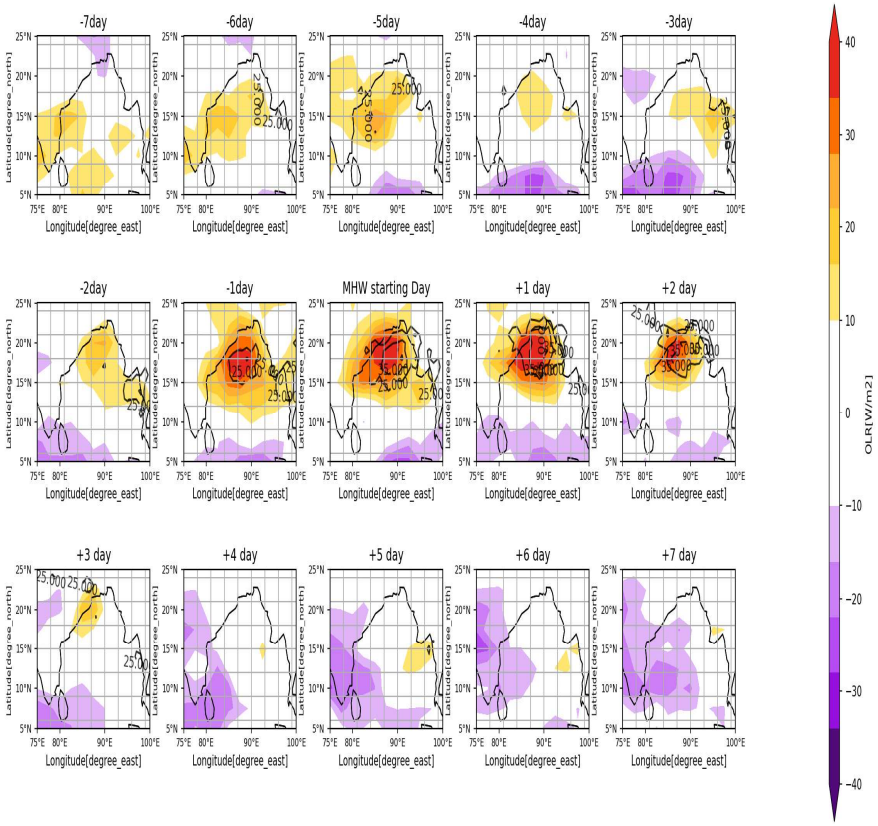

Figure 6.S11: The spatial plot of the composite of OLR & downward solar radiation anomalies of the 7 days before and after the starting date of MHW in the north Bay of Bengal (85°E–93°E–15°N–23°N) region. The colour bar represents the OLR and contours as downward solar radiation, using ERA5 datasets from 1982-2018.

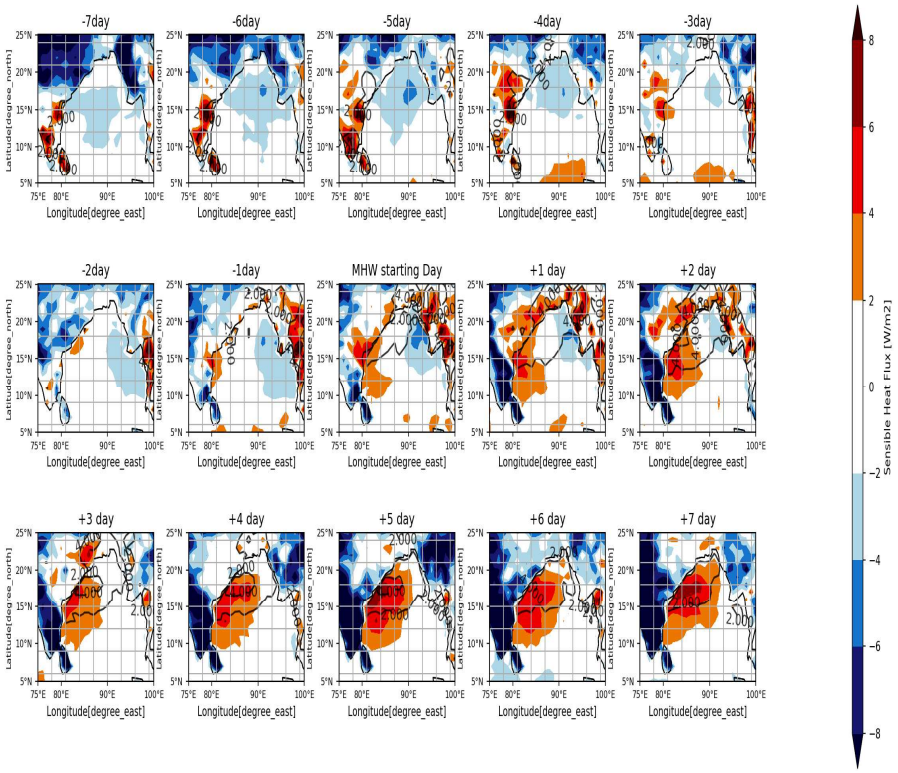

Figure 6.S12: The spatial plot of the composite of sensible heat flux and upward long wave radiation anomalies of the 7 days before and after the starting date of MHW north Bay of Bengal (85°E–93°E–15°N–23°N) region (using ERA5 datasets from 1982-2018).

6.2.2. Ocean mixed layer heat budget analysis using HYCOM Ocean current datasets in the north Bay of Bengal (85°E–93°E–15°N–23°N).

$$\partial T_{SST}/\partial t = -v_{(\text{vertically averaged over mld})} \bullet \nabla T_{SST} + Q_{0(ERA5)}/\rho C_p H_{m(hycom)} + Res$$

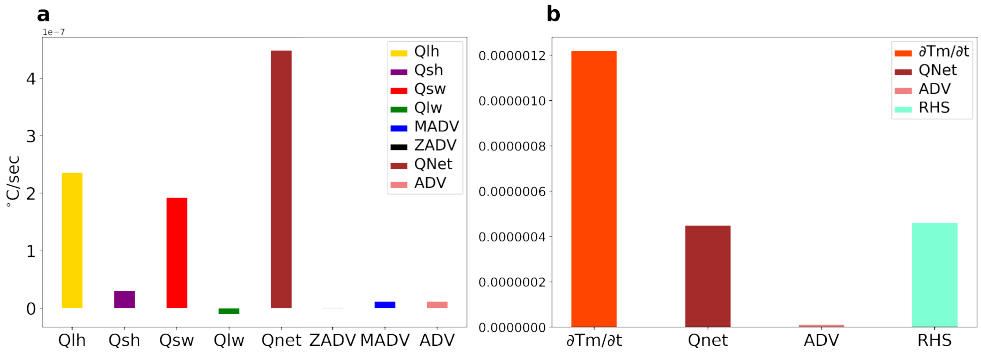

Figure 6.S13: The heat budget terms calculated for the 5 days before the starting date of MHW in the north Bay of Bengal (85°E–93°E–15°N–23°N), a) terms in the right-hand side of the temperature tendency equation, b) terms in both side of the temperature tendency equation, using the HYCOM Ocean current datasets and ERA5 fluxes from 1994 to 2015.

6.2.2. Ocean mixed layer heat budget analysis using GODAS Ocean current datasets in the north Bay of Bengal (85°E–93°E–15°N–23°N).

$$\partial T_{SST}/\partial t = -v_{(\text{vertically averaged over mld})} \cdot \nabla T_{SST} + Q_{0(ERA5)}/\rho C_p H_{m(GODAS)} + Res$$

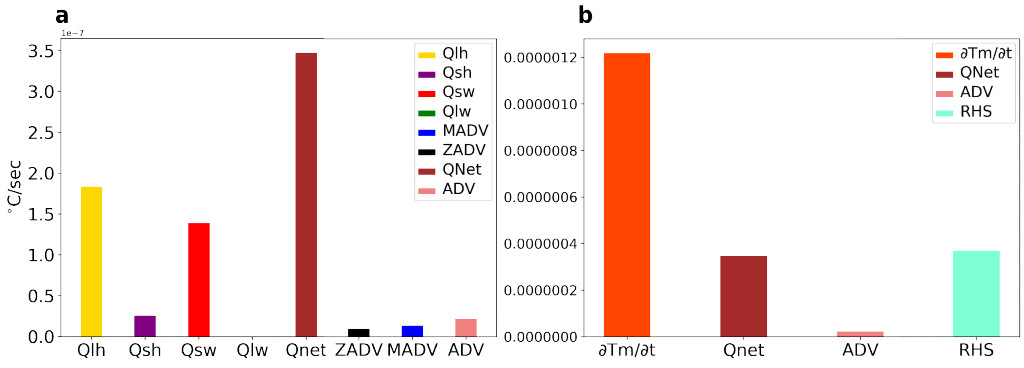

Figure 6.S14: The heat budget terms calculated for the 5 days before the starting date of MHW in the north Bay of Bengal (85°E–93°E–15°N–23°N), a) terms in the right-hand side of the temperature tendency equation, b) terms in both side of the temperature tendency equation, using the GODAS Ocean current datasets and ERA5 fluxes from 1994 to 2015.

REFERENCES

Arafeh-Dalmau, N., Montaño-Moctezuma, G., Martinez, J.A., Beas-Luna, R., Schoeman, D.S., Torres-Moye, G., 2019. Extreme Marine Heatwaves alter kelp forest community near its equatorward distribution limit. *Front. Mar. Sci.* 6: 499.

Arias-Ortiz, A., Serrano, O., Masqué, P., Lavery, P.S., Mueller, U., Kendrick, G.A., Rozaimi, M., Esteban, A., Fourqurean, J.W., Marbà, N., Mateo, M.A., Murray, K., Rule, M.J., Duarte, C.M., 2018. A marine heatwave drives massive losses from the world's largest seagrass carbon stocks. *Nat. Clim. Change*. 8(4): 338–344.

Balmaseda, M.A., Trenberth, K.E., Källén, E., 2013. Distinctive climate signals in reanalysis of global ocean heat content. *Geophys. Res. Lett*. 40(9): 1754–1759.

Behringer, D.W., 2007. 3.3 The Global Ocean Data Assimilation System (GODAS) at NCEP. In *Proceedings of the 11th Symposium on Integrated Observing and Assimilation Systems for the Atmosphere, Oceans, and Land Surface*.

Benthuysen, J.A., Tonin, H., Brinkman, R., Herzfeld, M., Steinberg, C., 2016. Intrusive upwelling in the Central Great Barrier Reef. *J. Geophys. Res. Oceans.* 121: 8395–8416.

Brandt, M.E., McManus, J.W., 2009. Disease incidence is related to the bleaching extent in reef-building corals. *Ecology*. 90(10): 2859–2867.

Brodeur, R.D., Auth, T.D., Phillips, A.J., 2019. Major Shifts in Pelagic Micronekton and Macrozooplankton Community Structure in an Upwelling Ecosystem Related to an Unprecedented Marine Heatwave. *Front. Mar. Sci.* 6: 212.

Charney, J.G., DeVore, J.G., 1979. Multiple Flow Equilibria in the Atmosphere and Blocking. *J. Atmospheric Sci.* 36(7): 1205–1216.

Chen, K., Gawarkiewicz, G., Kwon, Y.O., and Zhang, W.G. 2015. The role of atmospheric forcing versus ocean advection during the extreme warming of the Northeast US continental shelf in 2012. *J. Geophys. Res. Oceans*. 120(6): 4324-4339.

Cheung, W.W.L., Frölicher, T.L., 2020. Marine heatwaves exacerbate climate change impacts for fisheries in the northeast Pacific. *Sci. Rep*. 10(1): 1-10.

Cheung, W.W.L., Watson, R., Pauly, D., 2013. Signature of ocean warming in global fisheries catch. *Nature*. 497(7449): 365–368.

Darmaraki, S., Somot, S., Sevault, F., Nabat, P., Cabos Narvaez, W.D., Cavicchia, L., Djurdjevic, V., Li, L., Sannino, G., Sein, D.V., 2019. Future evolution of Marine Heatwaves in the Mediterranean Sea. *Clim. Dyn*. 53(3-4): 1371–1392.

Diaz, R.J., Rosenberg, R., 2008. Spreading Dead Zones and Consequences for Marine Ecosystems. *Science*. 321(5891): 926–929.

Dohan, K., Maximenko, N., 2010. Monitoring Ocean Currents with Satellite Sensors. *Oceanography.* 23(4): 94–103.

Edwards, M., Richardson, A.J., 2004. Impact of climate change on marine pelagic phenology and trophic mismatch. *Nature*. 430(7002): 881–884.

Elzahaby, Y., Schaeffer, A., 2019. Observational Insight Into the Subsurface Anomalies of Marine Heatwaves. *Front. Mar. Sci*. 6.

Evans, W., Hales, B., Strutton, P.G., Shearman, R.K., Barth, J.A., 2015. Failure to bloom: Intense upwelling results in negligible phytoplankton response and prolonged CO2 outgassing over the Oregon shelf. *J. Geophys. Res. Oceans*. 120(3): 1446–1461.

Feary, D.A., Pratchett, M.S., Emslie, M.J., Fowler, A.M., Figueira, W.F., Luiz, O.J., Nakamura, Y., Booth, D.J., 2014. Latitudinal shifts in coral reef fishes: why some species do and others do not shift. *Fish Fish*. 15(4): 593–615.

Feely, R.A., Hales, B., Sabine, C., Greeley, D., Lee, K., Alin, S., Juranek, L., 2008. A New Proxy Method for Estimating the Aragonite Saturation State of Coastal Waters Using Chemical and Hydrographic Data. AGU Fall Meet, 2008, Abstr. 33. p. OS33E-03.

Fewings, M.R., Brown, K.S., 2019. Regional Structure in the Marine Heat Wave of Summer 2015 Off the Western United States. *Front. Mar. Sci.* 6: 564.

Fordyce, A.J., Ainsworth, T.D., Heron, S.F., Leggat, W., 2019. Marine Heatwave Hotspots in Coral Reef Environments: Physical Drivers, Ecophysiological Outcomes, and Impact Upon Structural Complexity. *Front. Mar. Sci.* 6: 498.

Frölicher, T.L., 2019. Chapter 5 - Extreme climatic events in the ocean, in: Cisneros-Montemayor, A.M., Cheung, W.W.L., Ota, Y. (Eds.), *Predicting Future Oceans*. pp. 53–60. Elsevier.

Frölicher, T.L., Fischer, E.M., Gruber, N., 2018. Marine heatwaves under global warming. *Nature*. 560(7718): 360–364.

Garrabou, J., Coma, R., Bensoussan, N., Bally, M., Chevaldonné, P., Cigliano, M., Diaz, D., Harmelin, J.G., Gambi, M.C., Kersting, D.K., Ledoux, J.B., Lejeusne, C., Linares, C., Marschal, C., Pérez, T., Ribes, M., Romano, J.C., Serrano, E.,

Teixido, N., Torrents, O., Zabala, M., Zuberer, F., Cerrano, C., 2009. Mass mortality in Northwestern Mediterranean rocky benthic communities: effects of the 2003 heat wave. *Glob. Change Biol*. 15(5): 1090–1103.

Hobday, A.J., Alexander, L.V., Perkins, S.E., Smale, D.A., Straub, S.C., Oliver, E.C.J., Benthuysen, J.A., Burrows, M.T., Donat, M.G., Feng, M., Holbrook, N.J., Moore, P.J., Scannell, H.A., Sen Gupta, A., Wernberg, T., 2016. A hierarchical approach to defining marine heatwaves. *Prog. Oceanogr*. 141: 227–238.

Hoegh-Guldberg, O., 1999. Climate change, coral bleaching, and the future of the world's coral reefs. *Mar. Freshw. Res*. 50(8): 839–866.

Holbrook, N.J., Scannell, H.A., Gupta, A.S., Benthuysen, J.A., Feng, M., Oliver, E.C.J., Alexander, L.V., Burrows, M.T., Donat, M.G., Hobday, A.J., Moore, P.J., Perkins-Kirkpatrick, S.E., Smale, D.A., Straub, S.C., Wernberg, T., 2019. A global assessment of marine heatwaves and their drivers. *Nat. Commun*. 10(1): 1–13.

Hovel, K.A., Wahle, R.A., 2010. Effects of habitat patchiness on American lobster movement across a gradient of predation risk and shelter competition. *Ecology*. 91(7): 1993–2002.

Hughes, T.P., Kerry, J.T., Álvarez-Noriega, M., Álvarez-Romero, J.G., Anderson, K.D., Baird, A.H., Babcock, R.C., Beger, M., Bellwood, D.R., Berkelmans, R., and Bridge, T.C., 2017. Global warming and recurrent mass bleaching of corals. *Nature*. 543(7645): 373-377.

Jackson, J.M., Johnson, G.C., Dosser, H.V., Ross, T., 2018. Warming From Recent Marine Heatwave Lingers in Deep British Columbia Fjord. *Geophys. Res. Lett.* 45(16): 9757–9764.

Johnson, C.R., Banks, S.C., Barrett, N.S., Cazassus, F., Dunstan, P.K., Edgar, G.J., Frusher, S.D., Gardner, C., Haddon, M., Helidoniotis, F., Hill, K.L., Holbrook, N.J., Hosie, G.W., Last, P.R., Ling, S.D., Melbourne-Thomas, J., Miller, K., Pecl, G.T., Richardson, A.J., Ridgway, K.R., Rintoul, S.R., Ritz, D.A., Ross, D.J., Sanderson, J.C., Shepherd, S.A., Slotwinski, A., Swadling, K.M., Taw, N., 2011. Climate change cascades: Shifts in oceanography, species' ranges and subtidal marine community dynamics in eastern Tasmania. *J. Exp. Mar. Biol. Ecol*., Global change in marine ecosystems. 400(1-2): 17–32.

Kersting, D.K., Bensoussan, N., Linares, C., 2013. Long-Term Responses of the Endemic Reef-Builder Cladocora caespitosa to Mediterranean warming. *PLoS ONE 8*. 8(8): p.e70820.

Krishnamurti, T.N., Subrahmanyam, D., 1982. The 30–50 Day Mode at 850 mb During MONEX. *J. Atmospheric Sci.* 39: 2088–2095.

Krishnan, P., Roy, S.D., George, G., Srivastava, R.C., Anand, A., Murugesan, S., Kaliyamoorthy, M., Vikas, N., Soundararajan, R., 2011. Elevated sea surface temperature during May 2010 induces mass bleaching of corals in the Andaman. *Curr. Sci.* 100: 111–117.

Lau, K.-M., Chan, P.H., 1986. Aspects of the 40–50 Day Oscillation during the Northern Summer as Inferred from Outgoing Longwave Radiation. *Mon. Weather Rev.* 114(7): 1354–1367.

Lee, T., Fukumori, I., Tang, B., 2004. Temperature Advection: Internal versus External Processes. *J. Phys. Oceanogr.* 34(1): 1936–1944.

Leggat, W.P., Camp, E.F., Suggett, D.J., Heron, S.F., Fordyce, A.J., Gardner, S., Deakin, L., Turner, M., Beeching, L.J., Kuzhiumparambil, U., Eakin, C.M., Ainsworth,

T.D., 2019. Rapid Coral Decay Is Associated with Marine Heatwave Mortality Events on Reefs. *Curr. Biol.* 29(16): 2723-2730.

Maloney, E.D., Kiehl, J.T., 2002. MJO-Related SST Variations over the Tropical Eastern Pacific during Northern Hemisphere Summer. *J. Clim.* 15(6): 675–689. Available: https://doi.org/10.1175/15200442(2002)015<0675:MRSVOT>2.0.CO;2https://doi.org [28 June 2020].

Manta, G., Mello, S. de, Trinchin, R., Badagian, J., Barreiro, M., 2018. The 2017 Record Marine Heatwave in the Southwestern Atlantic Shelf. *Geophys. Res. Lett.* 45(2): Available: https://doi.org/10.1029/2018GL081070 [28 June 2020].

Marbà, N., Duarte, C.M., 2010. Mediterranean warming triggers seagrass (Posidonia oceanica) shoot mortality. *Glob. Change Biol.* 16(8): 2366–2375. Available: https://doi.org/10.1111/j.1365-2486.2009.02130.x [21 June 2020].

Marbà, N., Jorda, G., Agusti, S., Girard, C., Duarte, C.M., 2015. Footprints of climate change on Mediterranean Sea biota. *Front. Mar. Sci.* 2: 56.

Mills, K.E., Pershing, A.J., Brown, C.J., Chen, Y., Chiang, F.-S., Holland, D.S., Lehutha, S., Nye, J.A., Sun, J.C., Thomas, A.C., Wahle, R.A., 2013. Fisheries Management in a Changing Climate: Lessons from the 2012 Ocean Heat Wave in the Northwest Atlantic. *Oceanography*. 26(2): 191–195.

Mishra, V., Smoliak, B.V., Lettenmaier, D.P., Wallace, J.M., 2012. A prominent pattern of year-to-year variability in Indian Summer Monsoon Rainfall. *Proc*. *Natl. Acad. Sci.* 109(19): 7213–7217. Available: https://doi.org/10.1073/pnas.1119150109 [21 June 2020].

Muller-Parker, G., D'Elia, C., Cook, C., 2015. Interactions Between Corals and Their Symbiotic Algae. pp. 99–116.

Oliver, E.C., Benthuysen, J.A., Bindoff, N.L., Hobday, A.J., Holbrook, N.J., Mundy, C.N., and Perkins-Kirkpatrick, S.E., 2017. The unprecedented 2015/16 Tasman Sea marine heatwave. *Nat.commun. 8*(1): 1-12.

Oliver, E.C.J., Donat, M.G., Burrows, M.T., Moore, P.J., Smale, D.A., Alexander, L.V., Benthuysen, J.A., Feng, M., Gupta, A.S., Hobday, A.J., Holbrook, N.J., Perkins-Kirkpatrick, S.E., Scannell, H.A., Straub, S.C., Wernberg, T., 2018. Longer and more frequent marine heatwaves over the past century. *Nat. Commun.* 9(1): 1–12. Available: https://doi.org/10.1038/s41467-018-03732-9 [23 June 2020].

Orlowsky, B., Seneviratne, S.I., 2012. Global changes in extreme events: regional and seasonal dimension. *Clim. Change.* 110(3-4): 669–696. Available: https://doi.org/10.1007/s10584-011-0122-9 [22 June 2020].

Pearce, A.F., Feng, M., 2013. The rise and fall of the "marine heat wave" off Western Australia during the summer of 2010/2011. *J. Mar. Syst.* 111: 139–156.

Perkins, S.E., Alexander, L.V., 2012. On the Measurement of Heat Waves. *J. Clim.* 26(13): 4500–4517.

Perkins-Kirkpatrick, S.E., White, C.J., Alexander, L.V., Argüeso, D., Boschat, G., Cowan, T., Evans, J.P., Ekström, M., Oliver, E.C.J., Phatak, A., Purich, A., 2016. Natural hazards in Australia: heatwaves. *Clim. Change.* 139(1): 101–114.

Pinsky, M.L., Fogarty, M., 2012. Lagged social-ecological responses to climate and range shifts in fisheries. *Clim. Change.* 115(3-4): 883–891.

Reed, D., Washburn, L., Rassweiler, A., Miller, R., Bell, T., Harrer, S., 2016. Extreme warming challenges sentinel status of kelp forests as indicators of climate change. *Nat. Commun.* 7(1): 1–7.

Rodrigues, R.R., Taschetto, A.S., Gupta, A.S., Foltz, G.R., 2019. Common cause for severe droughts in South America and marine heatwaves in the South Atlantic. *Nat. Geosci.* 12(8): 620–626.

Roxy, M.K., Gnanaseelan, C., Parekh, A., Chowdary, J.S., Singh, S., Modi, A., Kakatkar, R., Mohapatra, S., Dhara, C., Shenoi, S.C., Rajeevan, M., 2020. Indian Ocean Warming, in: Krishnan, R., Sanjay, J., Gnanaseelan, Chellappan, Mujumdar, M., Kulkarni, A., Chakraborty, S. (Eds.), Assessment of Climate Change over the Indian Region: A Report of the Ministry of Earth Sciences (MoES), Government of India. Springer, Singapore, pp.191–206.Available: https://doi.org/10.1007/978-981-15-4327-2_10 [15 June 2020].

Roxy, M.K., Ritika, K., Terray, P., Masson, S., 2014. The Curious Case of Indian Ocean Warming. *J. Clim.* 27: 8501–8509. Available: https://doi.org/10.1175/JCLI-D-14-00471.1 [12 June 2020].

Roxy, M.K., Ritika, K., Terray, P., Murtugudde, R., Ashok, K., Goswami, B.N., 2015. Drying of Indian subcontinent by rapid Indian Ocean warming and a weakening land-sea thermal gradient. *Nat. Commun.* 6(1): 1–10.

Schaeffer, A., Gramoulle, A., Roughan, M., Mantovanelli, A., 2017. Characterizing frontal eddies along the East Australian Current from HF radar observations. *J. Geophys. Res. Oceans.* 122(5): 3964–3980.

Schlegel, R.W., Oliver, E.C.J., Wernberg, T., Smit, A.J., 2017. Nearshore and offshore co-occurrence of marine heatwaves and cold-spells. *Prog. Oceanogr.* 151: 189–205.

Simpson, S.D., Jennings, S., Johnson, M.P., Blanchard, J.L., Schön, P.-J., Sims, D.W., Genner, M.J., 2011. Continental Shelf-Wide Response of a Fish Assemblage to Rapid Warming of the Sea. *Curr. Biol.* 21(8): 1565–1570.

Smith, K.A., Dowling, C.E., Brown, J., 2019. Simmered Then Boiled: Multi-Decadal Poleward Shift in Distribution by a Temperate Fish Accelerates During Marine Heatwave. *Front. Mar. Sci.* 6: 407.

Sorte, C.J.B., Fuller, A., Bracken, M.E.S., 2010. Impacts of a simulated heat wave on composition of a marine community. *Oikos.* 119(12): 1909-1918.

Stott, P.A., Christidis, N., Otto, F.E.L., Sun, Y., Vanderlinden, J.-P., Oldenborgh, G.J. van, Vautard, R., Storch, H. von, Walton, P., Yiou, P., Zwiers, F.W., 2016. Attribution of extreme weather and climate-related events. *WIREs Clim. Change.* 7(1): 23-41. Available: https://doi.org/10.1002/wcc.380 [18 June 2020].

Stramma, L., Schmidtko, S., Levin, L.A., Johnson, G.C., 2010. Ocean oxygen minima expansions and their biological impacts. *Deep-Sea Res. Part Oceanogr. Res. Pap.* 57(4): 587-595. Available: https://doi.org/10.1016/j.dsr.2010.01.005 [18 June 2020].

Suhas, E., Neena, J.M., Goswami, B.N., 2013. An Indian monsoon intraseasonal oscillations (MISO) index for real time monitoring and forecast verification. *Clim. Dyn.* 40(11-12): 2605-2616. Available: https://doi.org/10.1007/s00382-012-1462-5 [20 June 2020].

Thomsen, M.S., Mondardini, L., Alestra, T., Gerrity, S., Tait, L., South, P.M., Lilley, S.A., Schiel, D.R., 2019. Local Extinction of bull kelp (Durvillaea spp.) due to a marine heatwave. *Front. Mar. Sci.* 6: 84.

Walker, H.J., Hastings, P.A., Hyde, J.R., Lea, R.N., Snodgrass, O.E., Bellquist, L.F., 2020. Unusual occurrences of fishes in the Southern California Current System during the warm water period of 2014–2018. *Estuar. Coast. Shelf Sci.* 236: 106634.

Wernberg, T., Smale, D.A., Tuya, F., Thomsen, M.S., Langlois, T.J., Bettignies, T. de, Bennett, S., Rousseaux, C.S., 2013. An extreme climatic event alters marine ecosystem structure in a global biodiversity hotspot. *Nat. Clim. Change.* 3(1): 78-82. Available: https://doi.org/10.1038/nclimate1627 [09 July 2020].

Wheeler, M.C., Hendon, H.H., 2004. An All-Season Real-Time Multivariate MJO Index: Development of an Index for Monitoring and Prediction. *Mon. Weather Rev.* 132(8): 1917-1932.

Yao, Y., Wang, J., Yin, J., Zou, X., 2020. Marine Heatwaves in China's Marginal Seas and Adjacent Offshore Waters: Past, Present, and Future. *J. Geophys. Res. Oceans.*125(3): p.e2019JC015801.

Zhang, N., Feng, M., Hendon, H.H., Hobday, A.J., Zinke, J., 2017. Opposite polarities of ENSO drive distinct patterns of coral bleaching potentials in the southeast Indian Ocean. *Sci. Rep.* 7(1): 1-10. Available: https://doi.org/10.1038/s41598-017-02688-y [07 June 2020].

MARINE HEAT WAVES IN THE INDIAN OCEAN AND THEIR IMPACTS ON ATMOSPHERIC CONVECTION

by

SARANYA, J. S

(2015-20-022)

ABSTRACT OF THE THESIS

Submitted in partial fulfillment of the requirements for the degree of

BSc-MSc (Integrated) CLIMATE CHANGE ADAPTATION

FACULTY OF AGRICULTURE
Kerala Agricultural University

ACADEMY OF CLIMATE CHANGE EDUCATION AND RESEARCH
VELLANIKKARA, THRISSUR - 680 656
KERALA, INDIA
2020

ABSTRACT

Marine heatwaves (MHWs) are anomalous warm water events, which have a definite start and end date, lasting there for at least five days. In this study, we have done a robust analysis of the MHWs events in the Indian Ocean. It found out that by taking the annual trend of MHWs events, they are more in the Western Indian Ocean, especially in the Somali (41°E–56°E–8°S–8°N) region, and experienced 66 events during the 1982-2018 periods. We further studied the trend of MHW frequency during the summer monsoon, and it turned out that MHWs are prominent in both the Somali and the North Bay of Bengal (85°E–93°E–15°N–23°N) region. The northern Bay of Bengal has 94 events, wherein 34 events occurred from June to September, while in the Somali region, it was 21 events. In addition to that, we also investigated the seasonal climatology of MHW metrics in both selected regions.

The correlation analysis between the SST and the number of MHWs in the two selected regions revealed that Somali MHWs have a connection with the El Niño and positive IOD (Indian Ocean Dipole), as in the case of North Bay of Bengal along with the El Niño, basin-wide warming influence the MHWs. In addition to these, global warming also triggers these events.

It is realized from the analysis that, before five days of the start date of MHWs, in the Somali region, wind showing a dipole pattern, which is the high wind speed in the south of Somali and weak wind speed on the north side. Thus the ocean currents are unable to transport the heat due to the weak wind speed into the north side. Along with that increased solar radiation and decreased evaporation cooling together lead to the genesis of MHW. As in the case of the North Bay of Bengal region, it revealed that the

weak wind, decreased evaporation and high solar radiation itself cause the piling up of heat in this region.

The composite analysis of Sea Surface Temperature (SST), Outgoing Longwave Radiation (OLR), wind (at 850 hPa), vertical velocity (omega) (at 500 hPa), vertically integrated moisture flux convergence anomalies, and rainfall anomalies over India during the MHW days (June to September) disclose that the MHWs in the Somali (North Bay of Bengal) connected with decreased (increased) rainfall over the Indian subcontinent.

Meanwhile, the pre-condition of MHW days in the North Bay of Bengal region has a relation with 1, 2 phase of Indian Monsoon Intra-seasonal Oscillation (MISO), and 3 and 4 phases of the MISO dominant over the entire MHW days. In the Somali region, there is no such striking relation with MISO phases, but they accompanied by the 1 and 2 phases of Madden-Julian Oscillation (MJO).

Keywords: MHWs, Indian Ocean, Indian summer Monsoon